AD/A-004 014

APPLICATION OF HIGH-FREQUENCY RESONANCE TECHNIQUES FOR BEARING DIAGNOSTICS IN HELICOPTER GEARBOXES

Mark S. Darlow, et al

Mechanical Technology, Incorporated

Prepared for:

Army Air Mobility Research and Development Laboratory

October 1974

UNCLASSIFIED

SECURITY CLASSIFICATION OF THIS PAGE (When Data Entered)

REPORT DOCUMENTATION PAGE		READ INSTRUCTIONS BEFORE COMPLETING FORM
1. REPORT NUMBER USAAMRDL-TR-74-77	2. GOVT ACCESSION NO.	3. RECIPIENT'S CATALOG NUMBER AD/A-004014
4. TITLE (and Subtitle) APPLICATION OF HIGH-FREQUENCY RESONANCE TECHNIQUES FOR BEARING DIAGNOSTICS IN HELICOPTER GEARBOXES		5. TYPE OF REPORT & PERIOD COVERED Final Technical Report 6. PERFORMING ORG. REPORT NUMBER MTI Technical Report 74TR25
7. AUTHOR(s) Mark S. Darlow Robert H. Badgley G. W. Hogg		8. CONTRACT OR GRANT NUMBER(s) DAAJ02-73-C-0086
9. PERFORMING ORGANIZATION NAME AND ADDRESS Mechanical Technology Incorporated 968 Albany-Shaker Road Latham, New York 12110		10. PROGRAM ELEMENT, PROJECT, TASK AREA & WORK UNIT NUMBERS Task 1F162205A11908
11. CONTROLLING OFFICE NAME AND ADDRESS Eustis Directorate U.S. Army Air Mobility Research & Development Laboratory, Fort Eustis, Virginia 23604		12. REPORT DATE October 1974 13. NUMBER OF PAGES 157
14. MONITORING AGENCY NAME & ADDRESS(if different from Controlling Office)		15. SECURITY CLASS. (of this report) Unclassified 15a. DECLASSIFICATION/DOWNGRADING SCHEDULE

16. DISTRIBUTION STATEMENT (of this Report)

Approved for public release; distribution unlimited.

17. DISTRIBUTION STATEMENT (of the abstract entered in Block 20, if different from Report)

18. SUPPLEMENTARY NOTES

19. KEY WORDS (Continue on reverse side if necessary and identify by block number)

Bearings
Antifriction Bearings
Diagnostic Equipment
High Frequency
Resonance

20. ABSTRACT (Continue on reverse side if necessary and identify by block number)

The feasibility of the High-Frequency Resonance Technique (HFRT) for defect analysis of rolling-element bearings found in a UH-1 helicopter main transmission was demonstrated. A study was conducted to determine optimum conditions under which to test each bearing. These included accelerometer location, speed, load, housing design and detection frequency. The results provided general testing criteria for each bearing. An analytical and experimental bearing race resonance study was conducted on each bearing. The bearings were then mounted

DD FORM 1 JAN 73 1473 EDITION OF 1 NOV 65 IS OBSOLETE

UNCLASSIFIED

SECURITY CLASSIFICATION OF THIS PAGE (When Data Entered)

EUSTIS DIRECTORATE POSITION STATEMENT

The Eustis Directorate of the U. S. Army Air Mobility Research and Development Laboratory is conducting a series of efforts directed at advancing the state of the art of vibration signal analysis techniques. These techniques are in support of efforts associated with improving the capability of diagnosing the mechanical condition of Army helicopter power train components.

This contract was awarded to investigate the feasibility of applying high-frequency resonant phenomenon analysis techniques to helicopter components. It includes both laboratory and on-board the helicopter investigations.

The conclusions presented herein are generally agreed with by the Eustis Directorate.

The technical monitor of this contract was Mr. G. William Hogg, Reliability and Maintainability Division.

19. (continued)

Helicopters
Gearboxes
Detection

20. (continued)

in a test rig and run at various speeds, loads and housing designs. Good bearings and bearings with artificially-induced discrete defects were run. The results showed order-of-magnitude increases in amplitudes of ball-pass or roller-pass frequency peaks for bearings with defects as compared to the same bearings without defects. Also, they showed that variations in speed and load have relatively little effect. Similar signals were recorded from accelerometers mounted on an installed UH-1 main transmission. This data, after reduction, vividly demonstrated that the HFRT could readily detect bearing defect signal components under conditions where normal data detection techniques were unsatisfactory due to background noise levels. In combination with the test rig results, these results infer that the HFRT is not only feasible for use with the bearings of a UH-1 helicopter transmission, but may also be applied to other bearing systems as well.

PREFACE

A major contribution to the program was made by Richard A. Cundiff, who was at MTI when the contract was initiated. He was responsible for the design of the rotating dynamic response test rig. Special credit is due to Mr. Leo W. Winn of MTI, who acted as a consultant in the area of bearing dynamics. The MTI Program Manager was Dr. Robert H. Badgley.

TABLE OF CONTENTS

Table of Contents (Cont.)

LIST OF ILLUSTRATIONS

LIST OF ILLUSTRATIONS (continued)

LIST OF ILLUSTRATIONS (continued)

LIST OF ILLUSTRATIONS (continued)

LIST OF ILLUSTRATIONS (continued)

LIST OF ILLUSTRATIONS (continued)

LIST OF ILLUSTRATIONS (concluded)

LIST OF TABLES

List of Tables (Cont.)

INTRODUCTION

The formation of defects in helicopter transmission bearings as a result of bearing wear is a serious maintenance problem. This problem is compounded by the fact that under normal maintenance procedures these bearing defects often cannot be detected before they present a significant danger to the safe operation of the helicopter.

A procedure is developed herein which applies an advanced vibration analysis technique to the need for diagnosis of the condition of rolling-element bearings in helicopter gearboxes. This technique, known as the High-Frequency Resonance Technique (HFRT), is based upon the fact that very small faults or defects in the rolling-element bearing races cause impacts as they are encountered by the balls or rollers. These impacts excite high-frequency resonances in the bearing races. The resonance characteristics are modified (modulated) at ball-pass or roller-pass frequency in a manner which can readily be detected. The presence of such modulations is a clear indication of the presence of the faults or defects. In the efforts presented herein, this powerful diagnostic technique is extended to demonstrate clearly its practical applications.

DESCRIPTION OF PROGRAM

This study of helicopter transmission bearing resonance was conducted in five tasks, the individual efforts of which are summarized below.

In this study, it was necessary to determine the resonant frequencies of each of the components of the system. The analyst learned from these results the frequency ranges upon which he must concentrate during the second portion of the study: the evaluation of vibration levels of the actual system in operation. The third portion of the study involved correlation of the resonant frequencies with system behavior, and relation of observed results to the physical condition of the actual system.

TASK I — BEARING SELECTION

Five different bearings from the UH-1 main rotor drive transmission were selected for detailed investigation.

TASK II — LABORATORY INVESTIGATION OF BEARING RESONANCE VIBRATIONS

This task consisted of three investigations. The first was an analytical investigation of the free-vibration resonances of the bearing races. The second was an experimental investigation of the free-vibration resonances of the bearings and their component parts (races and retainers). The third investigation involved recording the vibration levels of the bearings operating on a test rig under normal loading conditions. The results of the first two investigations were used to evaluate the results of the third investigation. The subsequent conclusions were used to develop a scheme for the determination of bearing wear through bearing resonance evaluation.

TASK III — MEASUREMENT OF BACKGROUND VIBRATION LEVELS IN UH-1 HELICOPTERS

A visit to Fort Eustis, Virginia was made to obtain and evaluate samples of background vibration levels on the external surface of an operating UH-1 helicopter main rotor drive gearbox. These measurements were taken from the standpoint of completeness and for possible use in constructing a complete picture of the bearing dynamics involved in a UH-1 helicopter transmission.

TASK IV — EVALUATION AND ANALYSIS OF TEST DATA

The conclusions of Task II were employed in the evaluation of the results of Task III, in order to identify the useful information available from the vibration level measurements in the UH-1 helicopter. The mode shape measurements made in Task II and structural resonance calculations conducted in that task were used to develop a suitable prediction method for identifying resonant frequencies for bearing defect diagnosis. This analysis correlates the vibration signal characteristics with various bearing defects, thus permitting early identification of impending bearing failures in operational equipment.

TASK V – ASSESSMENT OF UTILITY OF HIGH-FREQUENCY RESONANCE TECHNIQUES

The experimental findings of signal generation and transmissibility, along with improved knowledge of the generating mechanism and the noise background, were used to determine those bearing degradation levels that may be detected in the actual UH-1 installation.

The same techniques utilized in this task may also be applied to other helicopter installations.

BEARING SELECTION

A schematic diagram of a UH-1 helicopter transmission is presented in Figure 1. The primary components of this transmission are referenced in the figure and listed in Table I. Five of the bearings which are most prone to failure were chosen for this investigation. These bearings are as follows:

1. Input bevel gear shaft ball bearing (triplex set, Bell Helicopter Company part number 204-040-346).

2. Input bevel gear shaft roller bearing (Bell Helicopter Company part number 204-040-269).

3. Lower-stage sun gear shaft roller bearing (Bell Helicopter Company part number 204-040-271).

4. Lower-stage sun gear shaft ball bearing (duplex set, Bell Helicopter Company part number 204-040-345).

5. Upper mast bearing (Bell Helicopter Company part number 204-040-136).

Samples of these bearings are shown in Figure 2.

TABLE I. PRIMARY COMPONENTS OF UH-1 HELICOPTER TRANSMISSION

Schematic Reference No.	Part Number	Part Name
(1)	204-040-700	Driven Bevel Gear
(2)	204-040-701	Driven Bevel Gear
(3)	204-040-100	Generator Bevel Gear
(4)	205-040-101	Generator Spur Gear
(5)	205-040-102	Generator Spur Gear
(6)	205-040-103	Generator Spur Gear
(7)	204-040-329-1	Lower Sun Gear
(8)	204-040-108-7	Lower Planetary Pinions
(9)	204-040-331-5	Lower Ring Gear
(10)	204-040-330-1,3	Upper Sun Gear
(11)	204-040-108-7	Upper Planetary Pinions
(12)	204-040-331-5	Upper Ring Gear
(13)	204-040-763	Drive Spur Gear
(14)	204-040-762	Driven Spur Gear
(15)	204-040-103-7	Drive Bevel Gear
(16)	204-040-104-13	Driven Bevel Gear, Tail Rotor
(17)	204-040-105	Driven Bevel Gear, Accessories
(18)	204-040-112	Sprocket Wheel Assembly
(19)	204-040-113	Sprocket Wheel Hydraulic Pump
(23)	204-040-142-1	Input Quill Shaft Bearing

TABLE I - Continued

Schematic Reference No.	Part Number	Part Name
(24)	204-040-346-3	Input Quill Shaft Bearing Triplex Ball (Input Pinion)
(25)	204-040-269	Roller, Input Quill Shaft Bearing
(26)	204-040-345-3	Input Gear Shaft Bearing, Duplex Ball
(27)	204-040-271	Main Reduction Gear Bearing
(29)	204-040-105	Generator Drive Shaft Bearing
(30)	204-040-106	Generator Drive Shaft Bearing
(31)	204-040-107	Generator Drive Shaft Bearing
(32)	204-040-108	Generator Drive Shaft Bearing
(33)	204-040-725	Roller Set, Lower
(34)	204-040-135	Main Rotor Reduction Bearing, Lower
(35)	204-040-725	Roller Set, Upper
(36)	204-040-135	Main Rotor Reduction Bearing, Upper
(37)	204-040-136	Upper Mast Bearing
(38)	204-040-135	Lower Transmission Bearing
(39)	204-040-270	Lower Mast Bearing
(40)	204-040-143	Lower Transmission Input Duplex Bearing
(41)	204-040-310	Lower Transmission Input Bearing
(42)	204-040-310-1	Tail Rotor Drive Bearing and Accessory Drive Bearing
(43)	204-040-143-1	Tail Rotor Drive Duplex Bearing
(44)	204-040-145	Tachometer Drive Shaft Bearing
(48)	204-101-425	Swash Plate Bearing

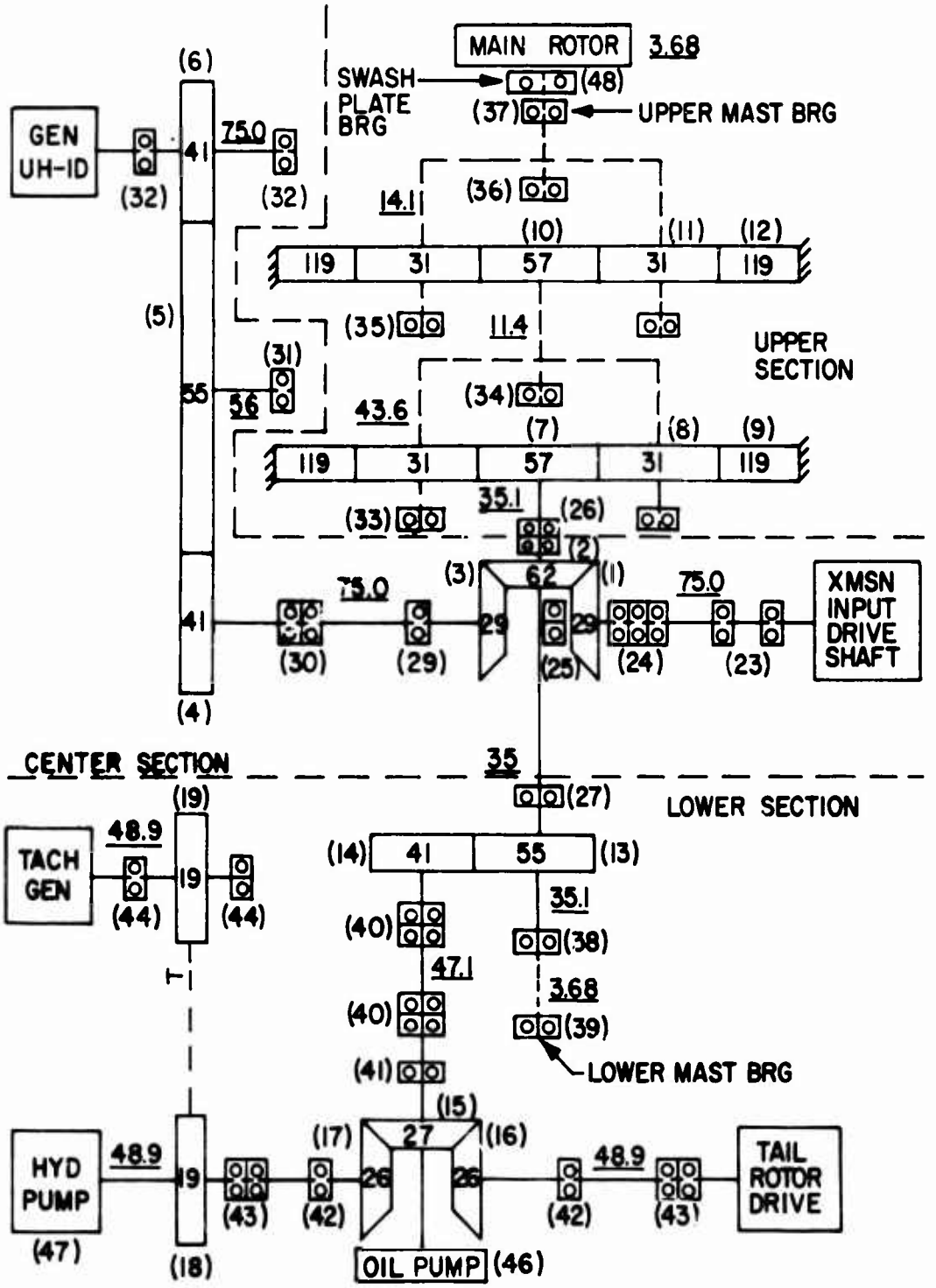

Figure 1. Gear Train Schematic – Model UH-1 Helicopter Main Rotor Transmission.

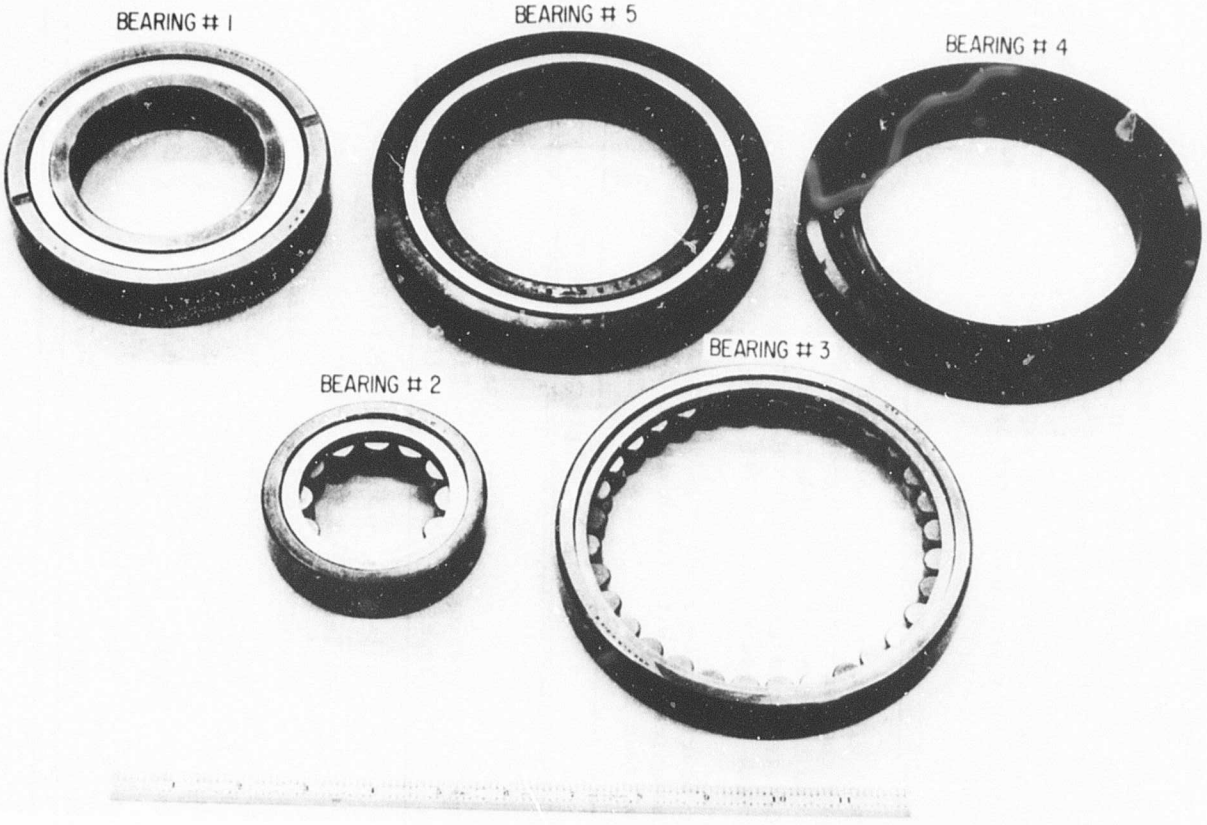

Figure 2. UH-1 Helicopter Transmission Bearings.

RESONANT FREQUENCIES OF BEARINGS AND BEARING COMPONENTS

As a first step in a bearing resonance study, it was necessary to investigate the natural, or resonant, frequencies of the individual bearings and their major components. These components are the inner and outer bearing races and the bearing retainers. The races of the UH-1 transmission bearings studied are made of SAE 52100 carbon-chromium steel. The retainers of all but one of the bearings are made of bronze. The other retainer is a phenolic composition. The resonant frequencies of the bearing races were investigated both analytically and experimentally. The resonant frequencies of the bearing retainers and of the assembled bearings were investigated experimentally, only.

FREE VIBRATION OF BEARINGS AND BEARING COMPONENTS

A thin-shell vibration computer program* was used to analytically determine a number of the resonant frequencies of five outer races and three inner races of the bearings of interest. Only the free-vibration portion of the program was required to determine these resonant frequencies. In all cases, a cylindrical reference surface was used.

All basic bearing dimensions were determined from design drawings and from direct communication with the designer. Some of these dimensions are presented in Table II.

TABLE II. BEARING DIMENSIONS

Bearing Number	Bearing Type	Pitch Diameter (in.)	Ball Roller Diameter (in.)	Number of Balls	Angle of of Contact (deg.)
1	Ball	4.3307	0.78125	15	25
2	Roller	2.5614	0.5512	12	-
3	Roller	5.6282	0.4724	32	-
4	Ball	5.7086	0.5938	26	25
5 (Design 1)	Ball	5.5118	0.71875	20	29
5 (Design 2)	Ball	5.5118	0.6875	21	40
5 (Design 3)	Ball	5.5118	0.6875	21	25
5 (Design 4)	Ball	5.5118	0.750	20	30

The four designs given for bearing No. 5 represent the differences in the

*Written by Dr. Arturs Kalnins, Lehigh University, 1963.

design of that bearing by various bearing manufacturers, any of which might be found in a UH-1 helicopter transmission. The inner surfaces of the outer races of bearings 1 and 4 were approximated as shown by the dashed line in Figure 3, where the value of ζ is of the order of 0.003 inch. The other bearing races were evaluated as they appear in the design drawings. Additional pertinent dimensions for each bearing race were calculated, using basic trigonometry. These dimensions were then used to mathematically describe the bearing races in sections, and to approximate the shell thickness variations for the purposes of programming. The curved surfaces were represented as a series of straight line segments.

Computer input data cards were prepared incorporating the above information, and the computer program was run for the eight races. Each of these cases was run for several different modes of vibration, and the resulting resonant frequencies were compared to the resonant frequencies determined experimentally. The experimental procedure involved the use of a magnetic driver to excite the bearing race and a B & K mini-accelerometer and amplification circuit to determine the existence and mode shape of several resonant frequencies. These resonant frequencies were found for the assembled bearings as well as for the races of the disassembled bearings.

The results for the five bearings are given in Tables III through VII. Circumferential Wave Number refers to the number of circumferential cycles, or half the number of circumferential nodes, around the circumference of the race as demonstrated in Figure 4. This quantity defines the mode of vibration.

For comparison, the resonances found experimentally and analytically for the free bearing races (bearings disassembled) are plotted together on line graphs in Figures 5 through 9. On these graphs, N represents the circumferential wave number and M represents the number of axial nodes. The resonances found experimentally for the five assembled bearings are given in Tables VIII through XII. The differences in the resonant frequencies observed during the various tests listed in Table VIII were due to the fact that none of the testing methods detected all of the resonant frequencies and that all of these tests contained a certain degree of inaccuracy.

As an additional source for comparison, the circumferential, or "bending", resonant modes of vibration may also be calculated from empirical equations. These are the modes of vibration with no axial nodes. The resonant frequency for the hoop mode is given by

$$f_s = \frac{1}{2\pi r}\frac{Eg}{\gamma} \qquad (1)$$

where E = Young's modulus, psi; g = gravitational constant, 386 in./sec^2; γ = weight density of steel, lb/in.^{3}; r = mean radius of steel ring, in.; f_s = hoop mode resonant frequency, Hz.

The resonant frequencies for modes of vibration with wave numbers of two

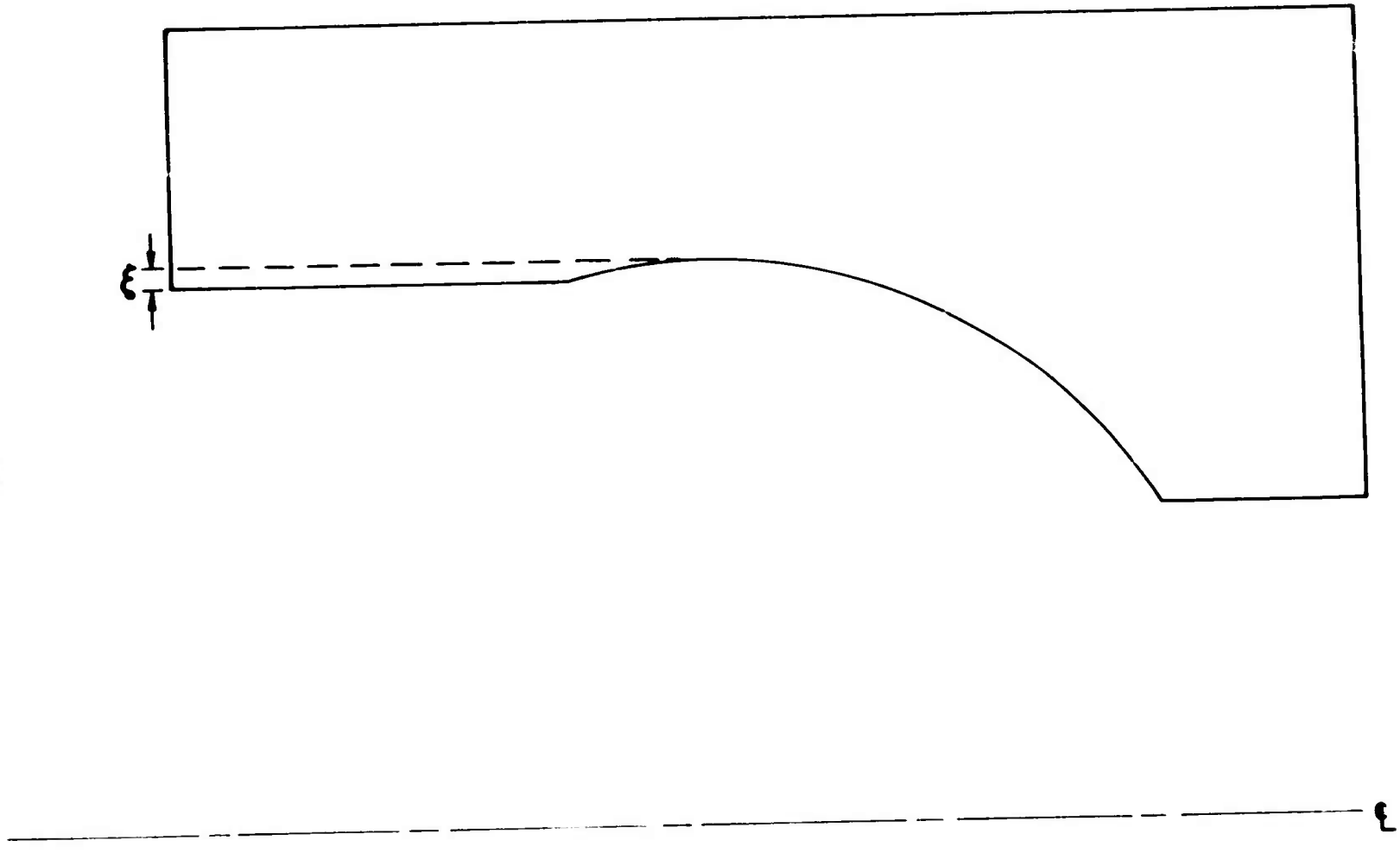

Figure 3. Cross Section of Outer Race of Bearings Numbers 1 and 4.

TABLE III. CALCULATED RESONANT FREQUENCIES AND MODE SHAPES FOR BEARING NO. 1 (Bell Helicopter Part No. 204-040-346)

Circumferential Wave Number	Number of Axial Nodes	Calculated Resonant Frequency (Hz)	Experimental Resonant Frequency (Hz)
		Outer Race	
0	0	12,100	12,460
2	0	1,060	1,030
3	0	2,940	2,830
4	0	5,550	5,220
5	0	8,800	8,360
6	0	12,600	11,840
7	0	16,900	15,590
8	0	21,700	19,850
2	1	-	1,920
		Inner Race	
0	0	19,100	18,640
2	0	3,060	3,000
3	0	8,500	8,100
4	0	16,100	14,480
5	0	25,600	21,800
6	0	36,700	30,400
2	1	-	3,460
3	1	-	9,570

TABLE IV. CALCULATED RESONANT FREQUENCIES AND MODE SHAPES FOR BEARING NO. 2 (Bell Helicopter Part No. 204-040-269)

Circumferential Wave Number	Number of Axial Nodes	Calculated Resonant Frequency (Hz)	Experimental Resonant Frequency (Hz)
		Outer Race	
0	0	19,200	19,730
0	2	50,100	-
2	0	2,370	2,430
2	1	5,460	4,380
3	0	7,180	6,980
4	0	13,800	12,770
5	0	22,400	19,860
6	0	33,000	28,230
7	0	44,700	37,190

TABLE V. CALCULATED RESONANT FREQUENCIES AND MODE SHAPES FOR BEARING NO. 3 (Bell Helicopter Part No. 204-040-271)

Circumferential Wave Number	Number of Axial Nodes	Calculated Resonant Frequency (Hz)	Experimental Resonant Frequency (Hz)
		Outer Race	
0	0	10,380	10,200
0	1	-	18,400
2	0	690	670
2	1	10,770	12,100
3	0	1,810	1,870
4	0	3,490	3,700
5	0	5,780	5,900
6	0	8,290	8,600
7	0	11,180	11,900
8	0	14,340	15,700

TABLE VI. CALCULATED RESONANT FREQUENCIES AND MODE SHAPES FOR BEARING NO. 4 (Bell Helicopter Part No. 204-040-345)

Circumferential Wave Number	Number of Axial Nodes	Calculated Resonant Frequency (Hz)	Experimental Resonant Frequency (Hz)
		Outer Race	
0	0	9,900	10,180
0	1	16,100	-
2	0	590	630
2	1	12,100	-
3	0	1,670	1,690
4	0	3,200	3,200
5	0	5,160	5,060
6	0	7,530	7,620
7	0	10,300	9,130
8	0	13,500	13,130
		Inner Race	
0	0	13,000	13,090
0	1	21,600	-
2	0	1,270	1,260
2	0	30,100	-
3	0	3,580	3,420
4	0	6,830	6,750
5	0	11,000	10,380
6	0	16,100	14,830
7	0	22,000	20,180
8	0	28,800	25,480

TABLE VII. CALCULATED RESONANT FREQUENCIES AND MODE SHAPES FOR BEARING NO. 5 (Bell Helicopter Part No. 204-040-136)

Circumferential Wave Number	Number of Axial Nodes	Calculated Resonant Frequency (Hz)	Experimental Resonant Frequency (Hz)
		Outer Race	
0	0	9,900	10,260
0	1	18,150	-
2	0	910	882
2	0	21,300	-
3	0	2,590	2,450
4	0	4,980	4,610
5	0	8,080	7,450
6	0	11,800	10,630
7	0	16,300	14,360
8	0	21,300	18,350
2	1	1,940	1,470
3	1	5,280	-
4	1	9,660	9,140
5	1	14,670	-
6	1	20,140	-
		Inner Race	
0	0	14,200	13,810
2	0	1,500	1,410
2	1	26,700	-
3	0	4,250	3,840
4	0	8,060	7,410
5	0	12,800	11,660
6	0	18,600	16,500
7	0	25,100	22,420
8	0	32,400	-

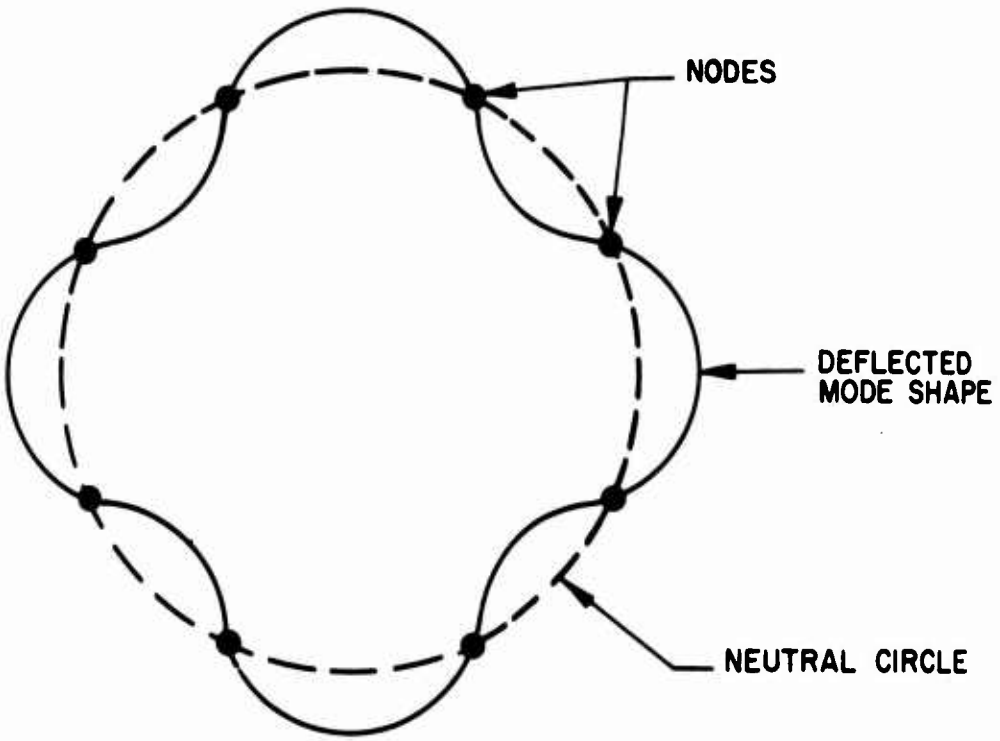

Figure 4. Sketch of Mode Shape for Circumferential Wave Number of 4.

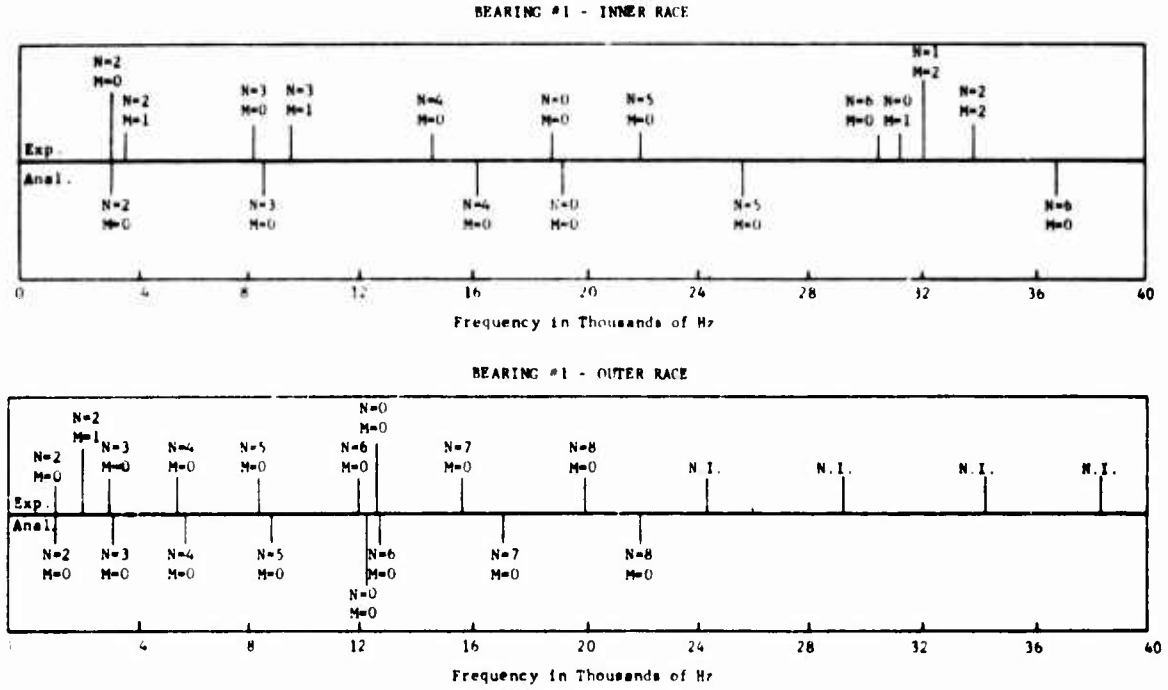

Figure 5. Resonant Frequencies for Races of Bearing No. 1.

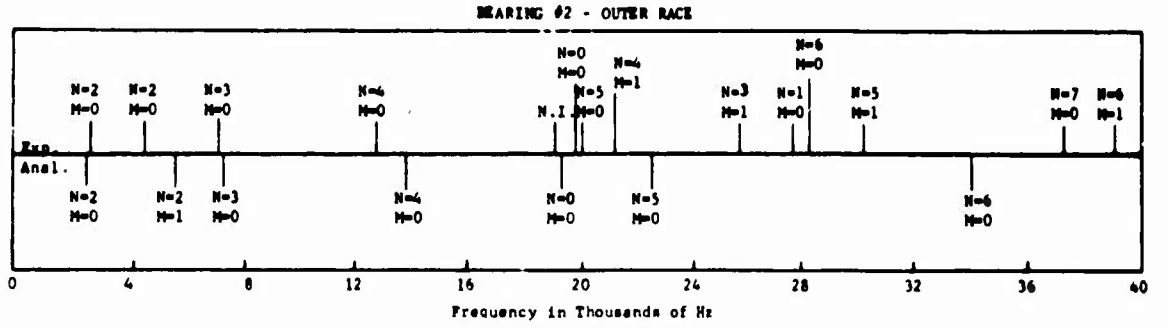

Figure 6. Resonant Frequencies for Races of Bearing No. 2.

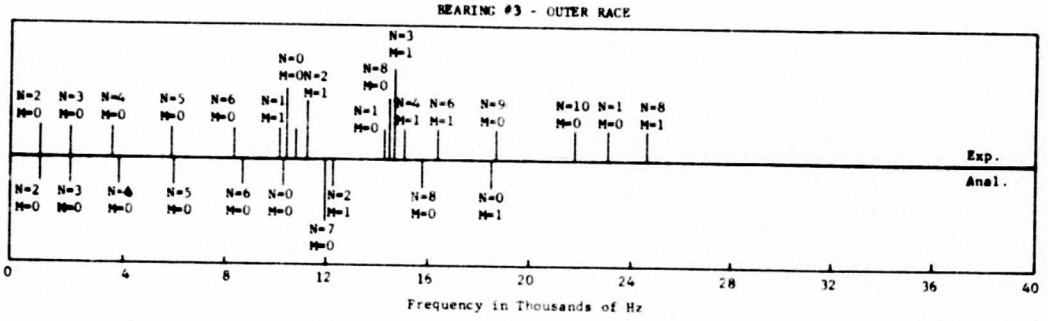

Figure 7. Resonant Frequencies for Races of Bearing No. 3.

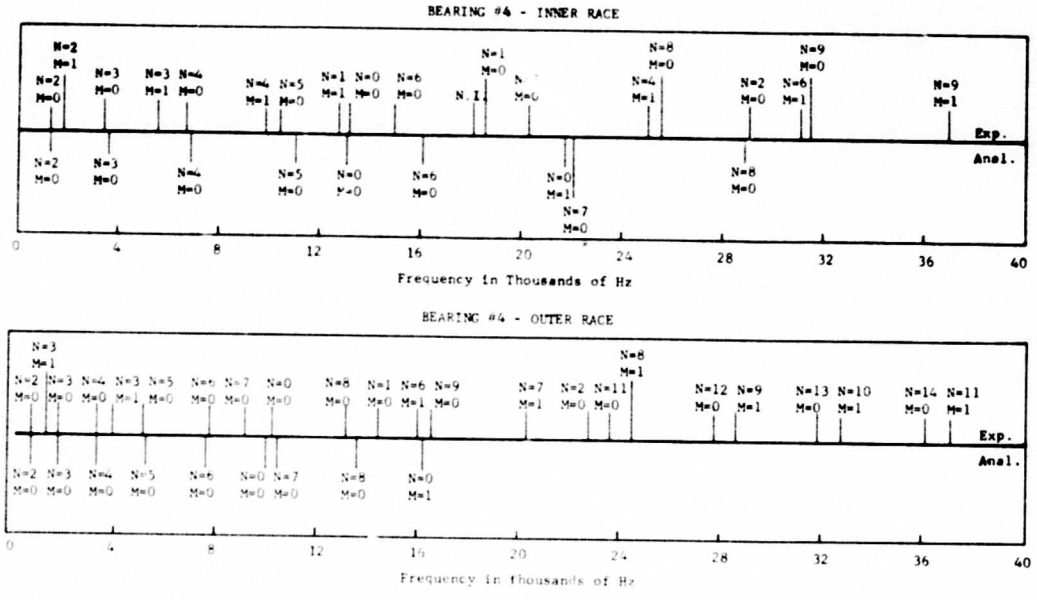

Figure 8. Resonant Frequencies for Races of Bearing No. 4.

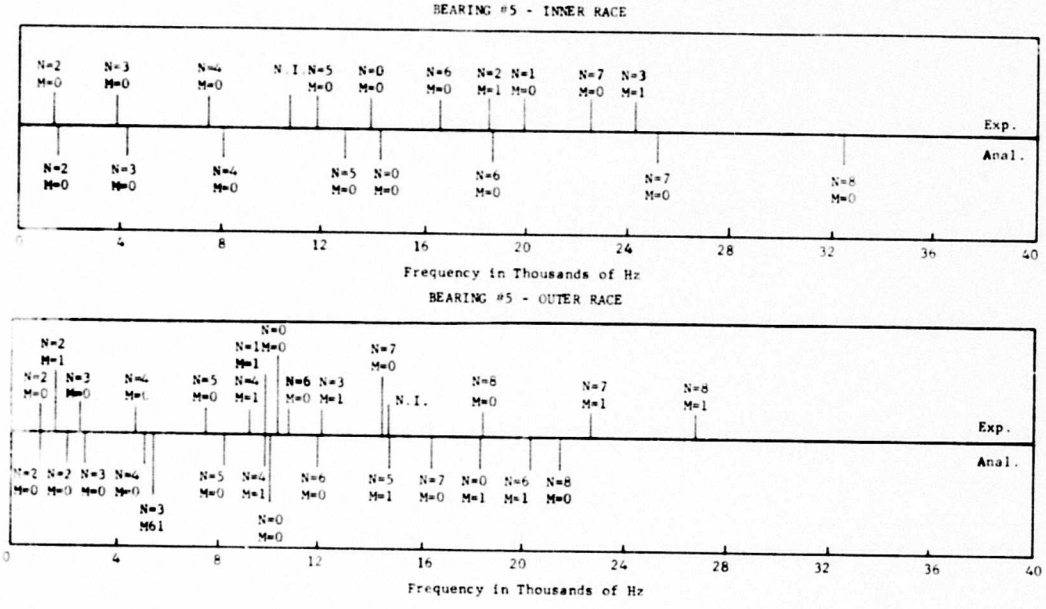

Figure 9. Resonant Frequencies for Races of Bea ing No. 5.

TABLE VIII. ASSEMBLED BEARING NO. 1

Test 1. Outer race driven with magnetic driver. Vibration picked up on outer race.

Resonant Frequencies

1.3 kHz	
2.7 kHz	
6.4 kHz	
11.0 kHz	
12.8 kHz	
16.2 kHz	(Strong Response)
24.8 kHz	
29.2 kHz	

Test 2. Outer race driven with miniature B&K accelerometer. Vibration picked up on outer race.

Resonant Frequencies

15.8 kHz
17.5 kHz
19.8 kHz
23.8 kHz
26.8 kHz
36.2 kHz

Test 3. Outer race impacted and transient response frequency picked up on outer race.

Resonant Frequencies

16 to 17 kHz

Test 4. Inner race driven with magnetic driver and vibration picked up on inner race.

Resonant Frequencies

1.36 kHz
2.8 kHz
16.4 kHz
20.6 kHz
21.2 kHz
21.6 kHz

TABLE IX. RESONANT FREQUENCIES FOUND EXPERIMENTALLY FOR ASSEMBLED BEARING NO. 2 (No Inner Race)

Test: Outer Race Driven With Magnetic Driver.
Vibration Picked up on Outer Race.

Resonant Frequency (kHz)	Circumferential Wave Number	Number of Axial Nodes
2.26	2	0
4.96	2	1
8.04	3	0
12.44	4	0
18.98	0	0
20.04	5	0
22.30	4	1
27.73	1	0
28.49	6	0
29.96	5	1
35.00	Not Identified	Not Identified
38.56	6	1
43.24	Not Identified	Not Identified
47.39	7	1

TABLE X. RESONANT FREQUENCIES FOUND EXPERIMENTALLY FOR ASSEMBLED BEARING NO. 3 (No Inner Race)

Test: Outer Race Driven With Magnetic Driver.
Vibration Picked up on Outer Race.

Resonant Frequency (kHz)	Circumferential Wave Number	Number of Axial Nodes
0.73	2	0
1.76	3	0
3.29	4	0
5.45	5	0
8.86	6	0
10.29	0	0
11.39	7	0
12.41	5	1
14.34	8	0
15.10	4	1
17.48	9	0
18.90	Not Identified	Not Identified
20.50	7	1
23.06	Not Identified	Not Identified
24.48	8	1

TABLE XI. RESONANT FREQUENCIES FOUND EXPERIMENTALLY FOR ASSEMBLED BEARING NO. 4

Test 1 Outer Race Driven With Magnetic Driver. Vibration Picked up on Outer Race

Resonant Frequency (kHz)	Circumferential Wave Number	Number of Axial Nodes
0.81	2	0
2.04	3	0
3.44	4	0
4.80	4	0
6.69	5	0
9.72	0	0
12.10	4	1
14.43	5	2
15.34	5	1
16.32	6	1
20.74	7	1

Test 2 Outer Race Driven With Magnetic Driver. Vibration Picked up on Inner Race

0.81	2	0
2.17	3	0
3.44	4	0
5.69	4	0
6.80	5	0
10.35	0	0
12.44	4	2
14.36	4	1

TABLE XI - Continued

Test 3. Inner Race Driven With Magnetic Driver. Vibration Picked up on Outer Race.

Resonant Frequency (kHz)	Circumferential Wave Number	Number of Axial Nodes
0.83	2	0
2.20	3	0
3.76	4	0
4.98	4	0
7.24	5	0
10.85	3	1
13.90	4	1
17.13	5	1
20.81	7	1

Test 4 Inner Race Driven With Magnetic Driver. Vibration Picked up on Inner Race.

0.83	2	0
2.20	3	0
3.93	4	0
4.98	4	0
7.24	5	0
10.85	3	1
13.50	4	1
17.13	5	1
20.81	7	1

TABLE XII. RESONANT FREQUENCIES FOUND EXPERIMENTALLY FOR ASSEMBLED BEARING NO. 5

Test 1 Outer Race Driven With Magnetic Driver. Vibration Picked up on Outer Race

Resonant Frequency (kHz)	Circumferential Wave Number	Number of Axial Nodes
0.95	2	0
2.16	3	0
3.72	4	0
5.39	4	0
7.52	5	0
9.28	0	0
12.42	2	1
14.43	3	1
18.40	Not Identified	Not Identified
23.00	4	1
27.40	9	0
35.50	10	0

Test 2 Outer Race Driven With Magnetic Driver. Vibration Picked up on Inner Race

0.95	2	0
2.16	2	0
3.72	3	0
4.87	3	0
6.94	0	0

TABLE XII - Continued

Test 3 Inner Race Driven With Magnetic Driver. Vibration Picked up on Outer Race.

Resonant Frequency (kHz)	Circumferential Wave Number	Number of Axial Nodes
1.00	2	0
2.54	3	0
4.44	3	0
9.38	0	0
10.92	4	0
13.43	3	1
16.20	4	1
19.20	5	0

Test 4 Inner Race Driven With Magnetic Driver. Vibration Picked up on Inner Race

1.00	2	0
2.54	3	0
3.54	3	0
9.38	3	0
10.92	4	0
13.43	3	1
16.20	4	1
19.20	5	0

through six* are given by

$$f_c = C \frac{h}{r^2} \times 10^4 \qquad (2)$$

where f_c = resonant frequency for other modes, Hz

h = thickness of steel ring, in.

C = empirical frequency constant such that for:

n	= 2	C	= 2.51
n	= 3	C	= 7.10
n	= 4	C	= 13.6
n	= 5	C	= 22.2
n	= 6	C	= 32.2

The circumferential resonant frequencies for the outer race of bearing No. 3 were calculated using the equations above. The results are listed in Table XIII.

TABLE XIII. CALCULATED RESONANT FREQUENCIES USING EMPIRICAL EQUATIONS FOR BEARING NO. 3 OUTER RACE (No Axial Nodes)

Circumferential Wave Number	Resonant Frequency (Hz)
0	10,200
2	695
3	1,960
4	3,760
5	6,140
6	8,920

In order to determine the relative significance of the resonant frequencies previously determined for each bearing race, the frequency spectrum of the free vibration of each bearing race was analyzed. This was done by rigidly attaching a B & K mini-accelerometer to the bearing race, suspending the race with a string, and exciting the race by dropping a ball on it directly opposite the location of the accelerometer. This was to insure that the accelerometer was not located on the vibrational node. The resulting transient response of the accelerometer was stored in a transient recorder. The frequency spectrum of this transient response was then analyzed by a frequency spectrum analyzer. In order to insure a characteristic frequency spectrum, each bearing race was excited ten times and the

*J.N. Macduff and R.P. Felgar, "Vibration Frequency Charts," Machine Design, February 7, 1957.

frequency spectrums were added and averaged. The resulting frequency spectrums for the eight bearing races tested are presented as Figures 10 through 17. The amplitudes in these spectrums are proportional to the force with which the ball was dropped. Since these amplitudes would be inconclusive and, possibly, misleading, they have not been included in the figures.

The resonant frequencies of the bearing retainers could not be calculated using the analytical methods employed above because the retainers are not axisymmetric. However, these resonances could be determined experimentally both by the use of the steady-state magnetic driver test and also by the transient frequency spectrum analysis method. The bearing retainer from bearing No. 1 was so tested. The results from the magnetic driver test are presented in Table XIV. The accelerometer signals were indistinct, and the modes of vibration were extremely difficult to define.

TABLE XIV. EXPERIMENTAL RESONANT FREQUENCIES AND MODE SHAPES FOR RETAINER BEARING NO. 1

Resonant Frequency (kHz)	Circumferential Wave Number	Number of Axial Nodes
0.64	2	0
1.03	2	0
2.60	3	0
4.43	4	0
5.38	4	1
6.25	3	1
7.21	0	0
7.71	5	0
8.54	0	1
9.78	1	0
10.58	5	1
13.34	6	0
14.22	5	1
16.76	6	1
18.55	7	1
25.60	7	1

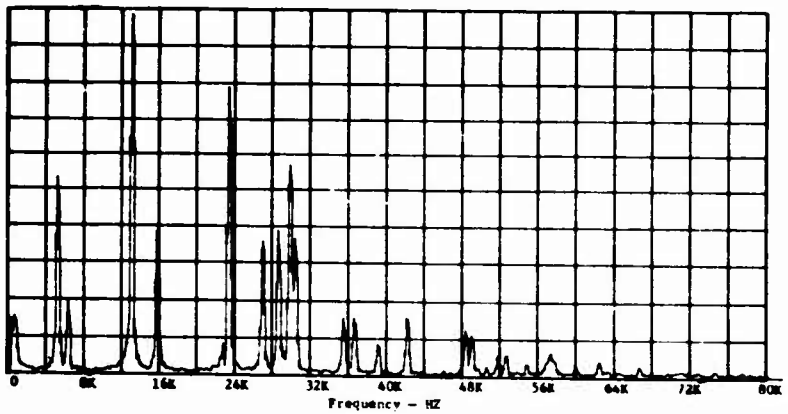

Figure 10. Free Vibration of Bearing No. 1 Inner Race, Ball Drop Excitation.

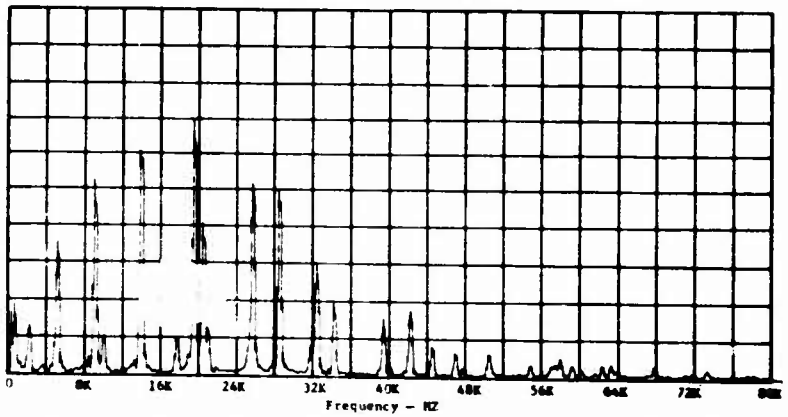

Figure 11. Free Vibration of Bearing No. 1 Oute Race, Ball Drop Excitation.

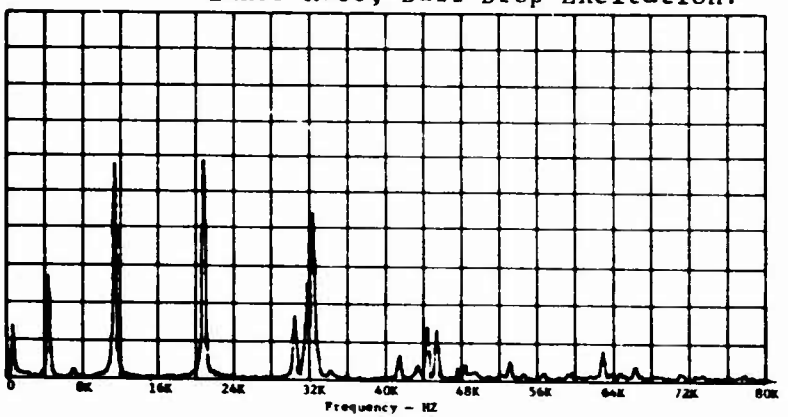

Figure 12. Free Vibration of Bearing No. 2 Outer Race, Ball Drop Excitation.

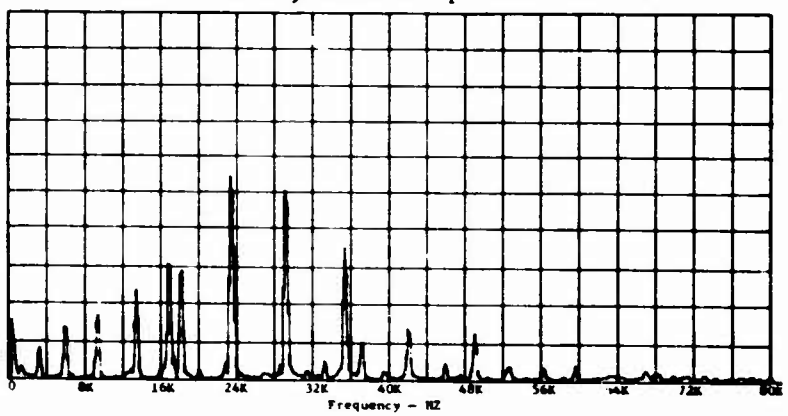

Figure 13. Free Vibration of Bearing No. 3 Outer Race, Ball Drop Excitation.

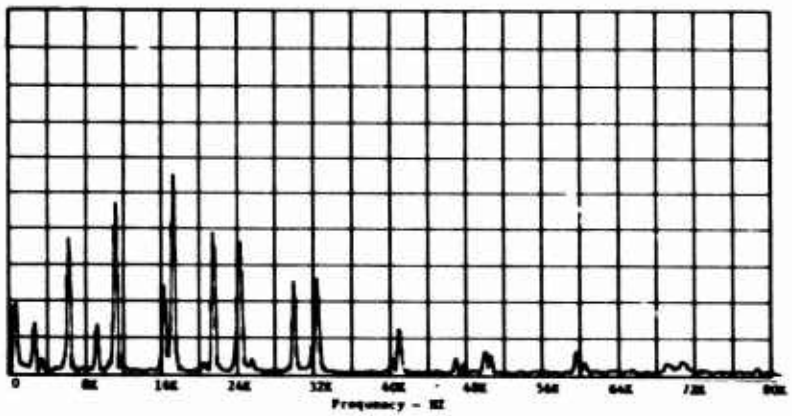

Figure 14. Free Vibration of Bearing No. 4 Inner Race, Ball Drop Excitation.

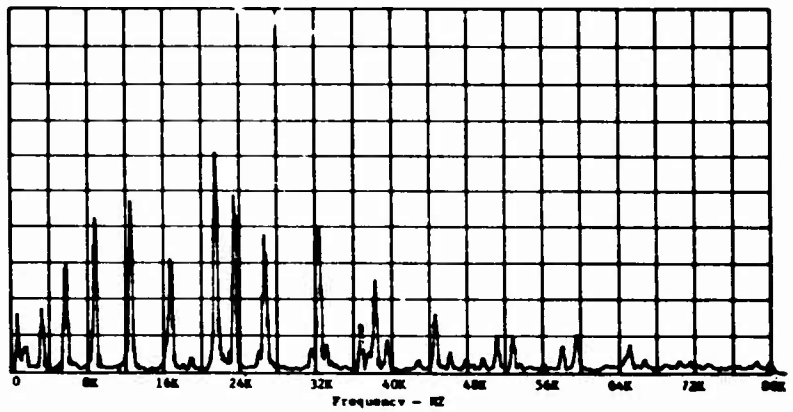

Figure 15. Free Vibration of Bearing No. 4 Outer Race, Ball Drop Excitation.

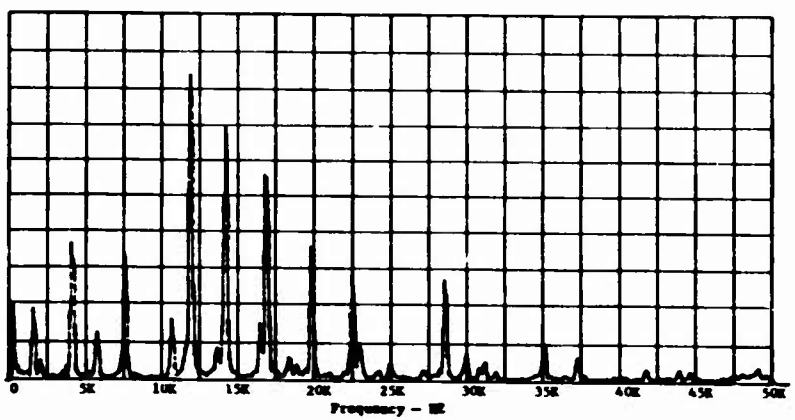

Figure 16. Free Vibration of Bearing No. 5 Inner Race, Ball Drop Excitation.

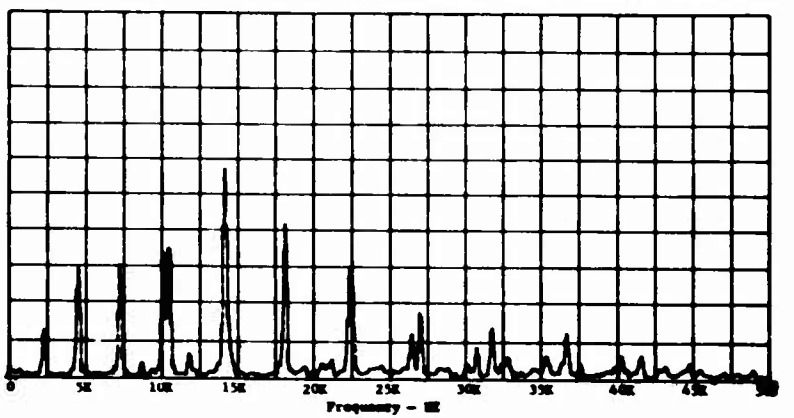

Figure 17. Free Vibration of Bearing No. 5 Outer Race, Ball Drop Excitation.

The remaining retainers were not tested by this method. However, frequency spectrums were obtained, by the ball drop method, for the free vibration of the retainers of all of the bearings except for bearing No. 4, whose retainer is phenolic. These frequency spectrums are presented as Figures 18 through 21. It would seem that during bearing operation, retainer resonances would not have as much effect as race resonances on overall bearing resonances, since the retainers are not in permanent contact with either the inner or the outer races and they are highly damped by their lubricant.

The results of the analytical and experimental resonant frequency investigations show that all procedures employed yield reasonably consistent results within the limits of accuracy of the analytical models and the experimental procedures. These results do provide a range of frequencies in which to look for useful resonances in an operating bearing. The relative amplitudes of the peaks in the frequency spectrums for the races, obtained by the ball drop method, show which resonances will probably tend to dominate. Incorporation of these results with the frequency spectrum analyses from the bearing test rigs and helicopter background vibration levels provides a substantially clearer picture of the bearing dynamics involved.

BEARING RESONANT FREQUENCIES WITH ELASTIC FOUNDATIONS

In actual operation, bearing outer races are not free to vibrate, but are instead fitted into semirigid housings which restrict their vibration. This added stiffness can have a significant effect on the bearing resonance frequencies, primarily the outer race resonances. In order to analytically determine what this effect is, the shell vibration computer program described previously was used to find the resonant frequencies for several modes of vibration of the outer race of bearing No. 5 with different values of elastic foundation modulus. Elastic foundation stiffness, which could also be called hoop stiffness, is a radial stiffness acting to restrain the circumferential vibration of a bearing race. The elastic foundation modulus represents the stiffness of the housing in which the bearing is to be mounted. This may not have been a rigorous representation in all cases, since the elastic foundation assumed by the program applied a retarding force to an inward radial race displacement as well as to outward displacement. For loose fits, the bearing housing applies a retarding force to an outward displacement only, whereas tight press-fits are closer to the analytical assumption. While the balls or rollers do apply a retarding force to the outer race for an inward deflection, this stiffness is probably not of the same order of magnitude as that of the housing.

The results of this analytical investigation are given in Table XV. The resonant frequencies of several specific modes of vibration are plotted as functions of the elastic foundation modulus in Figures 22 through 27. The data points for these plots are taken from Table XV. It can be seen clearly from these results that for circumferential wave numbers, other than zero, the foundation stiffness has much less of an effect on the resonances with one axial node than those with no axial nodes.

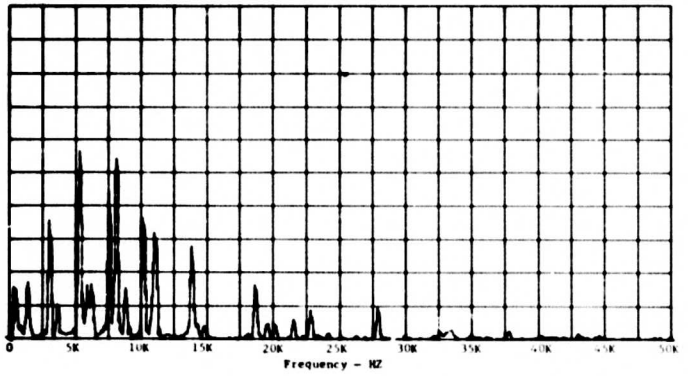

Figure 18. Free Vibration of Bearing No. 1 Retainer, Ball Drop Excitation.

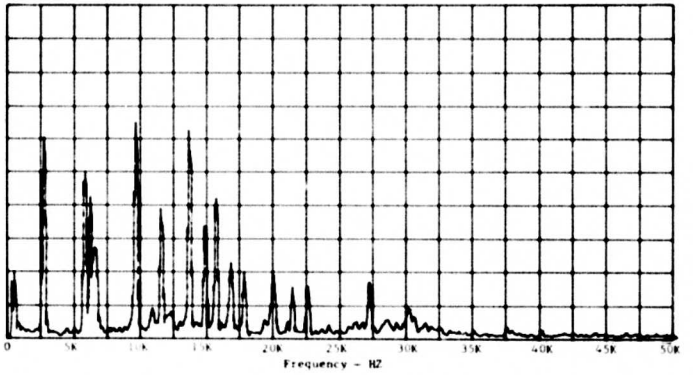

Figure 19. Free Vibration of Bearing No. 2 Retainer, Ball Drop Excitation.

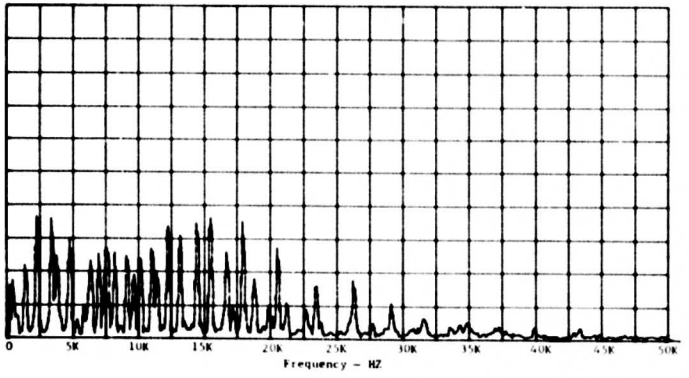

Figure 20. Free Vibration of Bearing No. 3 Retainer, Ball Drop Excitation.

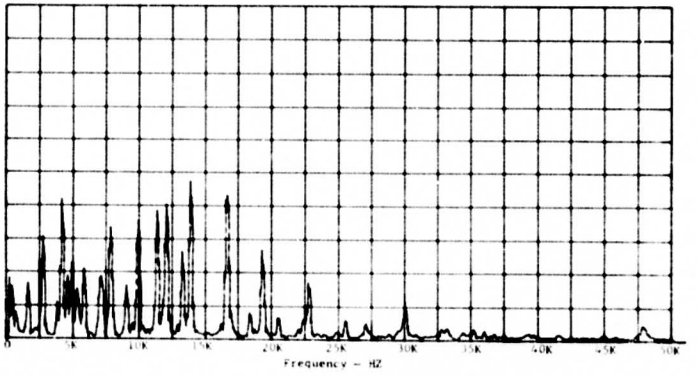

Figure 21. Free Vibration of Bearing No. 5 Retainer, Ball Drop Excitation.

TABLE XV. RESONANT FREQUENCIES OF BEARING NO. 5 OUTER RACE WITH ELASTIC FOUNDATION

Circumferential Wave Number	Number of Axial Nodes	Elastic Foundation Stiffness ($lb/in.^3$)	Calculated Resonant Frequency (Hz)
0	0	1,000,000	14,100
2	0	1,000,000	9,000
2	1(1/2 cycle)	1,000,000	2,540
3	1(1/2 cycle)	1,000,000	5,840
3	0	1,000,000	10,050
4	0	1,000,000	11,100
4	1(1/2 cycle)	1,000,000	10,100
0	1(1/2 cycle)	1,000,000	20,500
0	0	10,000	9,970
2	0	10,000	1,290
3	0	10,000	2,770
4	0	10,000	5,080
0	1(1/2 cycle)	10,000	18,200
2	1(1/2 cycle)	10,000	1,955
3	1(1/2 cycle)	10,000	5,290
4	1(1/2 cycle)	10,000	9,680
0	0	100,000	10,400
0	1(1/2 cycle)	100,000	18,400
2	0	100,000	3,030
2	1(1/2 cycle)	100,000	2,040
3	0	100,000	4,020
3	1(1/2 cycle)	100,000	5,360
4	0	100,000	5,900
4	1(1/2 cycle)	100,000	9,720
0	0	10,000,000	32,800
0	1(1/2 cycle)	10,000,000	35,600
2	0	10,000,000	18,300
2	1(1/2 cycle)	10,000,000	3,250
3	0	10,000,000	26,500
3	1(1/2 cycle)	10,000,000	6,830
4	0	10,000,000	31,100
4	1(1/2 cycle)	10,000,000	11,200
5	0	10,000	8,130
5	1(1/2 cycle)	10,000	14,680
6	0	10,000	11,900
6	1(1/2 cycle)	10,000	20,150

TABLE XV - Continued

Circumferential Wave Number	Number of Axial Nodes	Elastic Foundation Stiffness ($lb/in.^3$)	Calculated Resonant Frequency (Hz)
5	0	100,000	8,680
5	1(1/2 cycle)	100,000	14,700
6	0	100,000	12,300
6	1(1/2 cycle)	100,000	20,160
5	0	1,000,000	12,900
5	1(1/2 cycle)	1,000,000	15,080
6	0	1,000,000	15,600
6	1(1/2 cycle)	1,000,000	20,430
5	0	10,000,000	32,600
5	1(1/2 cycle)	10,000,000	16,170
6	0	10,000,000	34,000
6	1(1/2 cycle)	10,000,000	21,400

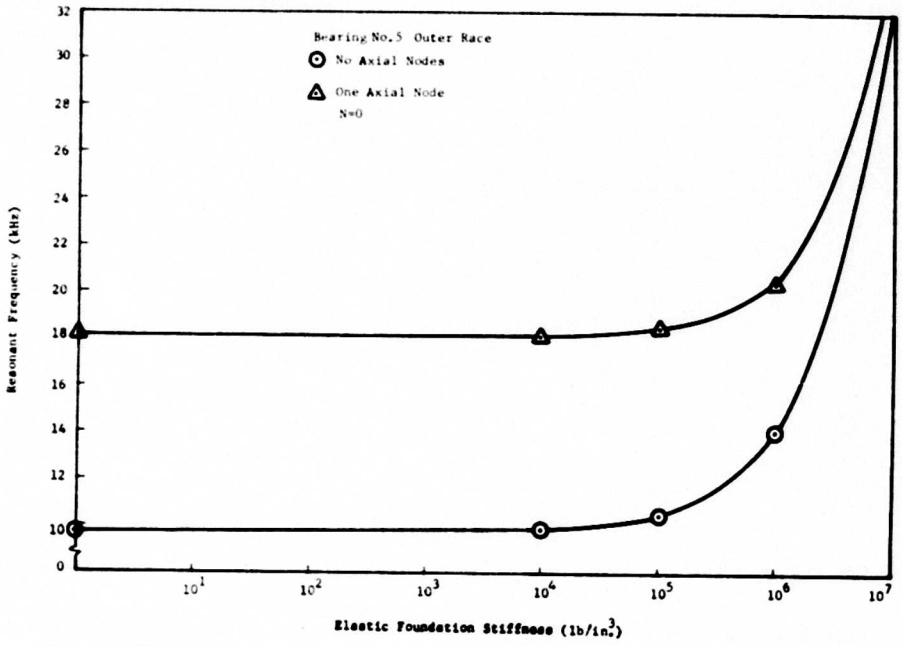

Figure 22. Bearing No. 5 Outer Race Resonant Frequencies as a Function of Foundation Stiffness for N=0.

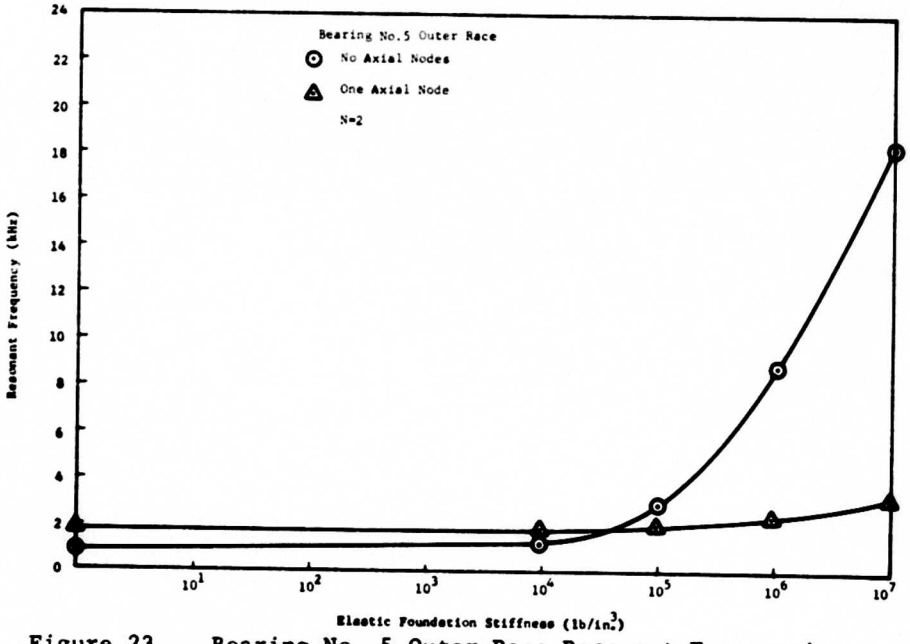

Figure 23. Bearing No. 5 Outer Race Resonant Frequencies as a Function of Foundation Stiffness for N=2.

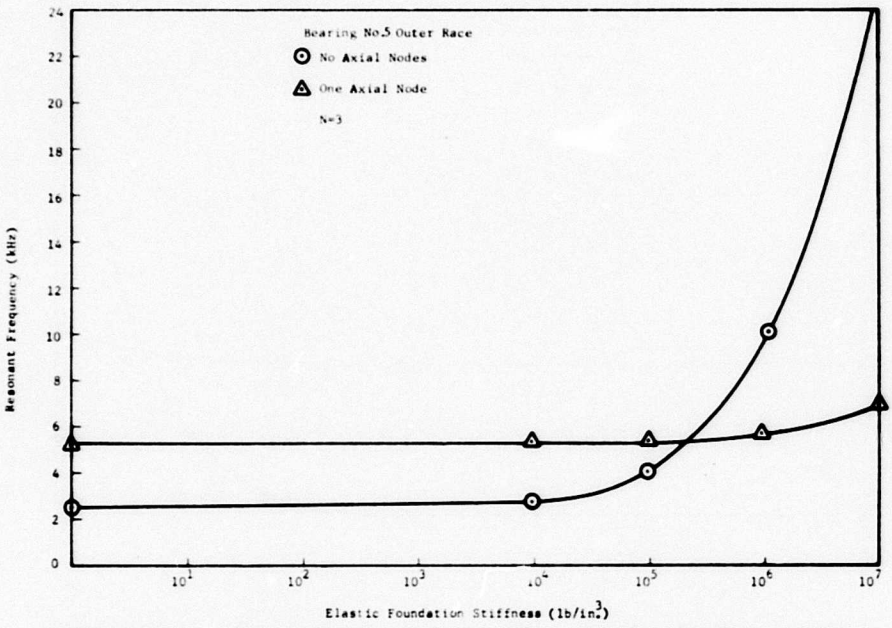

Figure 24. Bearing No. 5 Outer Race Resonant Frequencies as a Function of Foundation Stiffness for N=3.

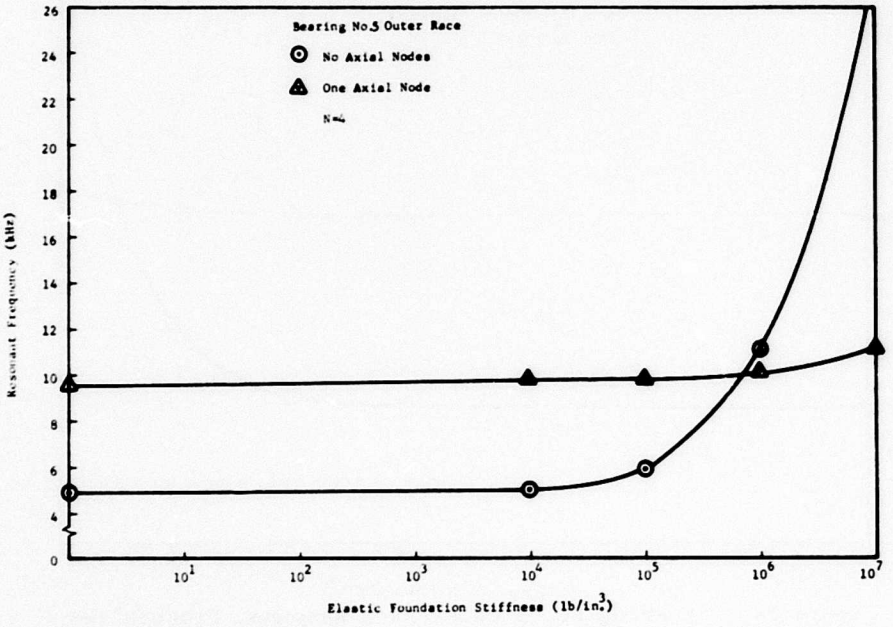

Figure 25. Bearing No. 5 Outer Race Resonant Frequencies as a Function of Foundation Stiffness for N=4.

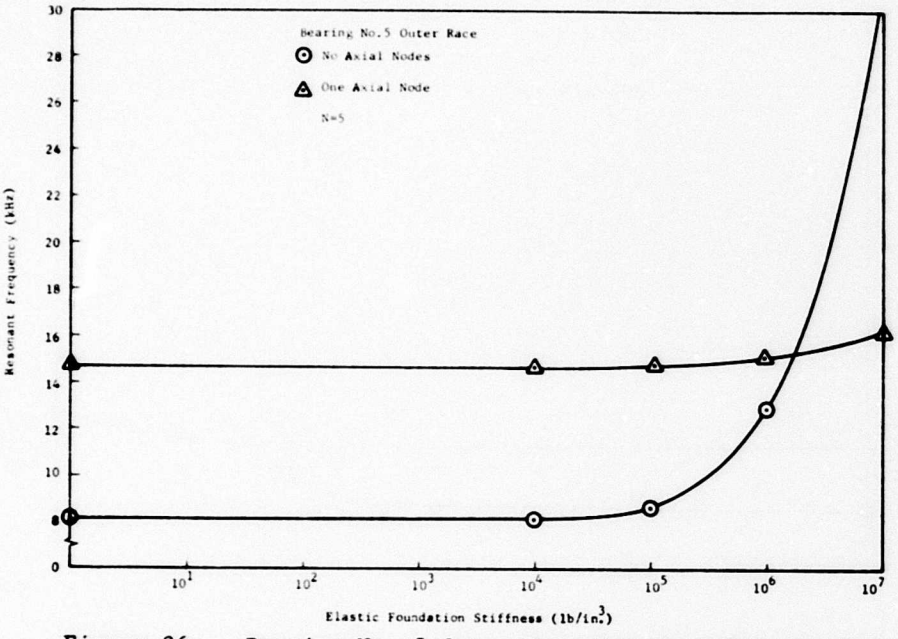

Figure 26. Bearing No. 5 Outer Race Resonant Frequencies as a Function of Foundation Stiffness for N=5.

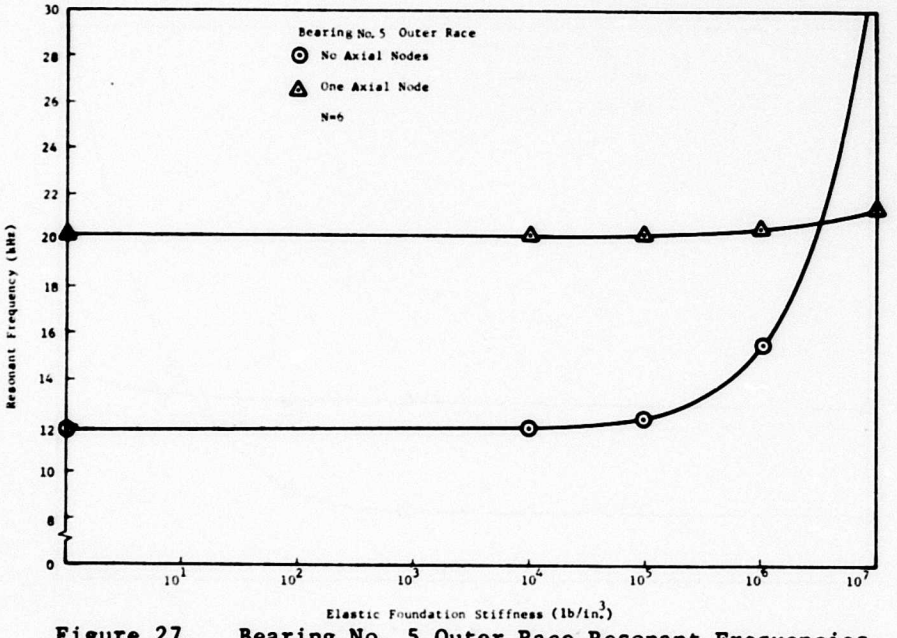

Figure 27. Bearing No. 5 Outer Race Resonant Frequencies as a Function of Foundation Stiffness for N=6.

ROTATING DYNAMIC RESPONSE TEST RIG

A test rig was designed and fabricated to allow representative loads and speeds to be applied to test bearings, and which permitted studies to be conducted on the transmission of high-frequency resonance signals across mechanical interfaces.

A commercially-fabricated (Whitnon) spindle capable of speeds up to 20,000 rpm and loads (radial and axial) up to several thousand pounds was adapted for use in the test rig.

The spindle, which was belt-driven by an electric motor, was used to mount the test bearings' inner races. The outer races were supported within a bearing housing which could be loaded radially and axially. A design drawing of the test rig is shown in Figure 28. Photographs of the entire test rig and its components are shown in Figures 29 through 36. Vibration measurements were made on the bearing supports.

The test rig was used for tests of bearings in simulated installation arrangements. High-frequency B&K mini-accelerometers were strategically located during these tests to assure that meaningful data would be recorded.

RADIAL STIFFNESSES OF TEST RIG BEARING HOUSINGS

The foundation stiffness model for the heavyweight bearing housing for bearing No. 1 is shown in Figure 37. The bearing support radial stiffness attributable to section A was calculated from equation (3) for deflection of a thick-walled vessel under uniform internal radial pressure.*

$$\Delta a = p\frac{a}{E}\left(\frac{b^2 + a^2}{b^2 - a^2} + \nu\right) \qquad (3)$$

where a = inside radius, in.

Δa = deflection of bearing housing, in.

b = outside radius, in.

p = pressure, lb/in.^{2}

E = Young's modulus, lb/in.^{2}

ν = Poisson's ratio

Solving for $p/\Delta a$, the unit stiffness of the bearing housing, and using the dimensions of Section A, the stiffness of this section was found to be equal to 3.0×10^6 pounds per cubic inch (psi/in.). Due to its thickness

* Raymond J. Roarke, Formulas for Stress and Strain, McGraw Hill, New York, 1938.

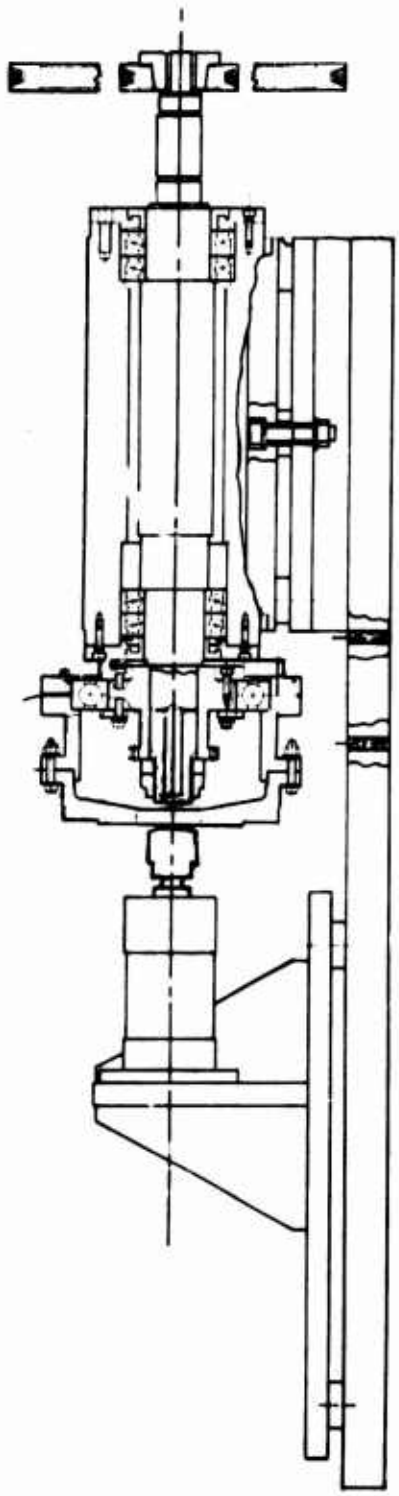

Figure 28. Design Drawing of Rotating Dynamic Response Test Rig.

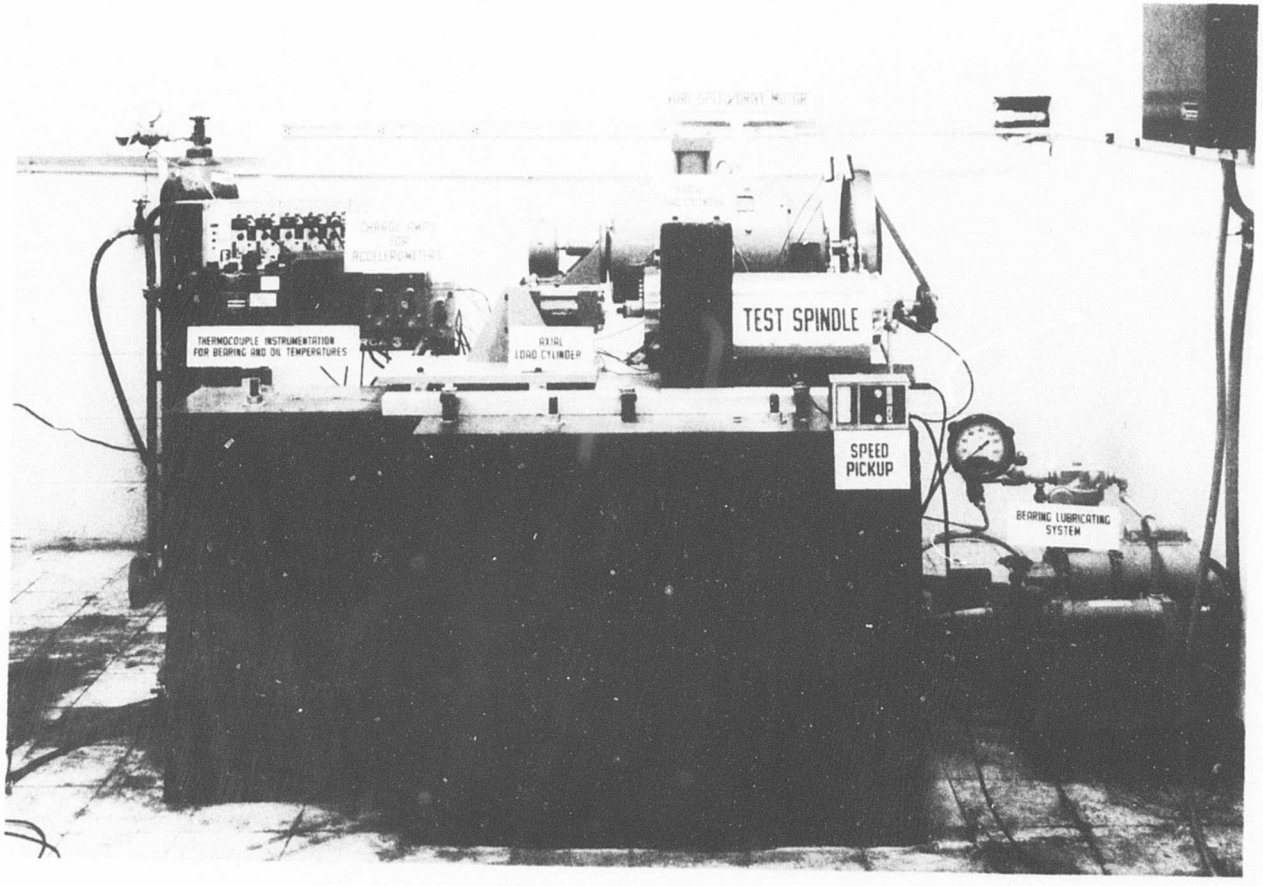

Figure 29. Rotating Dynamic Response Test Rig.

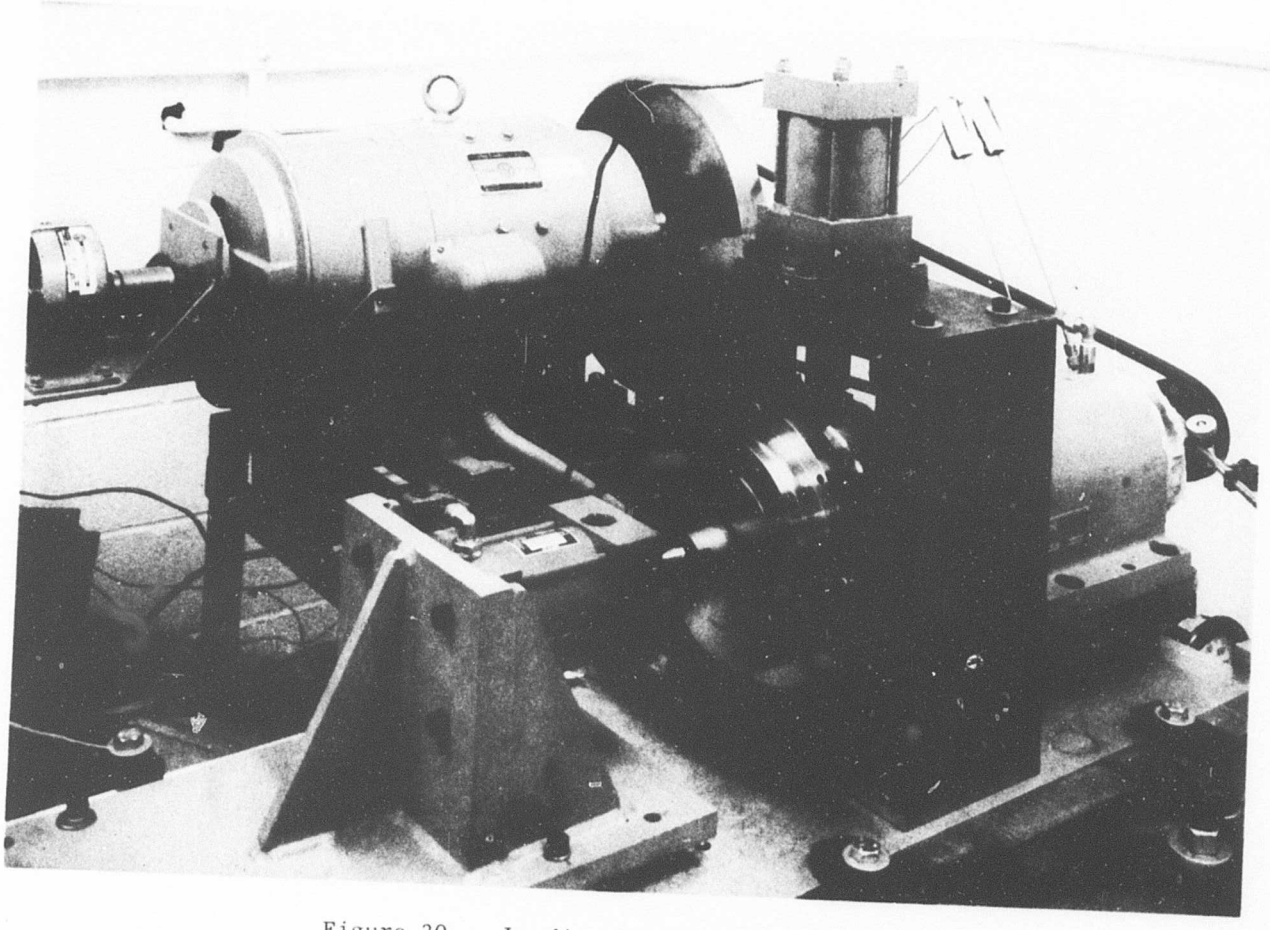

Figure 30. Loading Apparatus for Test Rig.

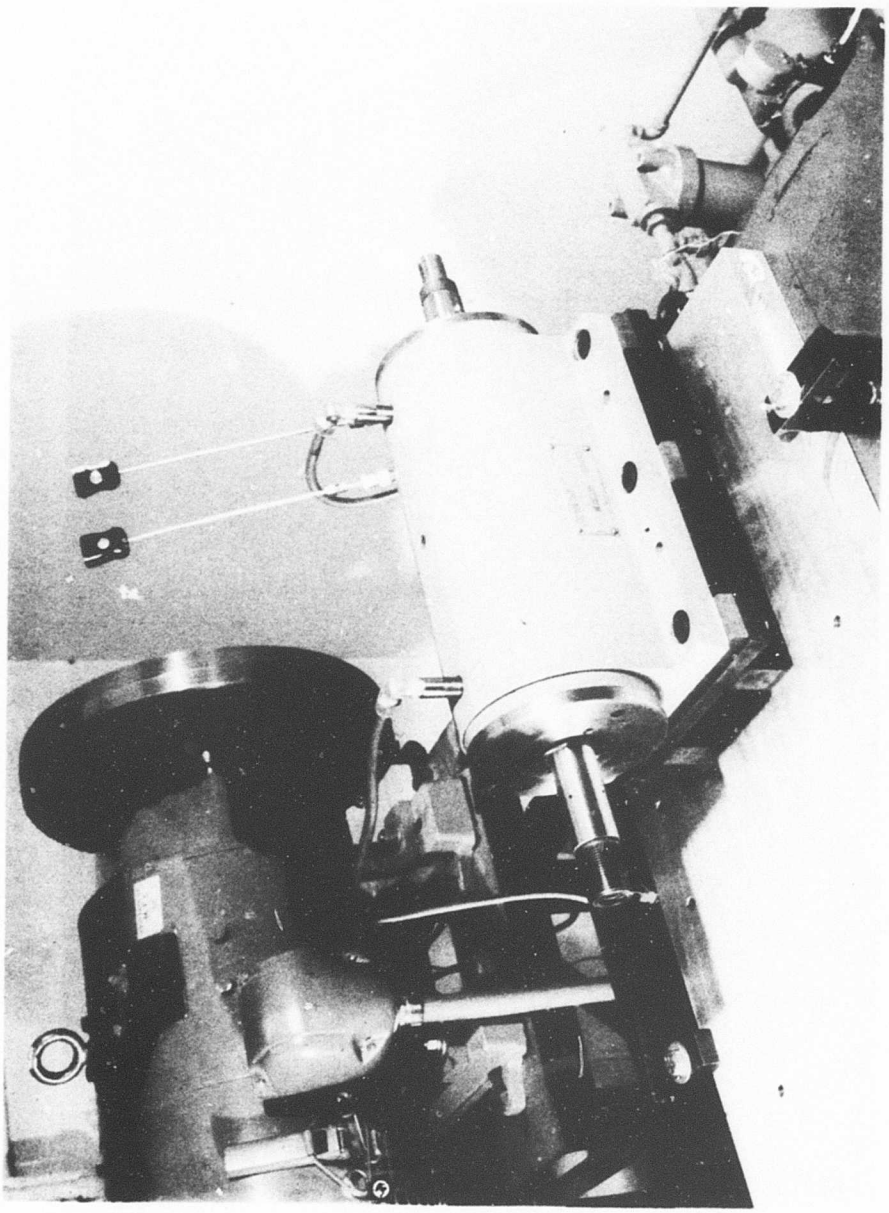

Figure 31. High-Speed Test Spindle.

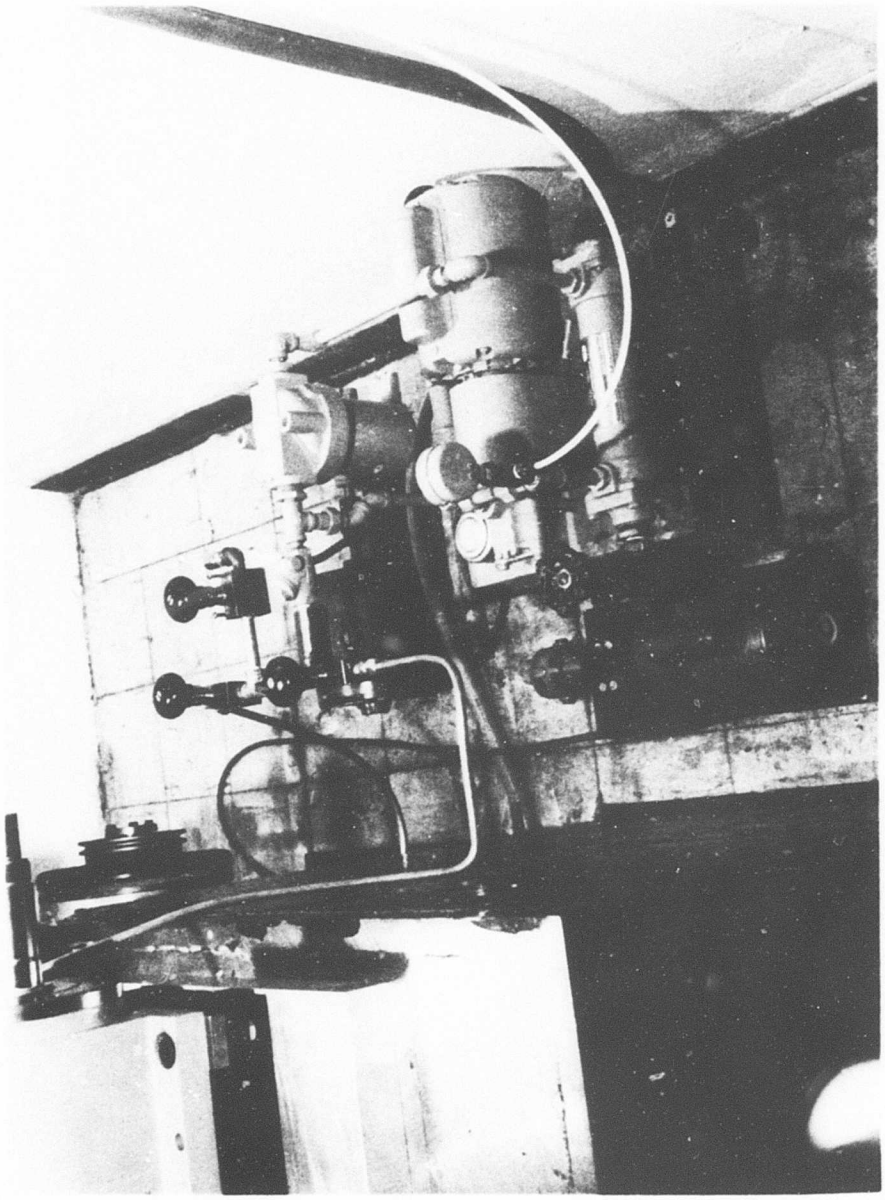

Figure 32. Lubrication System for Test Rig.

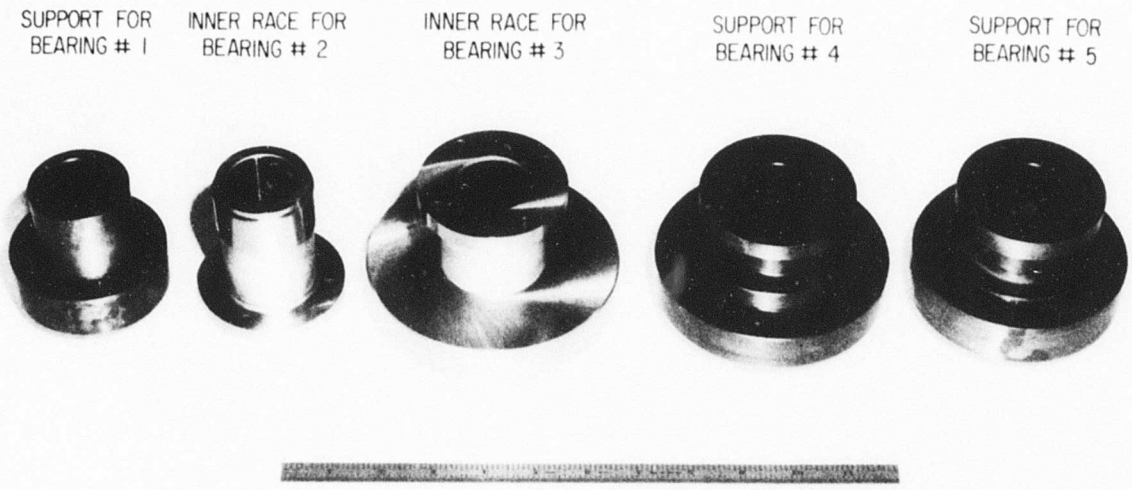

Figure 33. Inner Races or Inner Race Supports for Test Bearings.

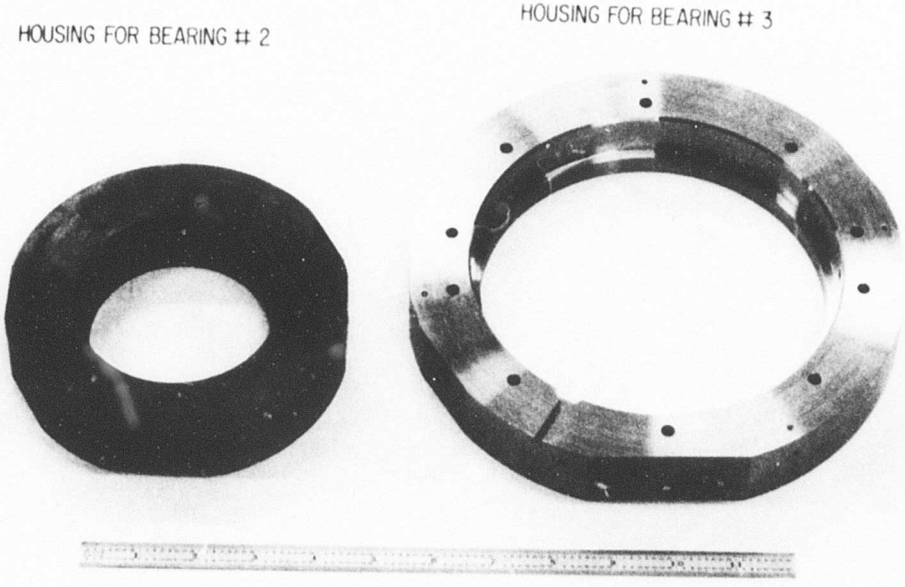

Figure 34. Bearing Housings for Roller Bearings Tested.

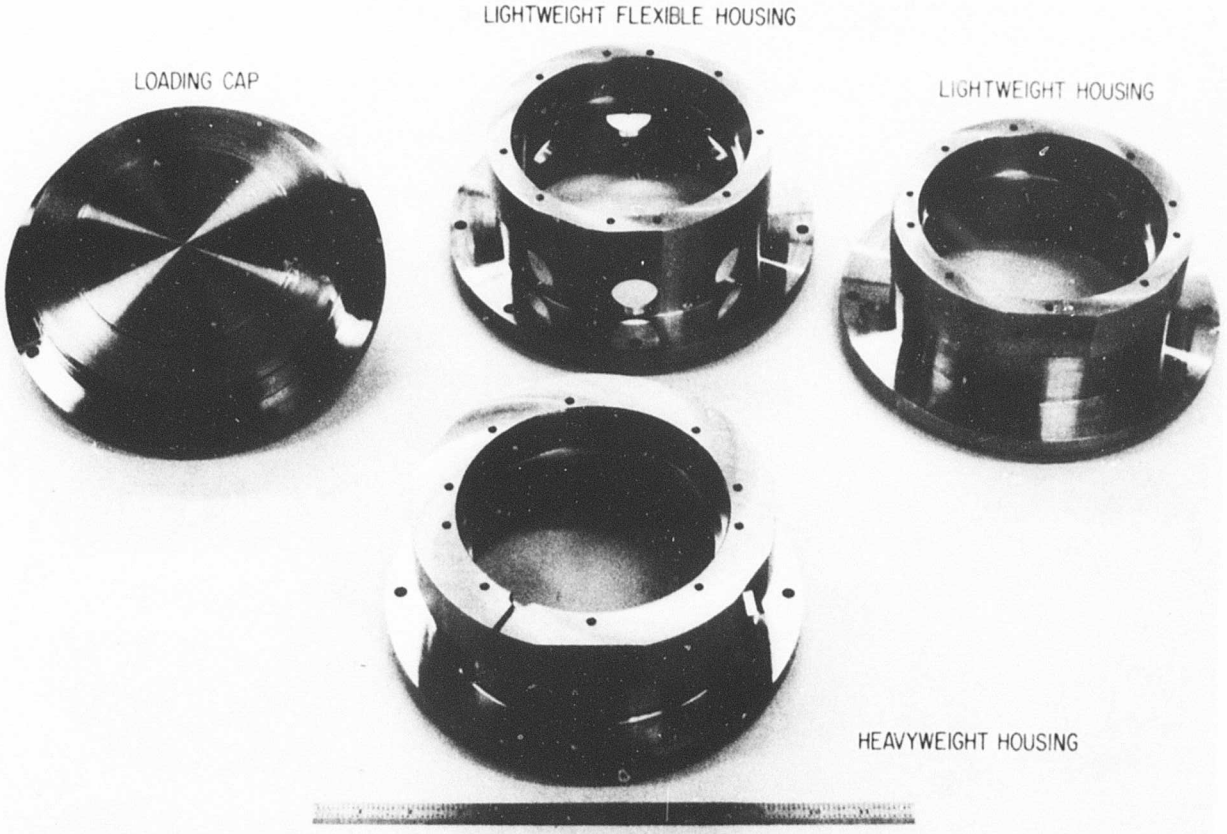

Figure 35. **Bearing** Housings for Bearing Number 1 and Loading Cap.

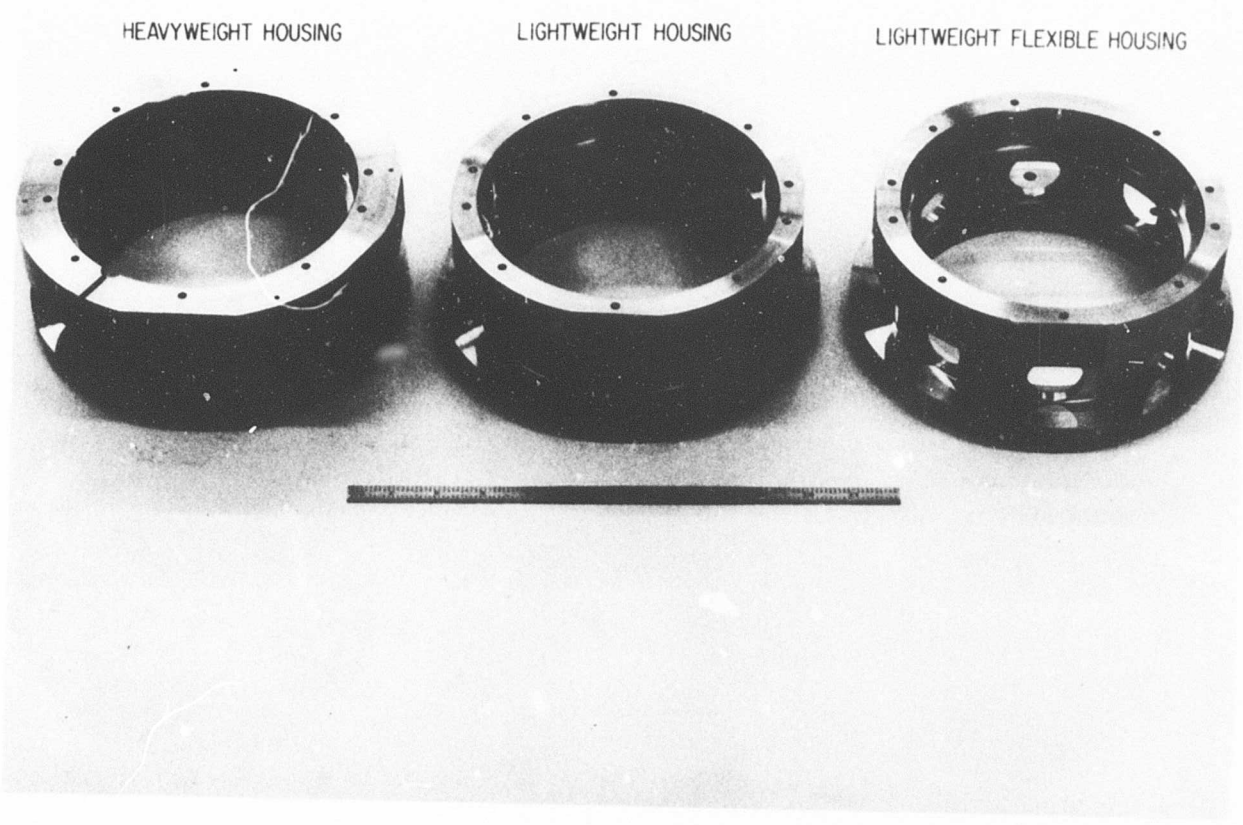

Figure 36. Bearing Housings for Bearings Numbers 4 and 5.

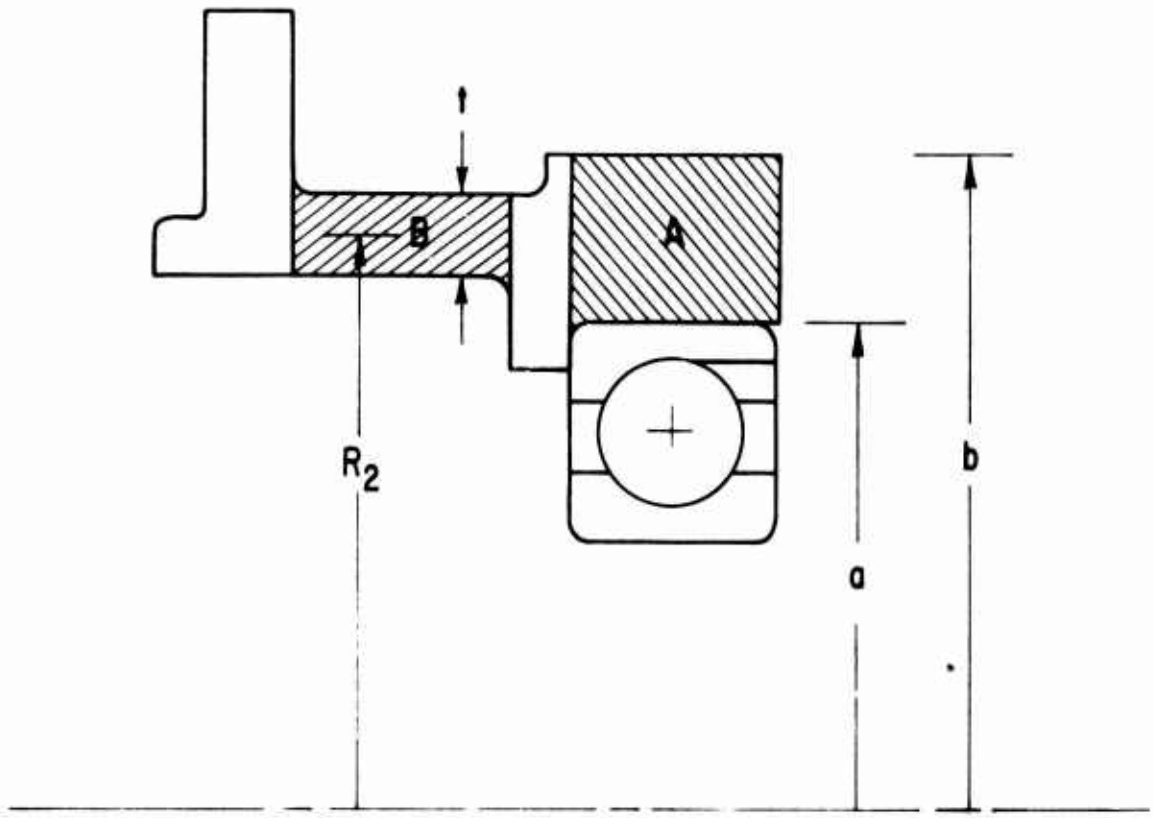

Figure 37. Foundation Stiffness Model for Bearing No. 1 Housing.

and proximity to the bearing, Section A contributes most of the foundation stiffness to the bearing. This was demonstrated by calculating the amount of foundation stiffness that Section B contributes to the bearing. This was calculated from equation (4) for the deflection of a thin-walled vessel due to a uniform radial shear:*

$$\Delta R_2 = \frac{V_o}{2D\lambda^3}, \text{ where } D = \frac{Et^3}{12(1-\nu^2)} \text{ and } \lambda = 4\frac{3(1-\nu^2)}{R_2^2\, t^2} \qquad (4)$$

R_2 = radius of wall, in.

ΔR_2 = deflection of bearing housing, in.

V_o = shear, lb/in.

E = Young's Modulus, $lb/in.^2$

t = wall thickness, in.

ν = Poisson's ratio

Solving for $V_o/\Delta R_2$, the unit stiffness of the bearing housing, using the dimensions of Section B and dividing by the bearing width of 1.02 inches, gave an addition to the foundation stiffness of 4.4×10^5 pounds per cubic inch. This is an order of magnitude lower than the stiffness of Section A.

The foundation stiffnesses for the other bearings, due only to Section A of the heavyweight bearing housings, were found in a manner similar to that demonstrated above. The results for all five bearings are given in Table XVI.

A similar procedure was carried out for the lightweight design of the bearing housings. For bearing No. 1, Section A contributed 2.09×10^6 pounds per cubic inch to the foundation stiffness, while Section B contributed 2×10^5 pounds per cubic inch. Section A of the lightweight flexible housing for bearing No. 1 also contributed 2.09×10^6 pounds per cubic inch to the foundation stiffness, but Section B of this housing contributed less than 2×10^5 pounds per cubic inch since it had a number of holes machined into it. The foundation stiffnesses due to Section A of the lightweight and lightweight flexible bearing housings for all of the bearings are given in Table XVII. There was no lightweight design for the bearing housings of bearings No. 2 and No. 3.

Regardless of whether the heavyweight or lightweight bearing housings are used, the bearing foundation stiffnesses are of the order of a million pounds per cubic inch. The analytical results presented previously showed that this is well within the region where there can be significant increases in the frequencies of several bearing race resonances.

* Raymond J. Roarke, Formulas for Stress and Strain, McGraw Hill, New York, 1938.

TABLE XVI. FOUNDATION STIFFNESSES FOR THE TEST RIG HEAVYWEIGHT BEARING HOUSINGS

Bearing No.	Foundation Stiffness Due to Section A ($lb/in.^3$)
1	3.0×10^6
2	7.2×10^6
3	2.5×10^6
4	2.1×10^6
5	2.1×10^6

TABLE XVII. FOUNDATION STIFFNESSES FOR THE TEST RIG LIGHTWEIGHT OR LIGHTWEIGHT FLEXIBLE BEARING HOUSINGS

Bearing No.	Foundation Stiffness Due to Section A ($lb/in.^3$)
1	2.1×10^6
2	no lightweight design
3	no lightweight design
4	1.5×10^6
5	1.5×10^6

TEST RIG INSTRUMENTATION SYSTEM AND OPERATION

The instrumentation system for the test rig is shown schematically in Figure 38.

The operation of the test rig and instrumentation were as follows: The bearing to be tested was chosen, and the necessary hardware assembled. The vari-speed drive and the loading hardware were adjusted for a chosen speed and load condition. The speed was checked with a Fotonic sensor and a frequency counter. The accelerometer locations were chosen and the amplified accelerometer signals were recorded using a multichannel magnetic tape recorder. This raw signal was then analyzed for frequency content using a real-time frequency spectrum analyzer. A peak to be envelope detected was chosen from the resulting frequency spectrum. The raw signal was then sent to the envelope detector which was set to envelope detect the previously chosen peak. A schematic diagram of the envelope detector is presented in Figure 39. In the envelope detector, the raw signal was first sent to a high-frequency bandpass filter to separate the high-frequency peak of interest from the rest of the raw signal. The bandwidth of this filter was $\pm$5% of the center frequency. The output of the bandpass filter was input to a half-wave rectifier and demodulator in order to remove the negative half of the signal and to separate the modulation envelope from the high-frequency signal. The output of the envelope detector was analyzed for frequency content using the real-time spectrum analyzer. The resulting frequency spectrum was examined for ball-pass frequencies. The analysis described above could be performed on either the live signal or the recorded signal.

Spindle Data

Before any of the test bearings were mounted, the test spindle was run by itself with accelerometers mounted directly on the outside of the spindle housing. The accelerometers were mounted in horizontal and vertical positions in the vicinity of each of the spindle bearing pairs. The purpose of collecting this data was to facilitate the identification of any spindle-bearing-caused background noise which might have been present in the test bearing data. The spindle was run at three different speeds during these tests, as shown in Table XVIII. The frequency spectrums obtained from some of the spindle bearing data are presented in Figure 40.

It was found that the amplitudes of the spindle data were much lower than those of the test bearing data. In addition, the spindle bearing signals would have been even more diminished by the time they reached the test bearing housings. Therefore, it could be safely assumed that the spindle bearings created a negligible contribution to the signals detected on the test bearing housings.

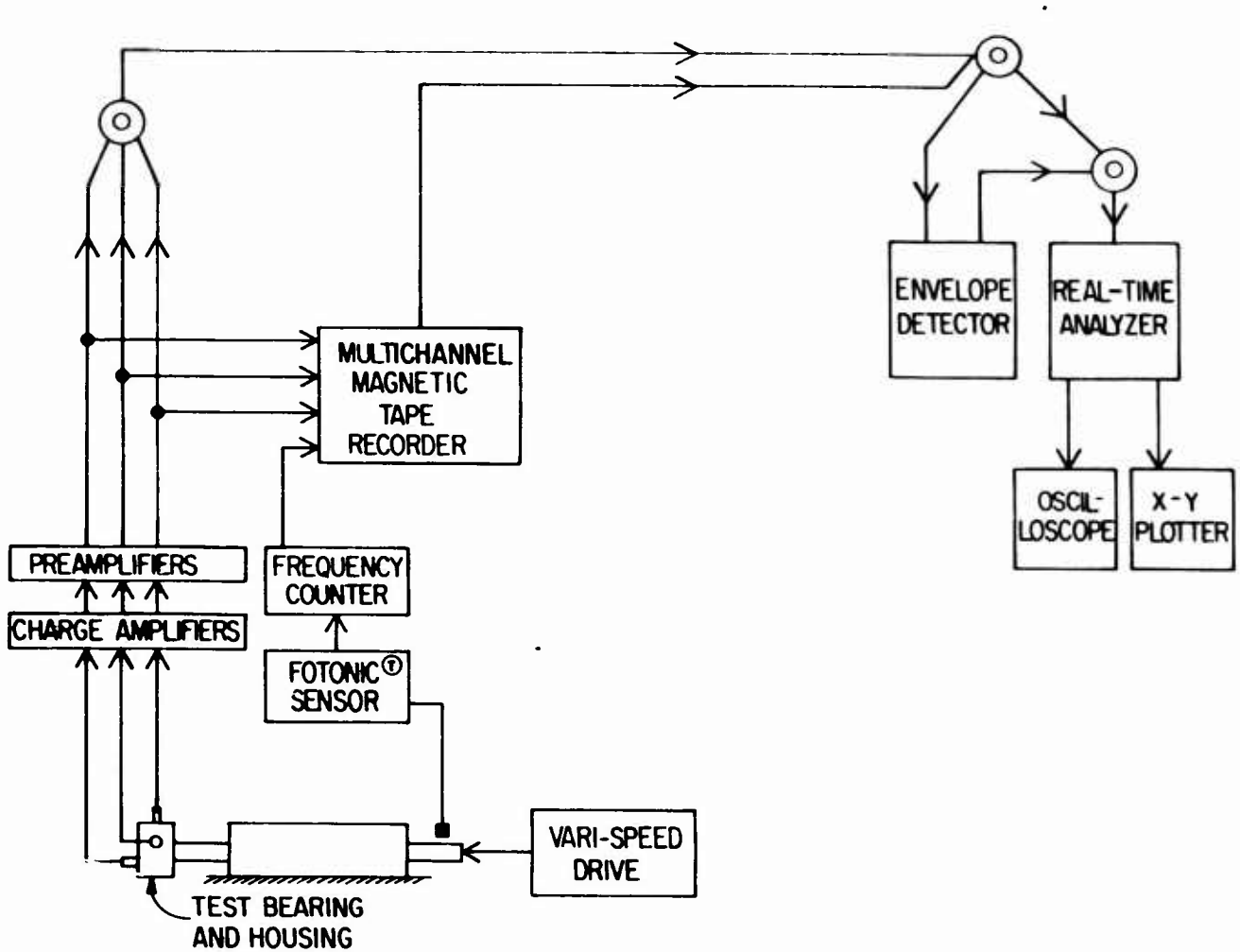

Figure 38. Schematic Diagram of Test Rig Instrumentation System.

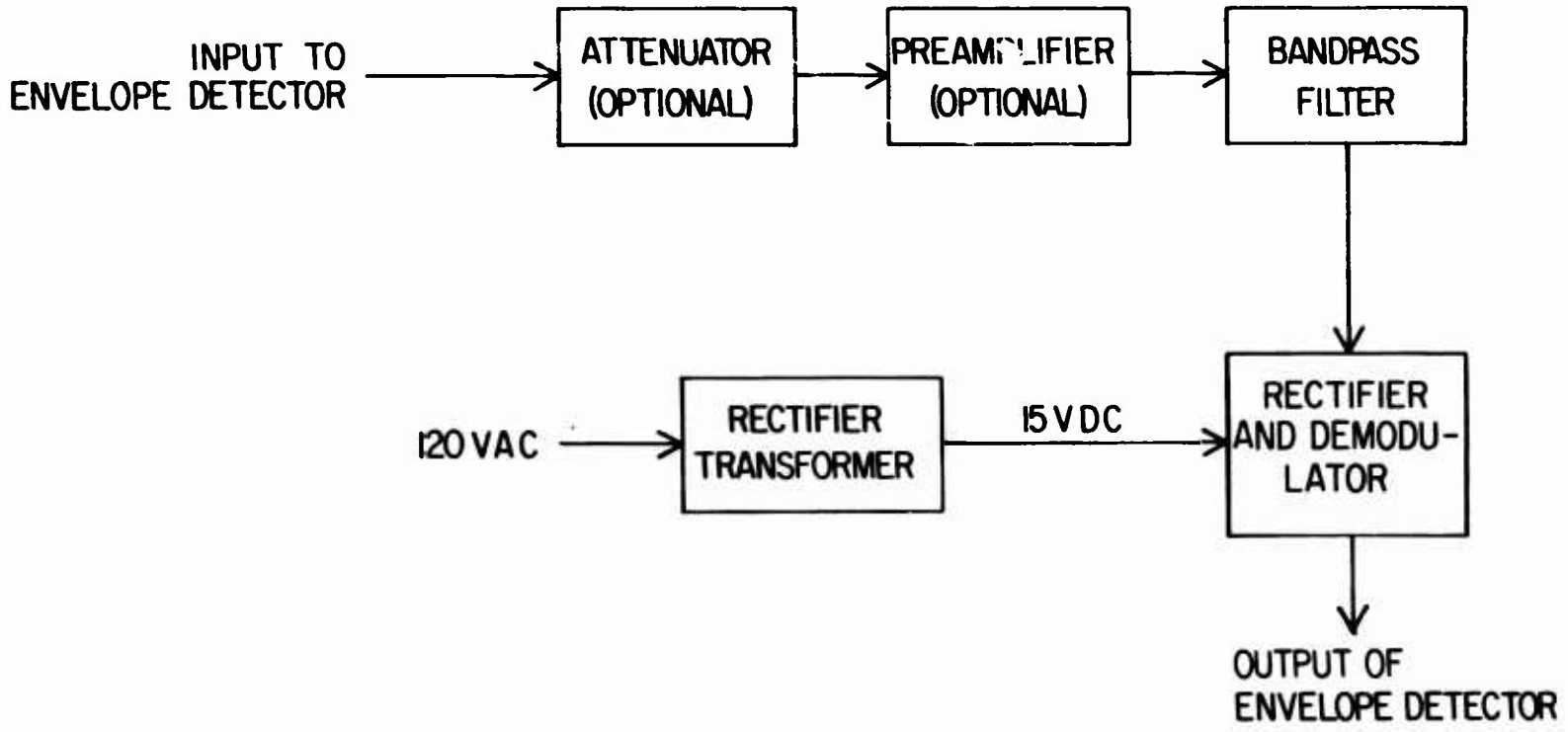
INPUT TO
ENVELOPE DETECTOR
ATTENUATOR
(OPTIONAL)
PREAMPLIFIER
(OPTIONAL)
BANDPASS
FILTER
120 VAC
RECTIFIER
TRANSFORMER
15 VDC
RECTIFIER
AND DEMODU-
LATOR
OUTPUT OF
ENVELOPE DETECTOR

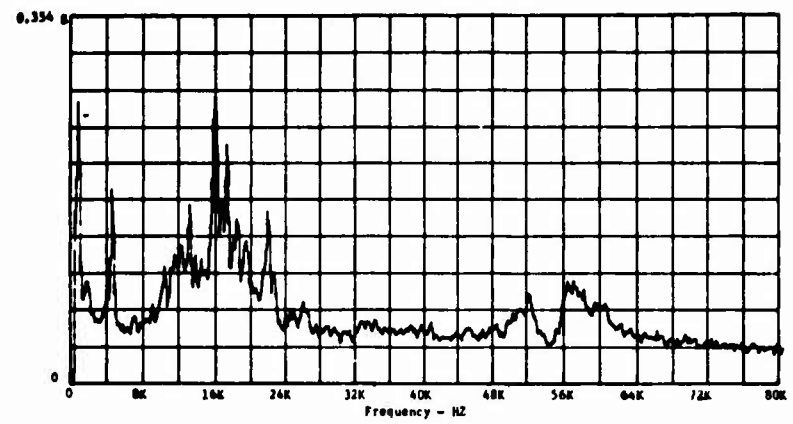

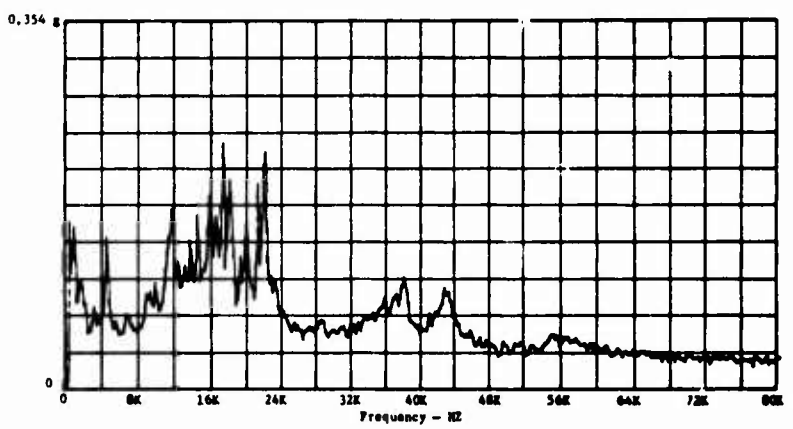

Figure 40. Spindle Background Data.

TABLE XVIII. DATA SUMMARY FOR SPINDLE BACKGROUND TESTS

Record	Speed (rpm)
1	6600
2	3050
3	324

Accelerometer Locations

Before the general testing procedure could begin, it was necessary to conduct an investigation of accelerometer locations. This investigation was conducted with bearing No. 2 mounted on the test rig. Data was taken and analyzed from a number of accelerometer locations in order to find the optimum locations both for getting good data and also for testing the effect of material interfaces. The accelerometer locations tested and chosen are shown in Figure 41. Of the accelerometer locations chosen, the one in the axial direction was designated accelerometer No. 1. Those located in the radial direction were designated accelerometers No. 2 and 3 with accelerometer No. 3 being the one located nearer the top of the bearing housing, as shown in Figure 41. The accelerometers had the same locations and designations for all of the bearings tested. For the ball bearings, the axially-mounted accelerometer was mounted on the loading cap in the same radial location as shown in Figure 41. For this investigation, the test rig was run at 6600 rpm with no load on bearing No. 2. The frequency spectrums obtained from the accelerometer location data are given in Figures 42 through 50.

Bearing Operating Loads and Frequencies

The maximum operating loads for the bearings are given in Table XIX, as obtained from Bell Helicopter Company. Table XX presents the rotational speeds of the five (5) bearings for various transmission input shaft speeds. These speeds are used as guides for the bearing tests. Table XXI gives the ball-pass frequencies for the five (5) bearings, for inner race, outer race, and ball defects for the input shaft speeds listed in Table XX.

BEARING TESTS

The test descriptions, results and analyses for the various bearings tested are presented in the same order as the tests were conducted.

Bearing No. 2

Bearing No. 2 was run with various speed and radial load combinations to determine the effect that these factors would have on the test data produced.

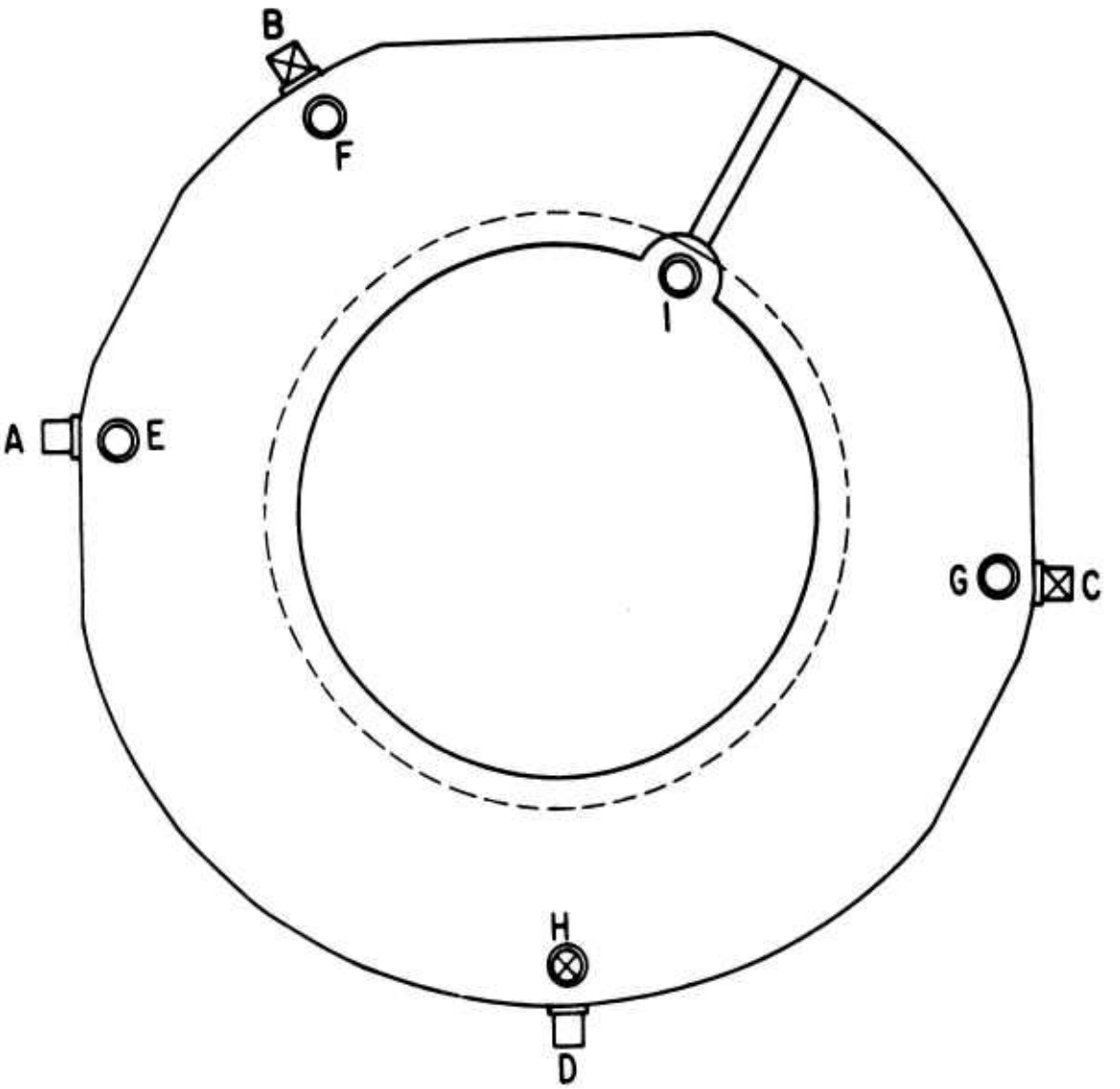

□, ○ - RADIAL OR AXIAL ACCELEROMETER LOCATION, RESPECTIVELY.

⊠, ⊗ - CHOSEN ACCELEROMETER LOCATION.

Figure 41. Accelerometer Locations on Bearing No. 2 Housing. (Refer to Figure 34)

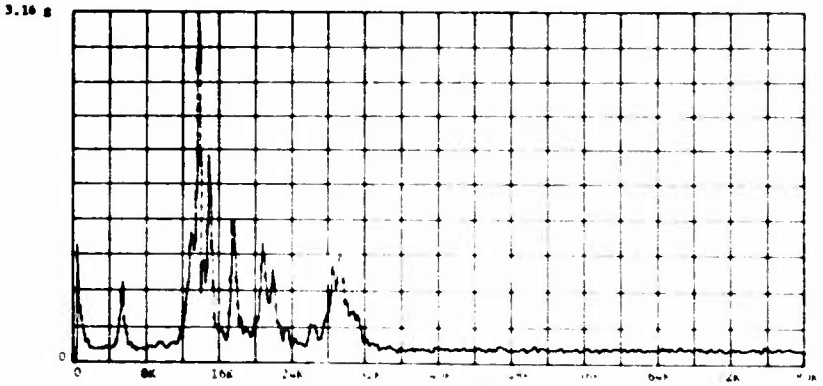

Figure 42. Accelerometer Test Location A.

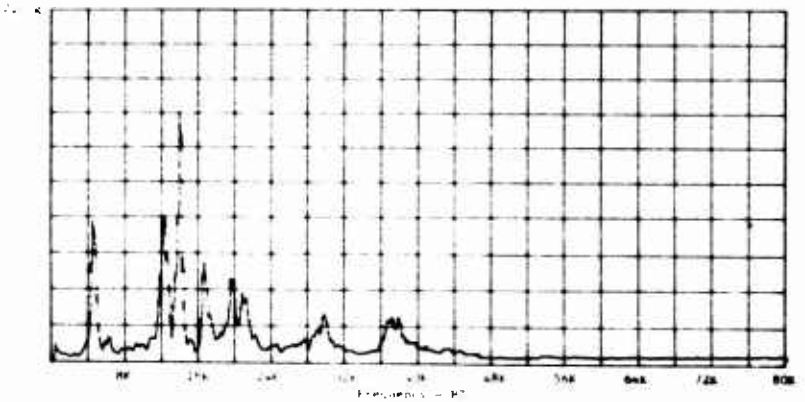

Figure 43. Accelerometer Test Location B.

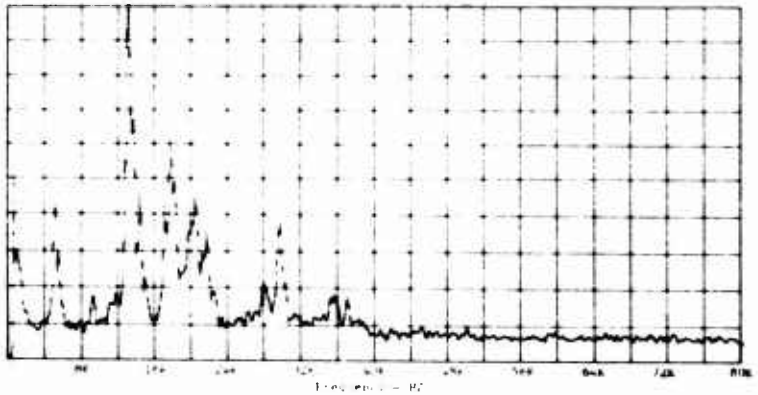

Figure 44. Accelerometer Test Location C.

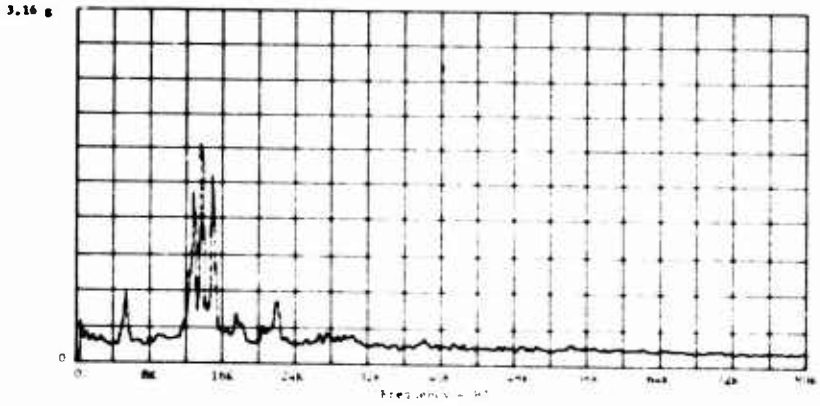

Figure 45. Accelerometer Test Location D.

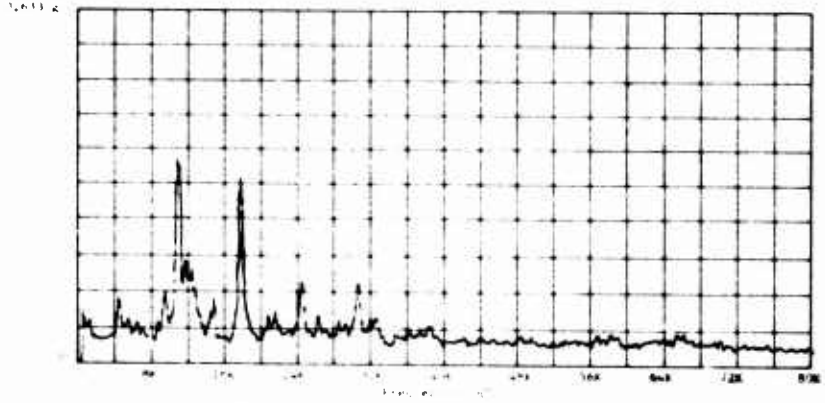

Figure 46. Accelerometer Test Location E.

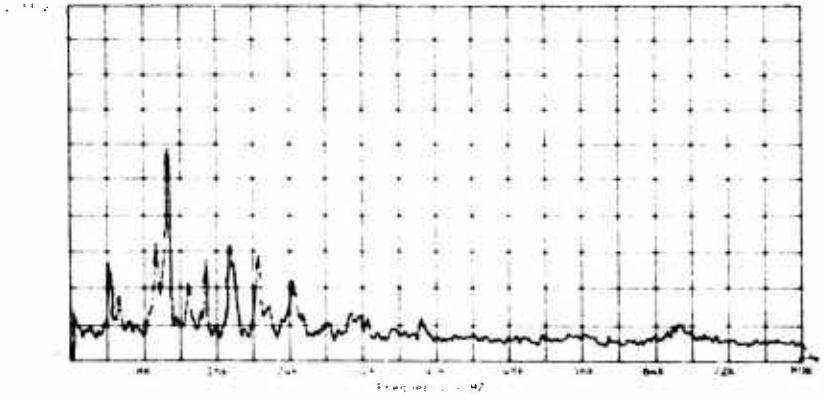

Figure 47. Accelerometer Test Location F.

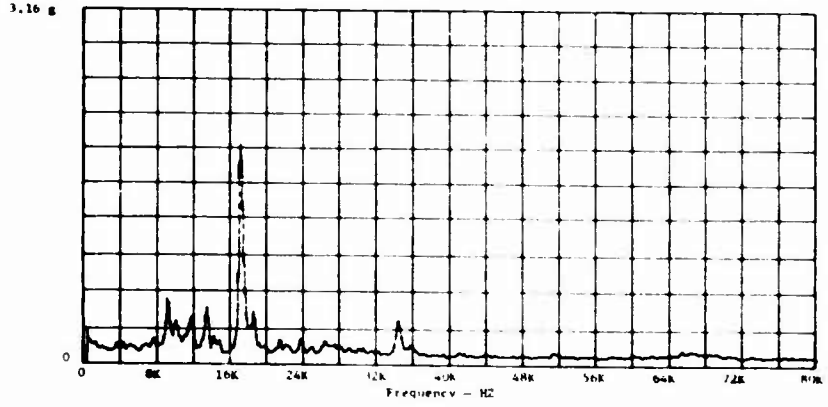

Figure 48. Accelerometer Test Location G.

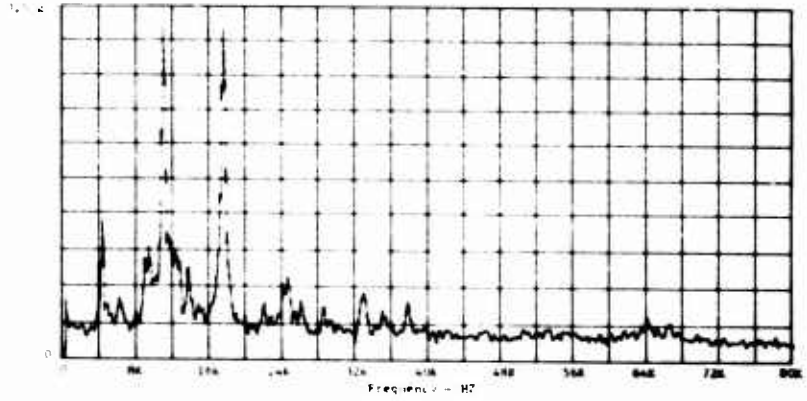

Figure 49. Accelerometer Test Location H.

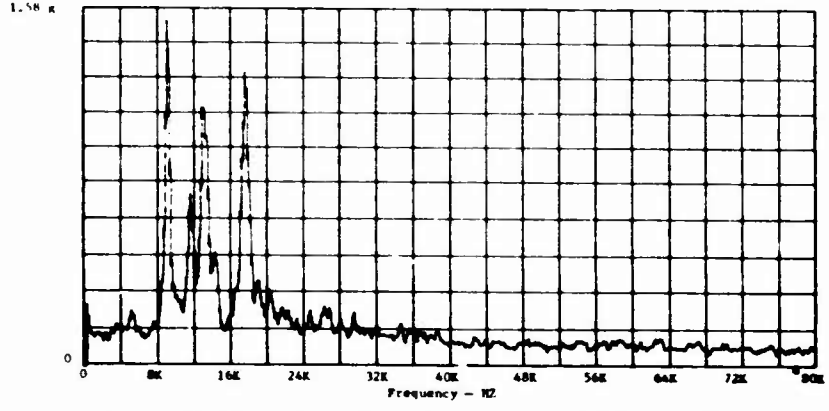

Figure 50. Accelerometer Test Location I.

TABLE XIX. MAXIMUM ACTUAL OPERATING LOADS FOR THE TEST BEARINGS

Bearing No.	Radial Load (lb)	Thrust Load (lb)
1	135	169
1	198	192
1	2860	4632
2	3633	0
3	1588	0
4	2134	1303
4	2668	1856
5	2000	10,000

TABLE XX. BEARING ROTATIONAL SPEEDS (rpm)

Transmission Input Shaft	Bearing No. 1	Bearing No. 2	Bearing No. 3	Bearing No. 4	Bearing No. 5
4000	4000	4000	1850	1850	196
4400	4400	4400	2040	2040	216
6000	6000	6000	2780	2780	294
6600	6600	6600	3050	3050	324

TABLE XXI. TEST BEARING BALL-PASS FREQUENCIES (Hz)

	Bearing No.	Input Shaft Speed (rpm)			
		4000	4400	6000	6600
	1 e	418	460	627	690
	i	582	640	873	960
	n	360	396	540	594
	2 e	314	345	471	518
	i	486	535	729	802
	n	295	325	443	487
	3 e	457	503	686	755
	i	540	596	811	892
	n	369	406	554	609
	4 e	367	404	551	606
	i	443	488	666	732
	n	297	327	446	491
Design 1	5 e	29	32	43	48
	i	37	40	55	60
	n	25	28	37	41
Design 2	5 e	31	34	47	51
	i	37	41	56	62
	n	26	29	39	43
Design 3	5 e	31	33	46	50
	i	38	42	57	63
	n	26	29	39	43
Design 4	5 e	28	31	42	47
	i	37	41	56	61
	n	23	26	35	39

e = outer race defect
i = inner race defect
n = ball defect

It was not possible to load bearing No. 2 in the axial direction since it is a roller bearing. Table XXII summarizes the tests conducted on bearing No. 2.

TABLE XXII. DATA SUMMARY FOR TESTS OF BEARING NO. 2

Record	Speed (rpm)	Radial Load (lb)	Bearing Condition
1	4000	0	Undamaged
2	4400	0	Undamaged
3	6000	0	Undamaged
4	6600	0	Undamaged
5	6600	726	Undamaged
6	4400	726	Undamaged
7	6600	1817	Undamaged
8	6600	3633	Undamaged
9	6600	0	Damaged Outer Race
10	6600	3633	Damaged Outer Race

It should be noted that for all the bearing test data, channel 2 corresponded to accelerometer No. 1, channel 4 to accelerometer No. 2, and channel 6 to accelerometer No. 3. The frequency spectrums obtained from some of the data taken for the speed and load variations of the undamaged bearing No. 2 are shown in Figures 51 and 52. They show that although variations in speed and load affected the relative magnitudes of the frequency peaks, they did not affect the locations of those peaks.

The results of these tests show that for bearing No. 2, speed had virtually no effect on the locations or relative magnitudes of the frequency peaks found in the frequency spectrums of the signals generated. Since bearings No. 2 and No. 3 are both roller bearings, that conclusion can be safely extended to cover both bearings.

Bearing No. 2 was then removed from the test spindle and replaced with another bearing No. 2 sample onto whose outer race a defect had been introduced. This defect was a score, shown in Figure 53, which was chemically etched into the race in order to simulate a bearing spall. Chemical etching was chosen for scoring the race, as opposed to using some mechanical method such as vibro-engraving, because chemical etching would not create raised ridges around the defect, and would thereby better simulate a spall. This artifically damaged bearing was run in the test rig at no load and at full radial load (3633 pounds) at full speed (6600 rpm).

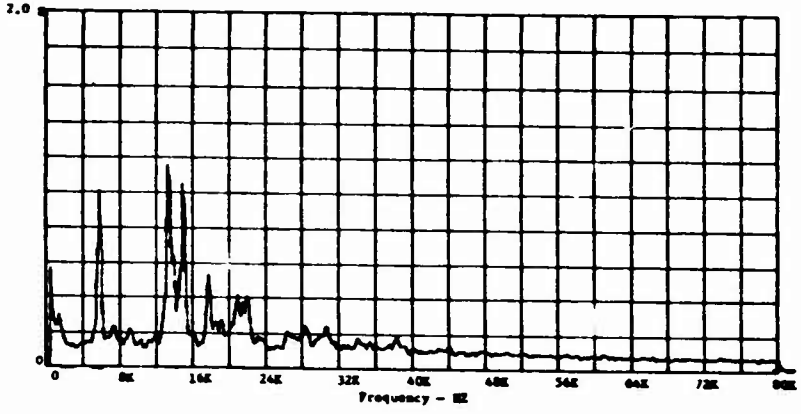

a) No Load

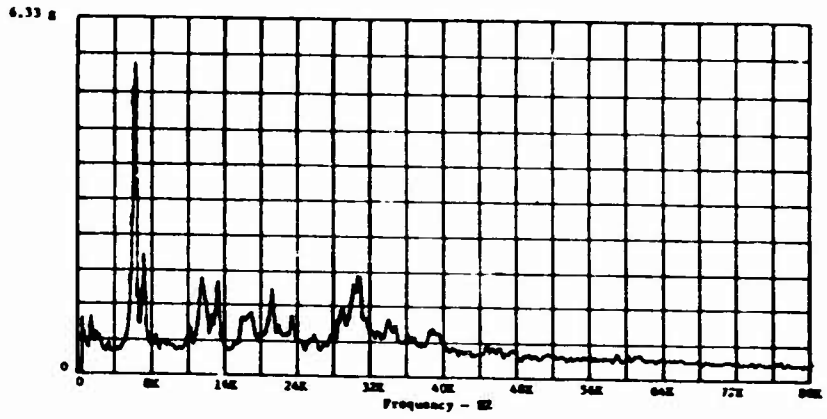

b) 726-Lb Radial Load

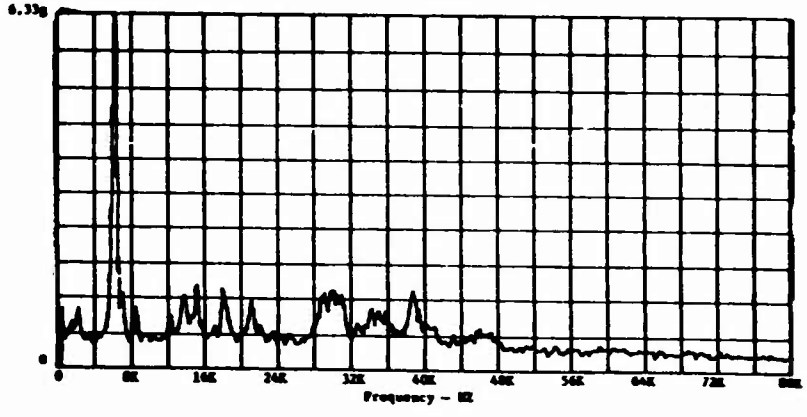

c) 3633-Lb Radial Load

Figure 51. Bearing No. 2, Undamaged, 6600 RPM, Accelerometer No. 3.

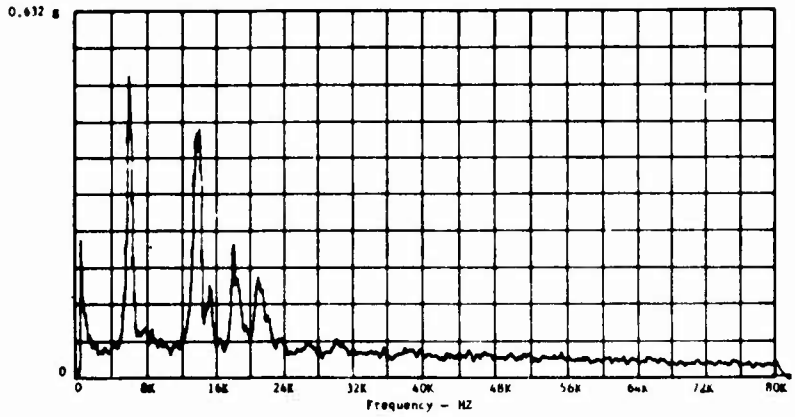

a) 4000 RPM, No Load

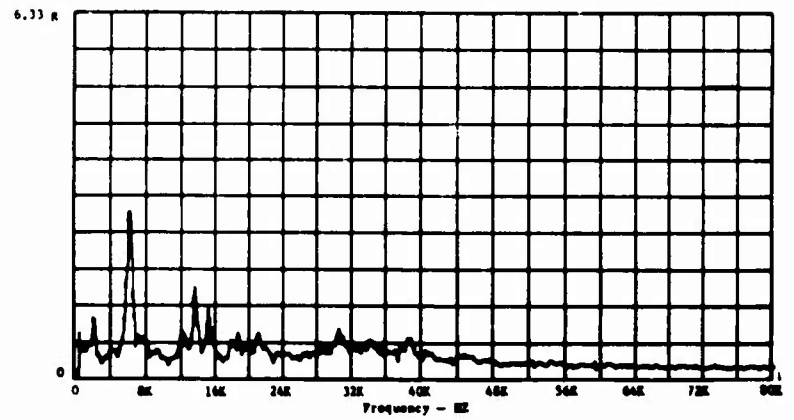

b) 4400 RPM, 726-Lb Radial Load

Figure 52. Bearing No. 2, Undamaged, Accelerometer No. 3.

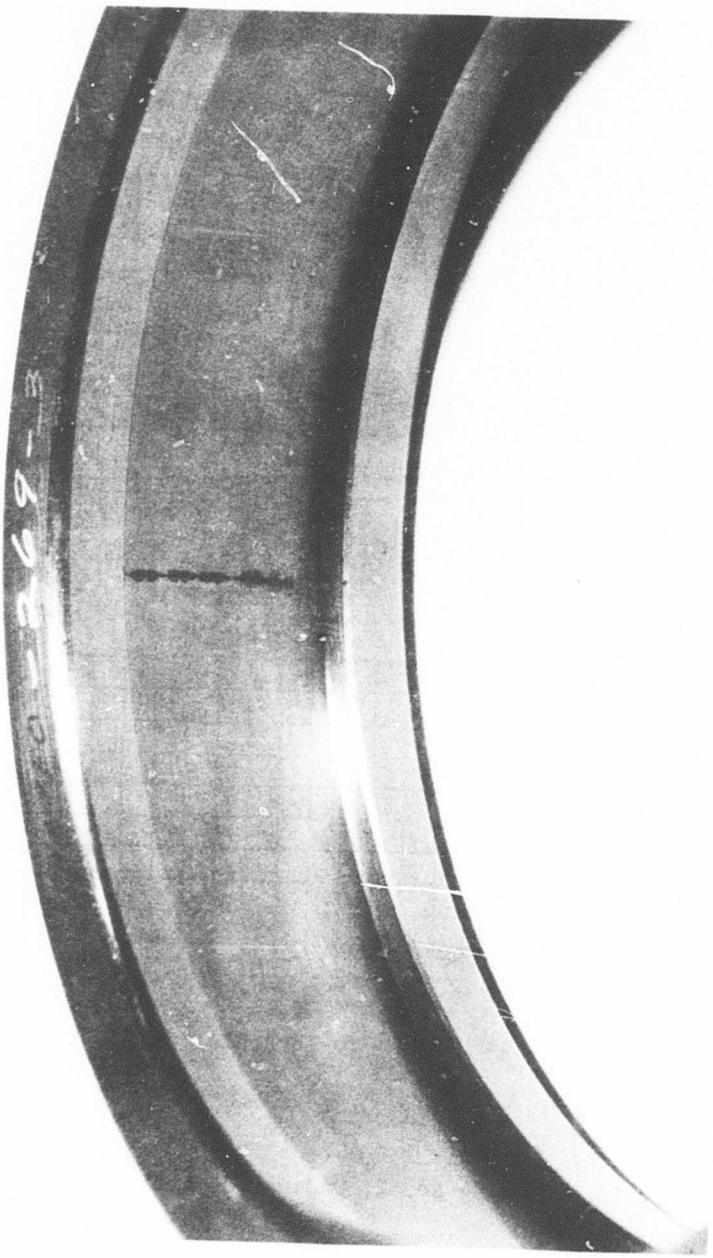

Figure 53. Outer Race Score for Bearing No. 2.

The raw data frequency spectrums for some of the runs are given in Figure 54.

Bearing No. 3

Based on the conclusions mentioned above, it was decided to test this bearing under the full-load (1588 pounds) and full-speed (3050 rpm) conditions only. The same is true for the artificially damaged bearing No. 3, whose defect is shown in Figure 55. The frequency spectrums obtained from some of the raw data for these two bearings are given in Figure 56. Table XXIII summarizes the tests conducted on bearing No. 3.

TABLE XXIII. DATA SUMMARY FOR TESTS OF BEARING NO. 3

Record	Speed (rpm)	Radial Load (lb)	Bearing Condition
1	3050	1588	Undamaged
2	3050	1588	Damaged Outer Race

Bearing No. 1

The first ball bearing to be tested was bearing No. 1. This bearing was run for various speed, radial load and thrust load combinations in order to determine the effect that these factors would have on the test data produced. The speed was varied from 4000 to 6600 rpm, the radial load was varied from zero to 2860 pounds, and the thrust load was varied from zero to 4632 pounds, as shown in Table XXIV. The frequency spectrums obtained from some of the data taken for the speed and load variations of bearing No. 1, given in Figures 57 through 62, show that frequency peak locations for bearing No. 1 were no more affected by speed and load variations than were those generated by bearing No. 2. Therefore, the speed and load independence conclusions stated as concerning roller bearings can also be assumed to be true concerning ball bearings. The speed and load variations for bearing No. 1 were run for both the good bearing and the bearing with the artificially damaged outer race, whose defect is shown in Figure 63. For both cases the heavyweight bearing housing was used. The bearing with the artificially damaged outer race was also run with lightweight and lightweight flexible bearing housings at maximum speed (6600 rpm) and maximum load (2860 lb radial and 4632 lb thrust) only. The bearing with the artificially damaged inner race, whose defect is shown in Figure 64, was run with the heavyweight housing at maximum speed and maximum load only. The frequency spectrums for some of the data from these tests are given in Figures 65 and 66.

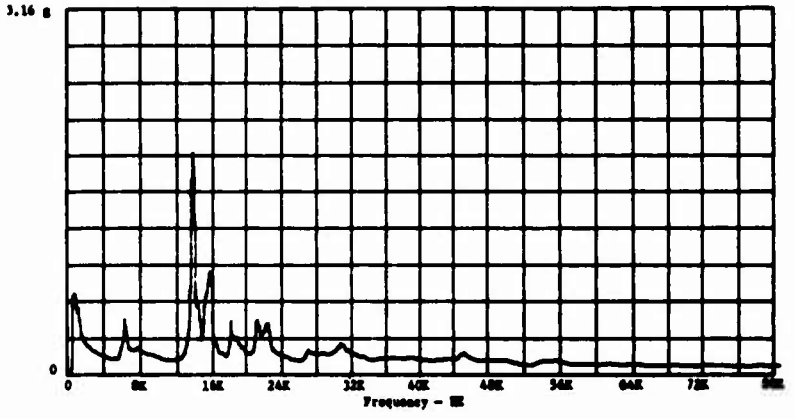

a) No Load

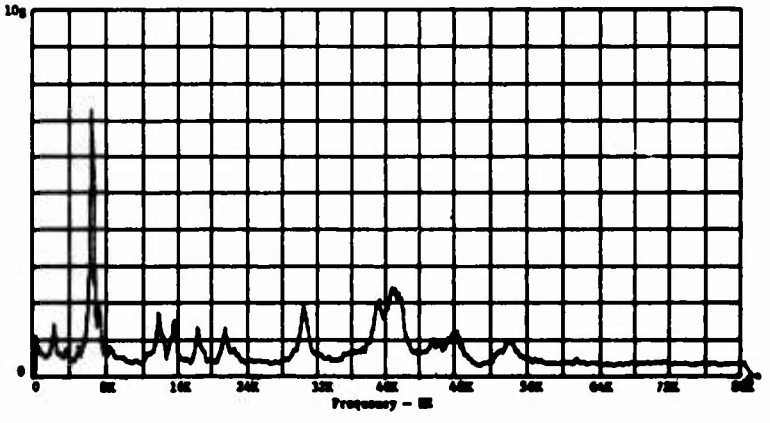

b) 3633-Lb Radial Load

Figure 54. Bearing No. 2, Damaged Outer Race, 6600 RPM, Accelerometer No. 3.

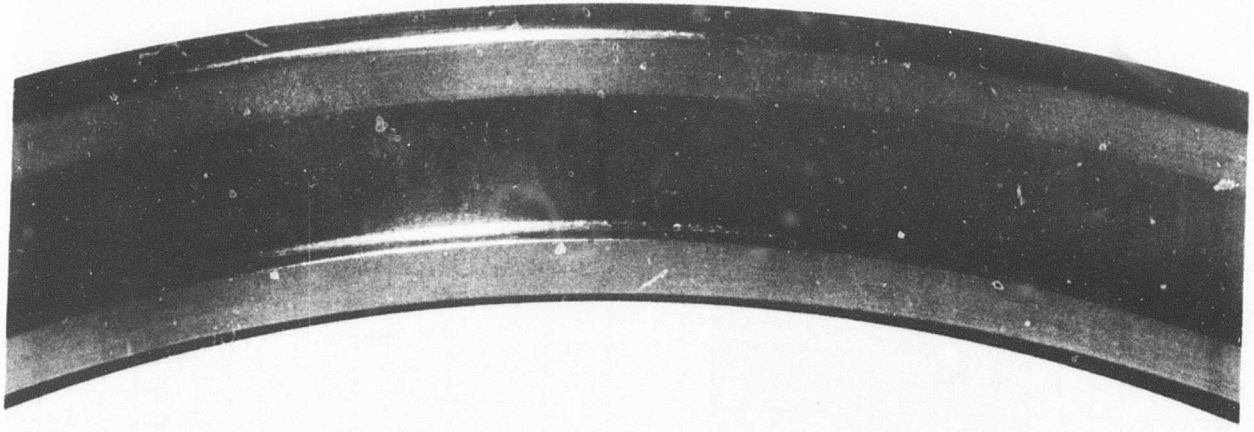

Figure 55. Outer Race Score for Bearing No. 3.

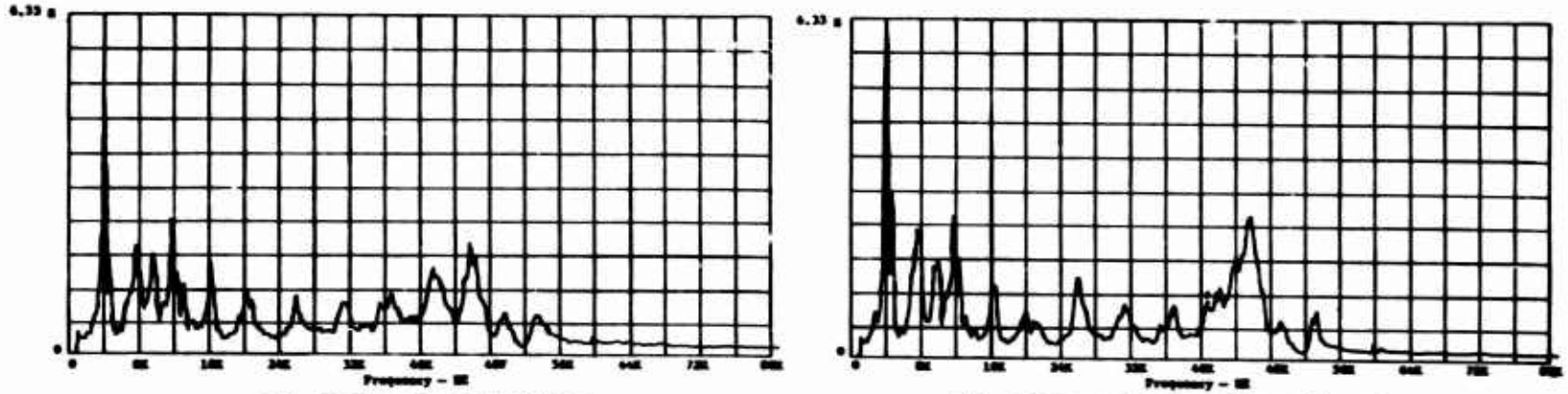

a) Undamaged Bearing

b) Damaged Outer Race Bearing

Figure 56. Bearing No. 3, 3050 RPM, 1588-Lb Radial Load, Accelerometer No. 3.

TABLE XXIV. DATA SUMMARY FOR TESTS OF BEARING NO. 1

Record	Speed (rpm)	Radial Load (lb)	Thrust Load (lb)	Bearing Condition	Bearing Housing
1	6600	0	0	Undamaged	Heavyweight
2	6600	0	4632	Undamaged	Heavyweight
3	6600	198	192	Undamaged	Heavyweight
4	4400	198	192	Undamaged	Heavyweight
5	6600	2860	0	Undamaged	Heavyweight
6	6600	2860	4632	Undamaged	Heavyweight
7	6000	2860	4632	Undamaged	Heavyweight
8	4400	2860	4632	Undamaged	Heavyweight
9	4000	2860	4632	Undamaged	Heavyweight
10	6600	2860	4632	Damaged Inner Race	Heavyweight
11	6600	0	0	Damaged Outer Race	Heavyweight
12	6600	0	4632	Damaged Outer Race	Heavyweight
13	6600	198	192	Damaged Outer Race	Heavyweight
14	4400	198	192	Damaged Outer Race	Heavyweight
15	6600	2860	0	Damaged Outer Race	Heavyweight
16	6600	2860	4632	Damaged Outer Race	Heavyweight
17	6000	2860	4632	Damaged Outer Race	Heavyweight
18	4400	2860	4632	Damaged Outer Race	Heavyweight
19	4000	2860	4632	Damaged Outer Race	Heavyweight
20	6600	2860	4632	Damaged Outer Race	Lightweight
21	6600	2860	4632	Damaged Outer Race	Lightweight Flexible

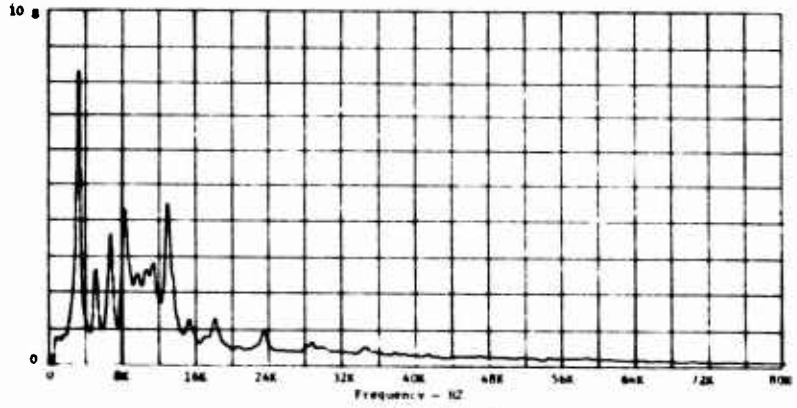

a) No Load

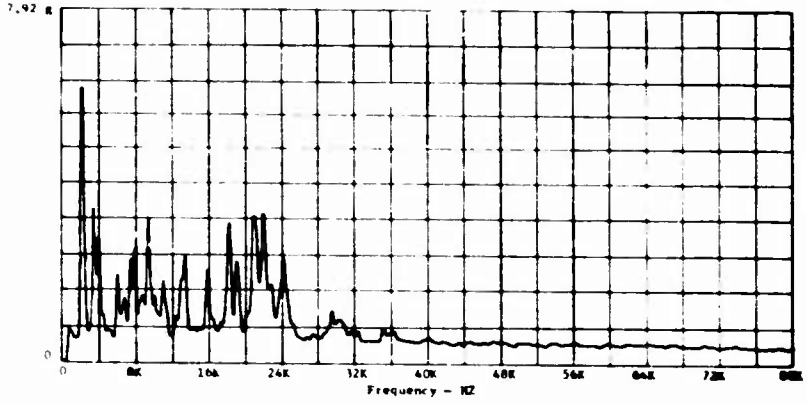

b) 4632-Lb Thrust Load Only

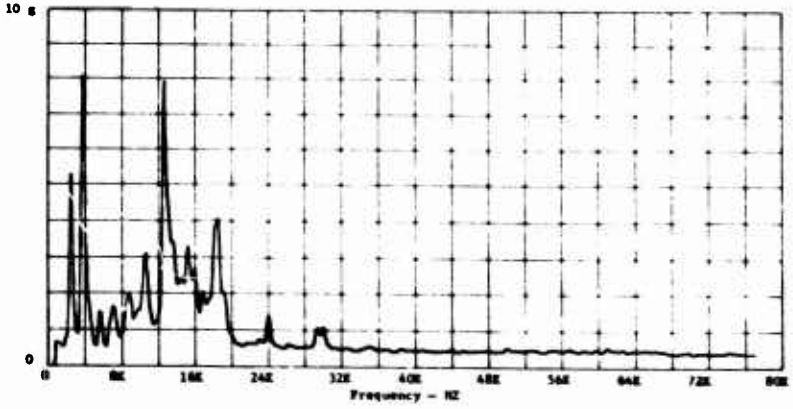

c) 198-Lb Radial Load, 192-Lb Thrust Load

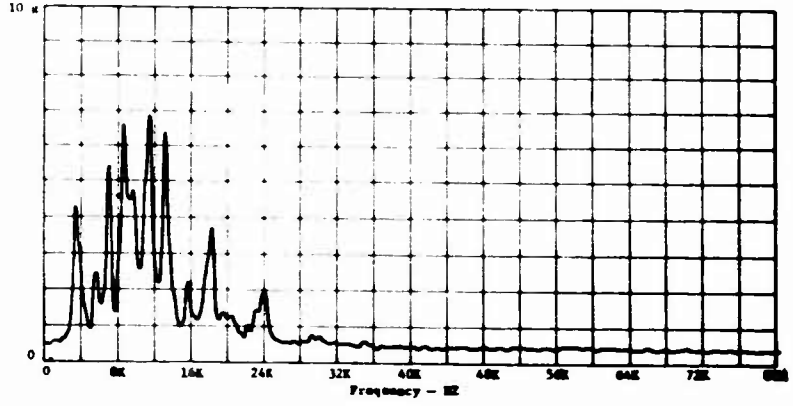

d) 2860-Lb Radial Load Only

Figure 57. Bearing No. 1, Undamaged, 6600 RPM, Accelerometer No. 3.

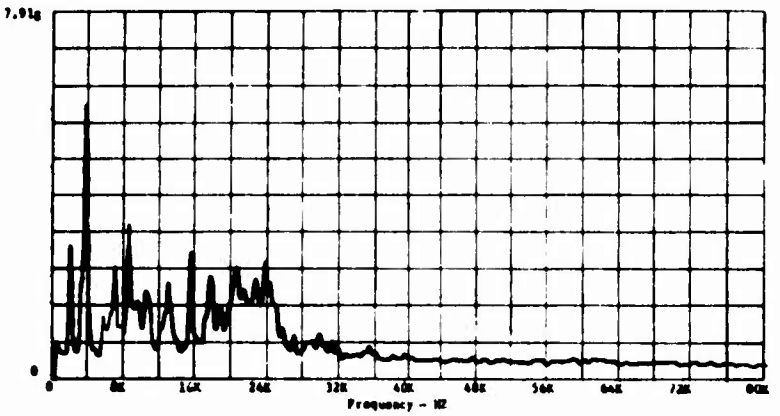

a) 6600 RPM

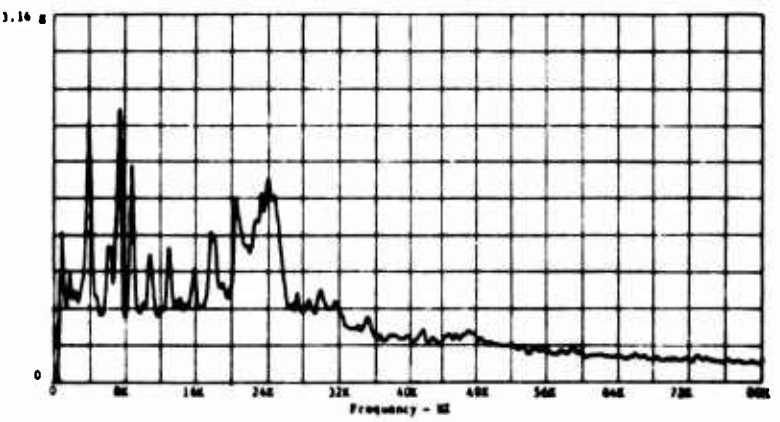

b) 4400 RPM

Figure 58. Bearing No. 1, Undamaged, 2860-Lb Radial Load, 4632-Lb Thrust Load, Accelerometer No. 3.

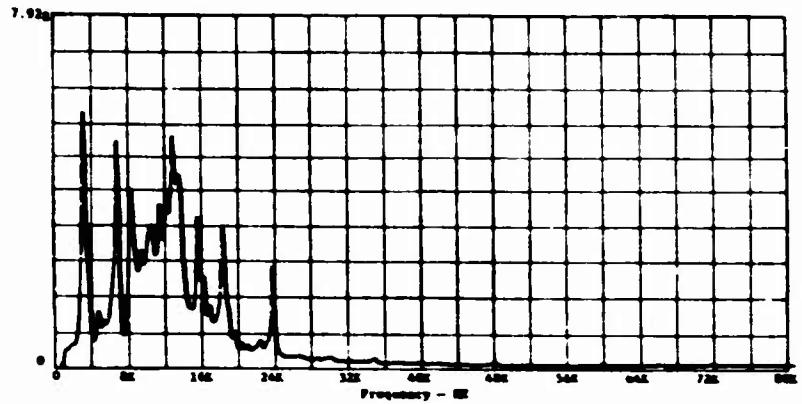

a) No Load

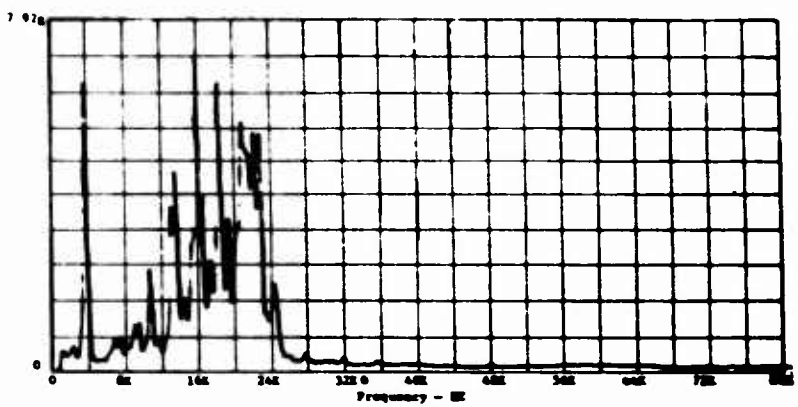

b) 4632-Lb Thrust Load Only

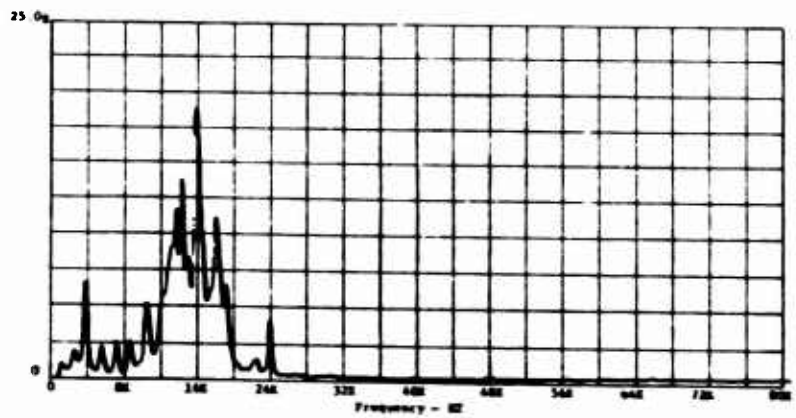

c) 198-Lb Radial Load, 192-Lb Thrust Load

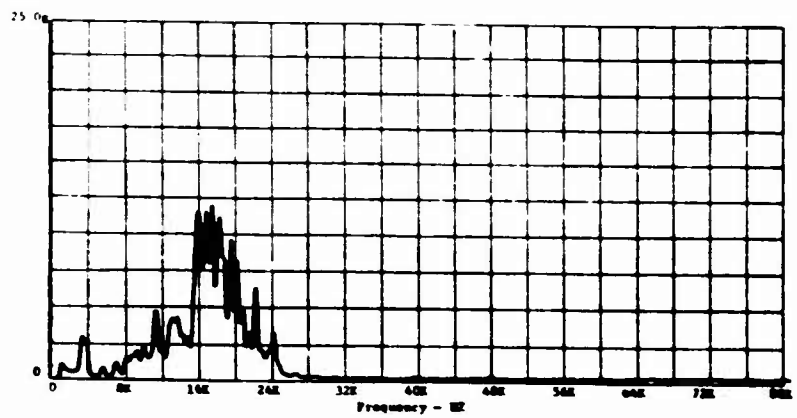

d) 2860-Lb Radial Load Only

Figure 59. Bearing No. 1, Damaged Outer Race, 6600 RPM, Accelerometer No. 3.

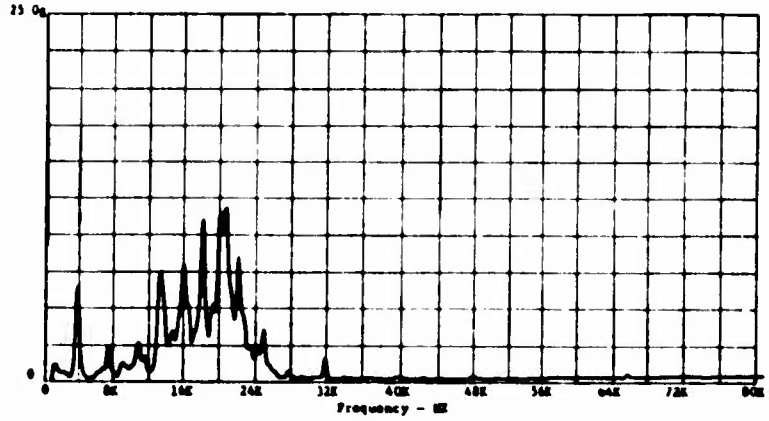

a) 6600 RPM

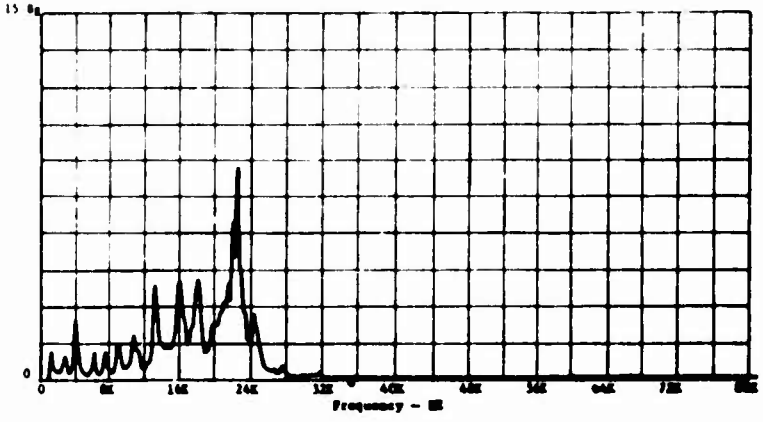

b) 4400 RPM

Figure 60. Bearing No. 1, Damaged Outer Race, 2860-Lb Radial Load, 4632-Lb Thrust Load, Accelerometer No. 3.

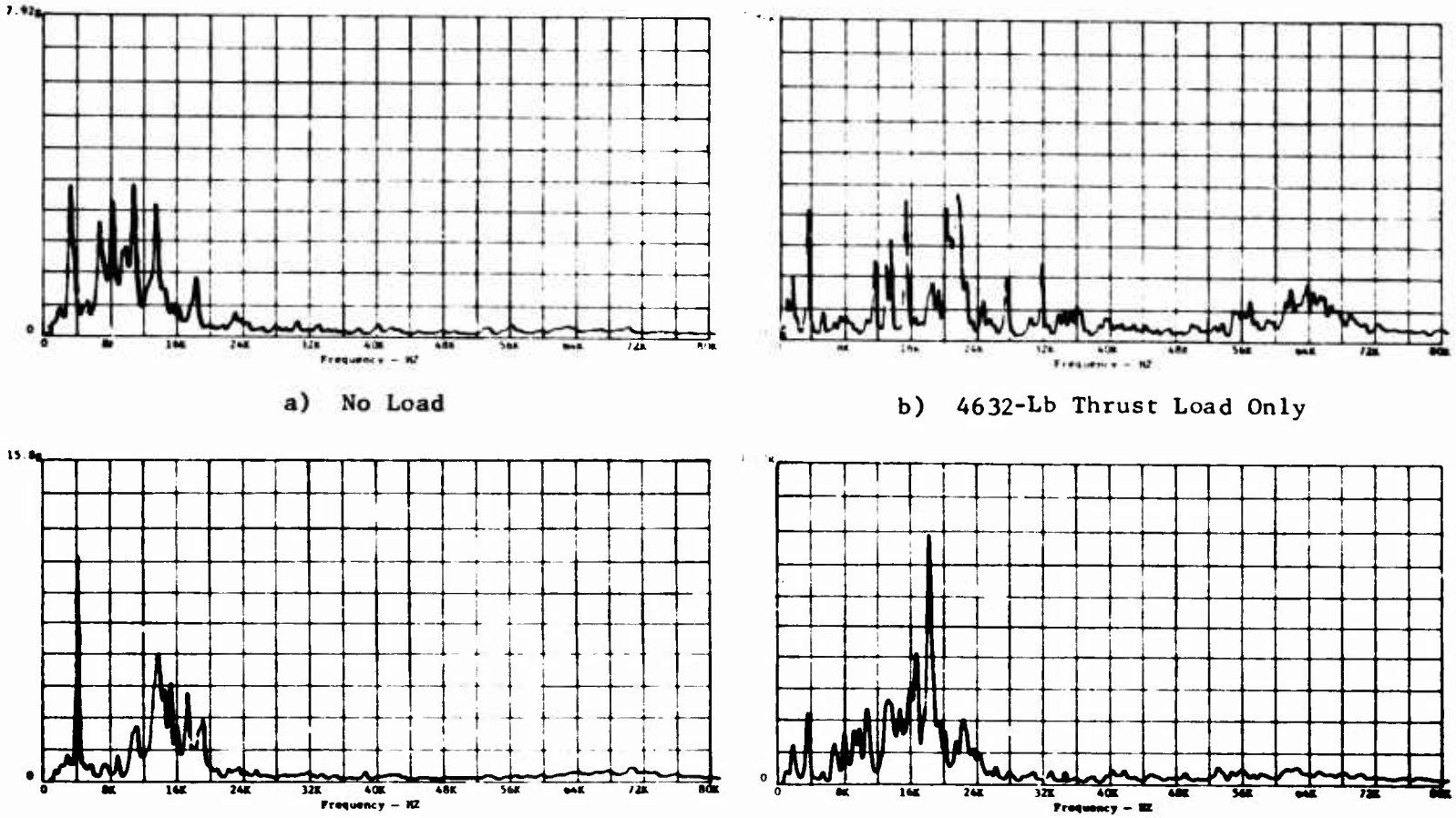

a) No Load

b) 4632-Lb Thrust Load Only

c) 198-Lb Radial Load, 192-Lb Thrust Load

d) 2860-Lb Radial Load Only

Figure 61. Bearing No. 1, Damaged Outer Race, 6600 RPM, Accelerometer No. 1.

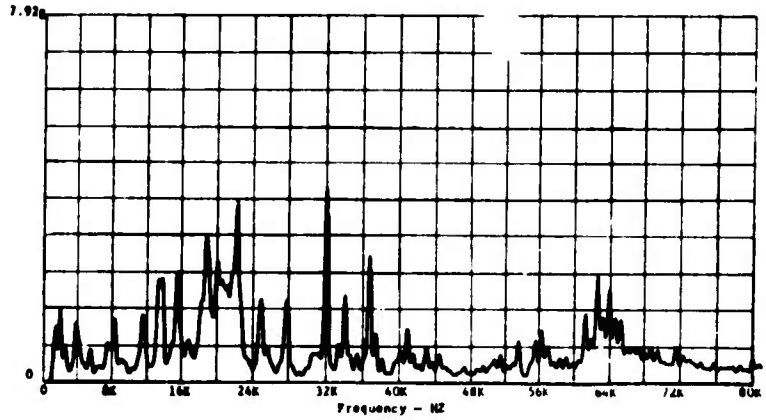

a) 6600 RPM

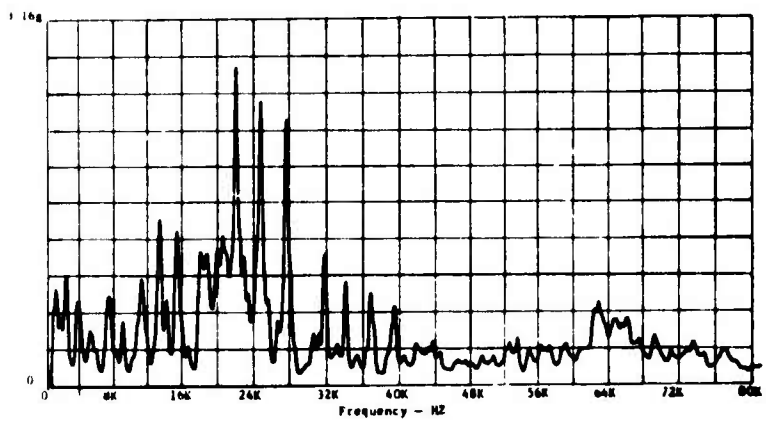

b) 4400 RPM

Figure 62. Bearing No. 1, Damaged Outer Race, 2860-Lb Radial Load, 4632-Lb Thrust Load, Accelerometer No. 1.

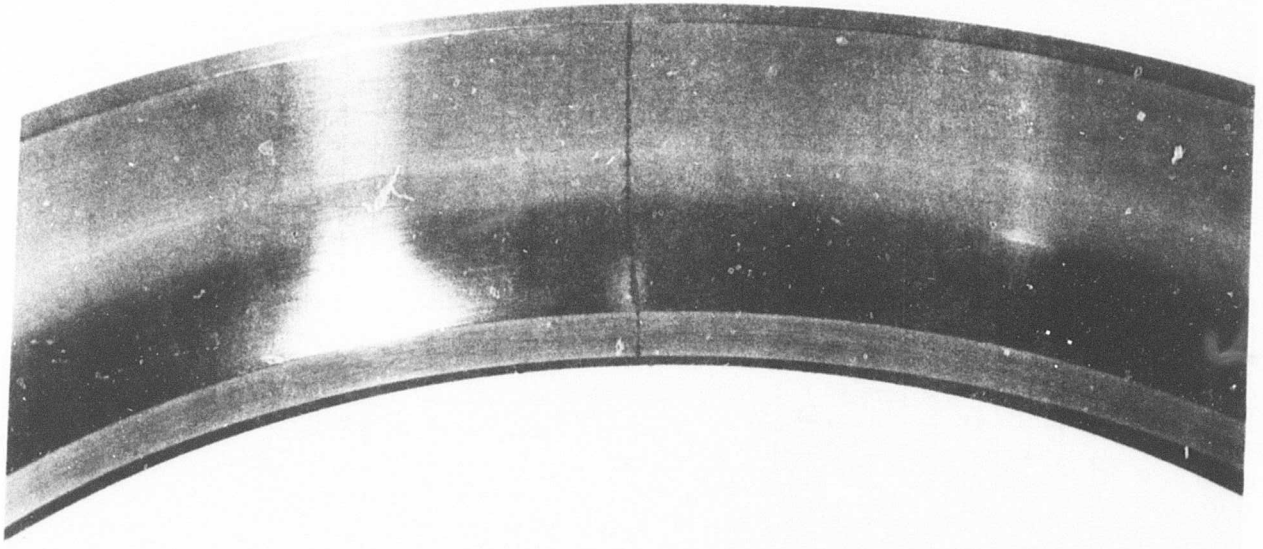

Figure 63. Outer Race Score for Bearing No. 1.

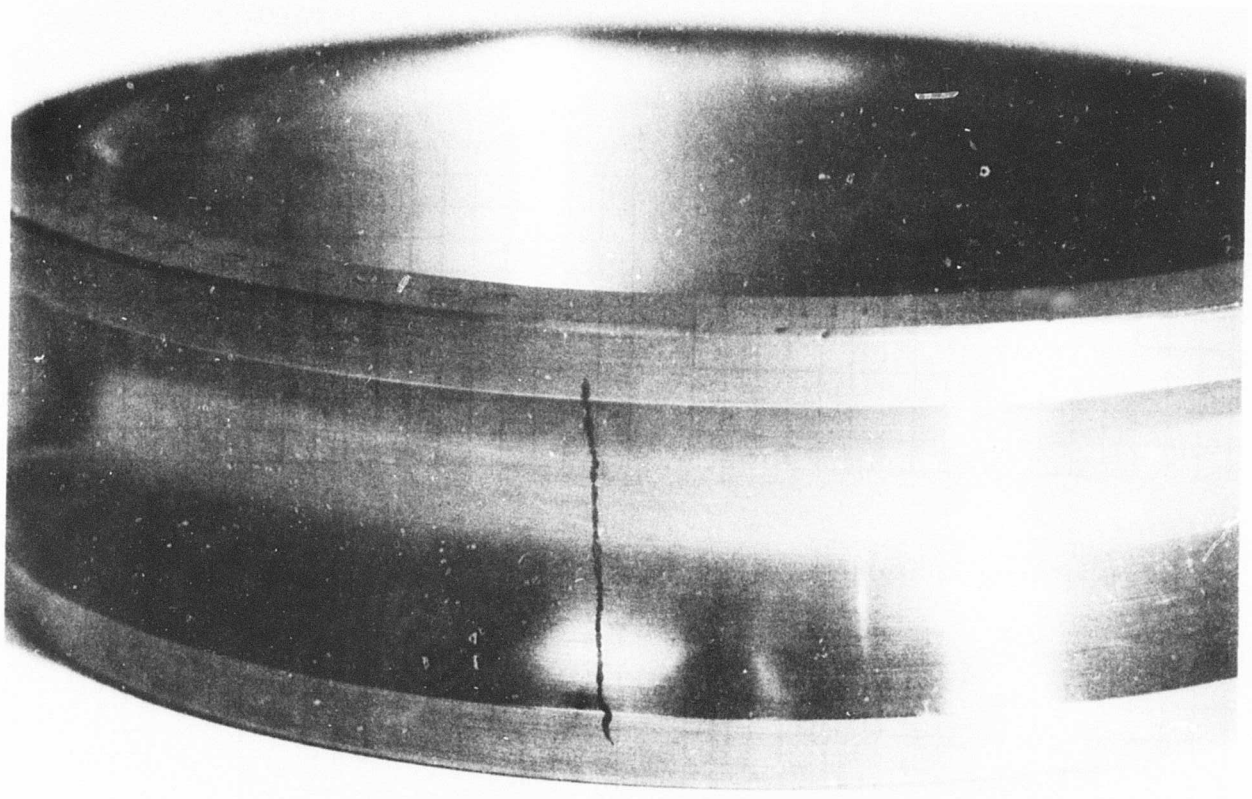

Figure 64. Inner Race Score for Bearing No. 1.

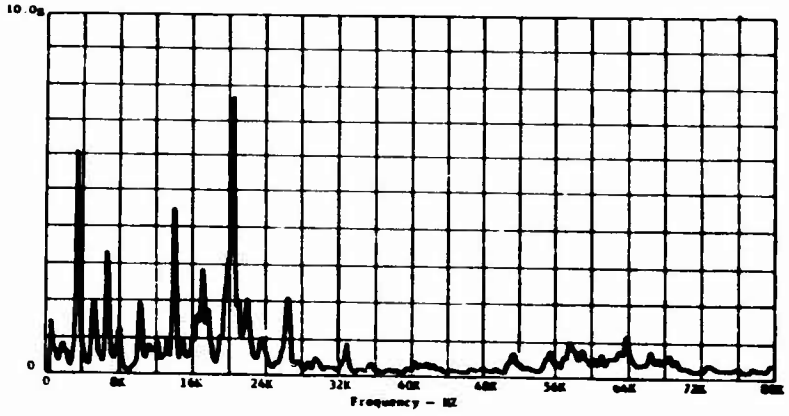

a) Lightweight Housing, Accelerometer No. 1

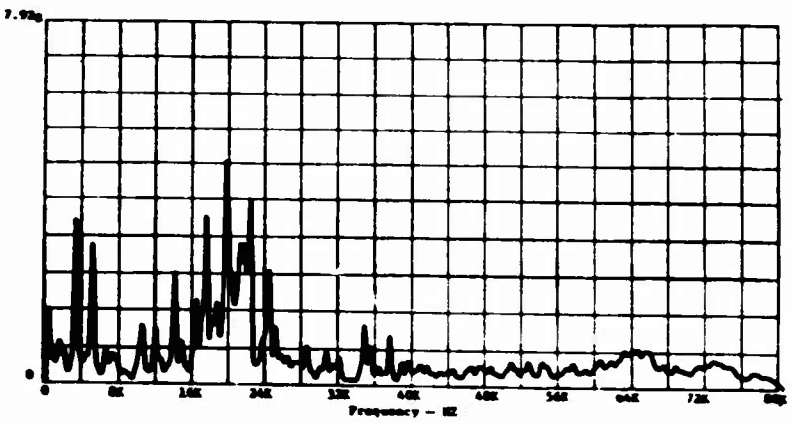

b) Lightweight Flexible Housing, Accelerometer No. 1

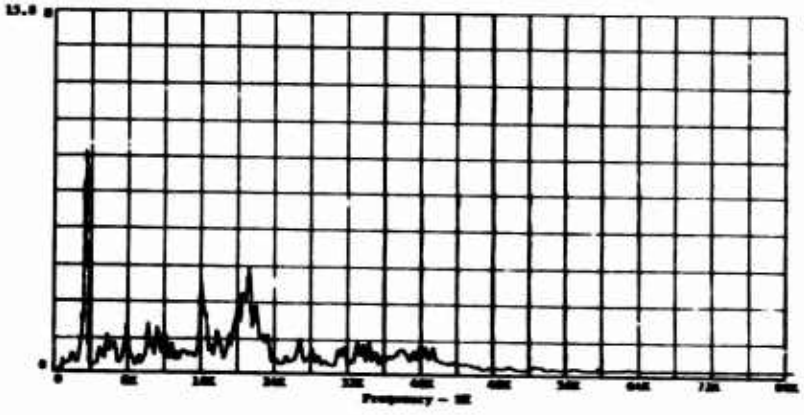

c) Lightweight Housing, Accelerometer No. 3

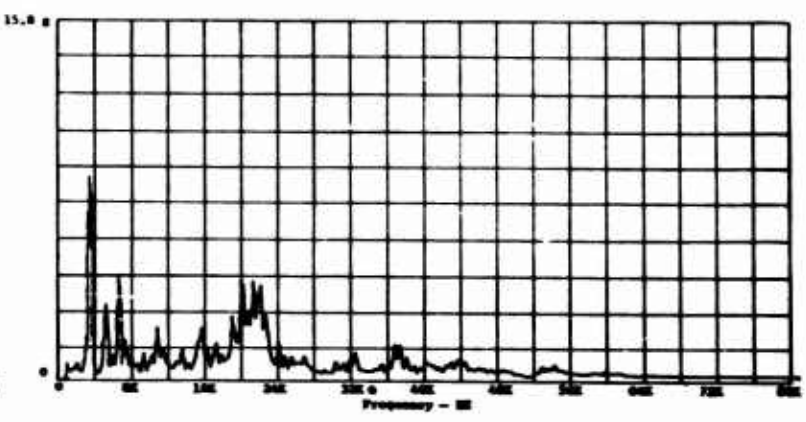

d) Lightweight Flexible Housing, Accelerometer No. 3

Figure 65. Bearing No. 1, Damaged Outer Race, 6600 RPM, 2860-Lb Radial Load, 4632-Lb Thrust Load.

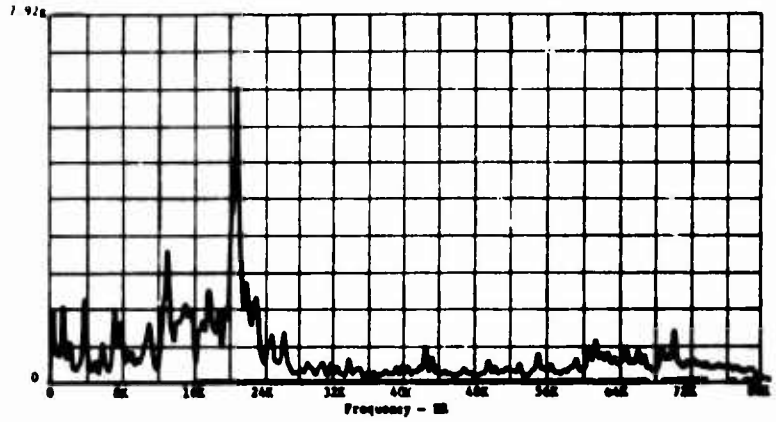

a) Accelerometer No. 1

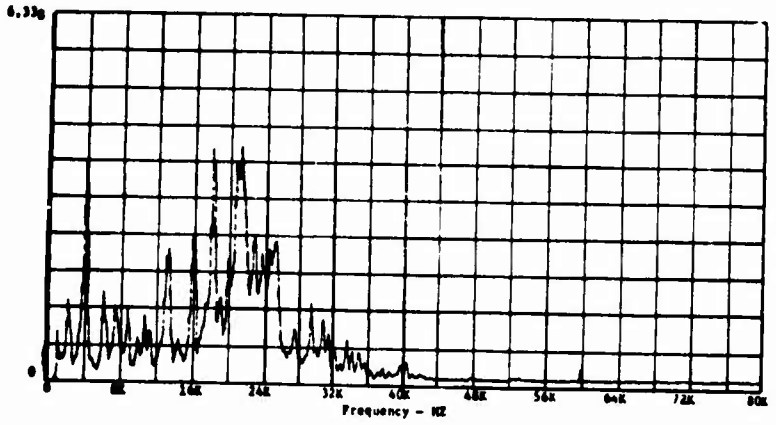

b) Accelerometer No. 3

Figure 66. Bearing No. 1, Damaged Inner Race, 6600 RPM, 2860-Lb Radial Load, 4632-Lb Thrust Load.

Bearing No. 4

In a UH-1 helicopter transmission, bearing No. 4 is found in a set. Each member of the pair undergoes similar, though not identical, loading conditions, as shown in Table XIX. The good bearing, the bearing with the artificially damaged inner race, and the bearing with the artificially damaged outer race were all run with the heavyweight housing at maximum speed (3050 rpm) and under both sets of operating loads as shown in Table XXV. The defects created in the damaged outer race and damaged inner race bearings are shown in Figures 67 and 68, respectively.

TABLE XXV. DATA SUMMARY FOR TESTS OF BEARING NO. 4

Record	Speed (rpm)	Radial Load (lb)	Thrust Load (lb)	Bearing Condition	Bearing Housing
1	3050	2134	1303	Undamaged	Heavyweight
2	3050	2668	1856	Undamaged	Heavyweight
3	3050	2668	1856	Damaged Outer Race	Lightweight
4	3050	2134	1303	Damaged Outer Race	Heavyweight
5	3050	2668	1856	Damaged Outer Race	Heavyweight
6	3050	2668	1856	Damaged Outer Race	Lightweight Flexible
7	3050	2134	1303	Damaged Inner Race	Heavyweight
8	3050	2668	1856	Damaged Inner Race	Heavyweight

In addition, the bearing with the artificially damaged outer race was run with the lightweight and lightweight flexible bearing housings at maximum speed under the larger of the two sets of operating loads only. The frequency spectrums obtained from the data for some of the bearing No. 4 tests are given in Figures 69 through 72.

Bearing No. 5

This bearing was run at maximum operating speed (324 rpm) and under a 2000-pound radial load and a 5000-pound thrust load, as shown in Table XXVI. The applied radial load is the approximate maximum operating load. The maximum operating thrust load is approximately 10,000 pounds. However, the thrust loading apparatus associated with the test rig was capable of applying a load of only 5000 pounds. The good bearing, the bearing with the artificially damaged inner race, whose defect is shown in Figure 73, and the bearing with the artificially damaged outer race, whose defect is shown

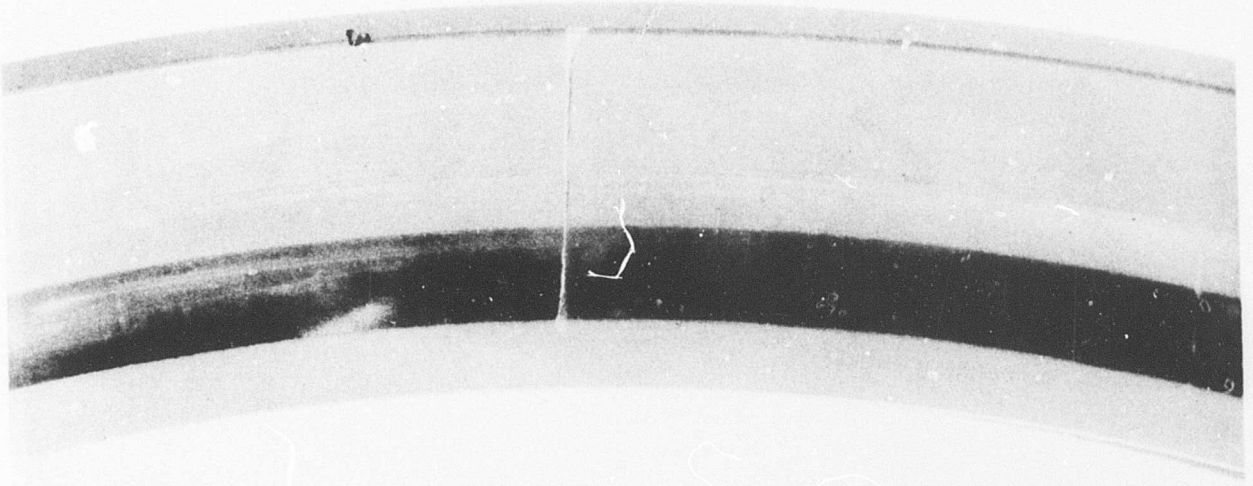

Figure 67. Outer Race Score for Bearing No. 4.

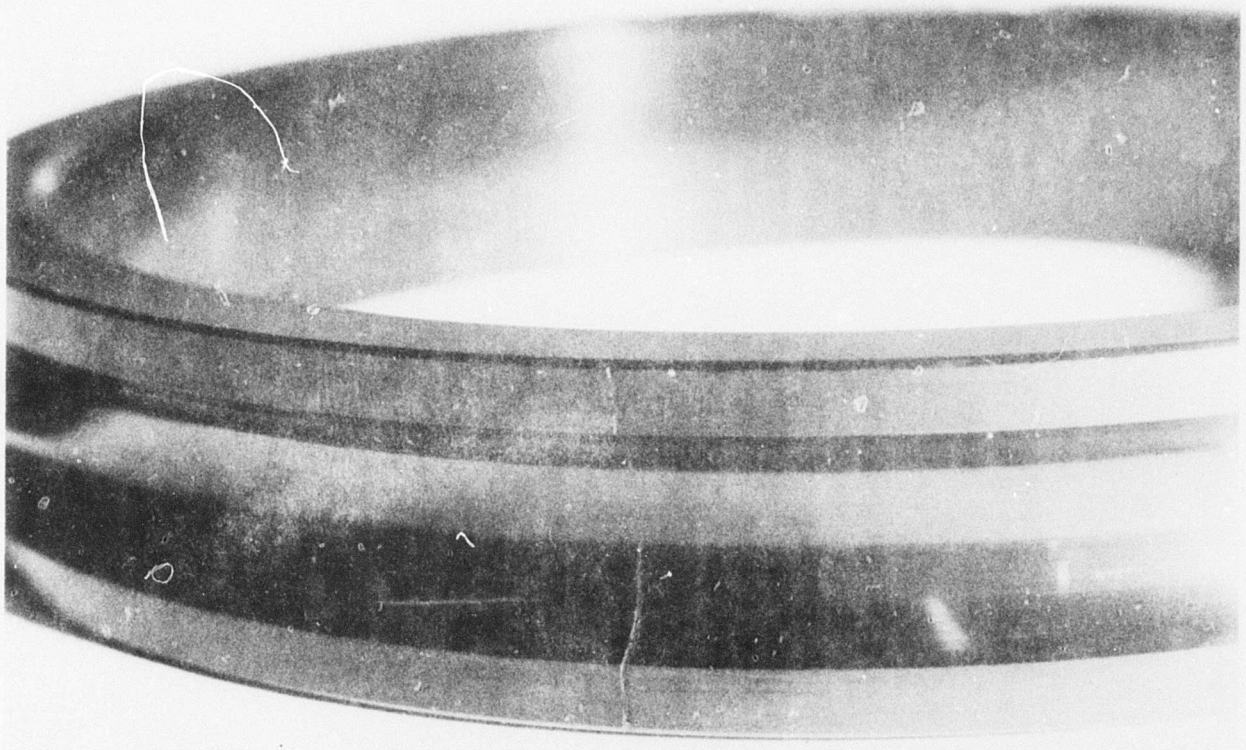

Figure 68. Inner Race Score for Bearing No. 4.

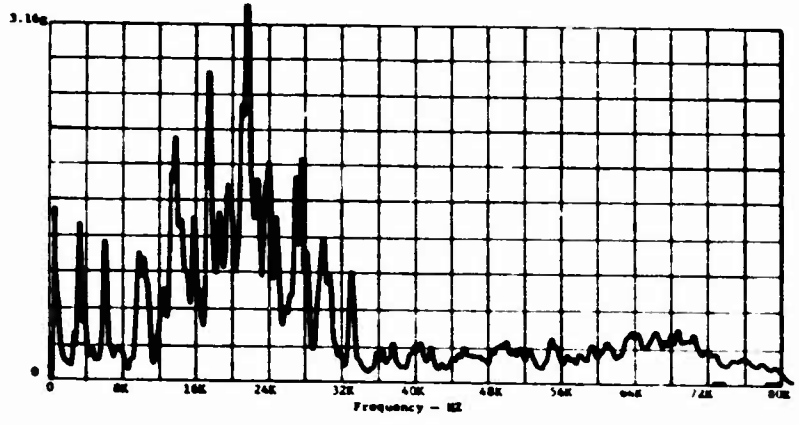

a) 2134-Lb Radial Load, 1303-Lb Thrust Load Accelerometer No. 1.

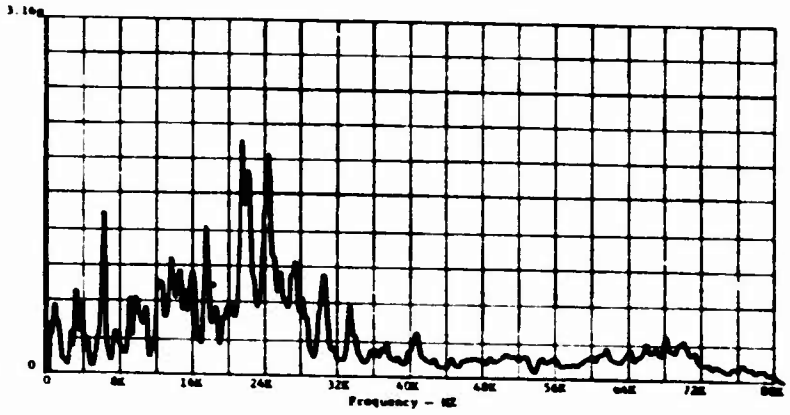

b) 2668-Lb Radial Load, 1856-Lb Thrust Load, Accelerometer No. 1.

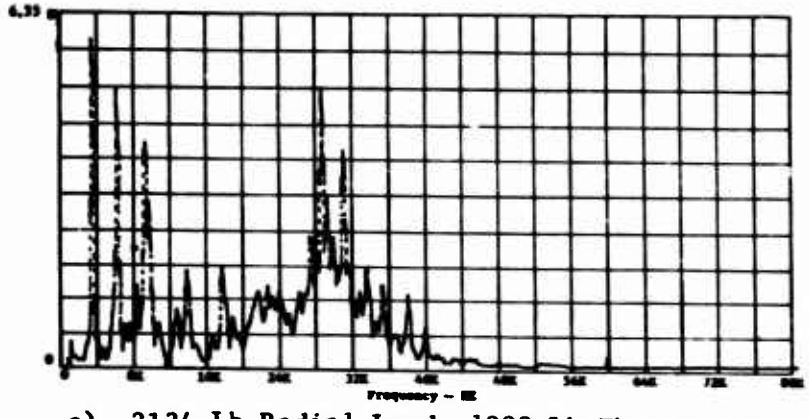

c) 2134-Lb Radial Load, 1303-Lb Thrust Load, Accelerometer No. 3.

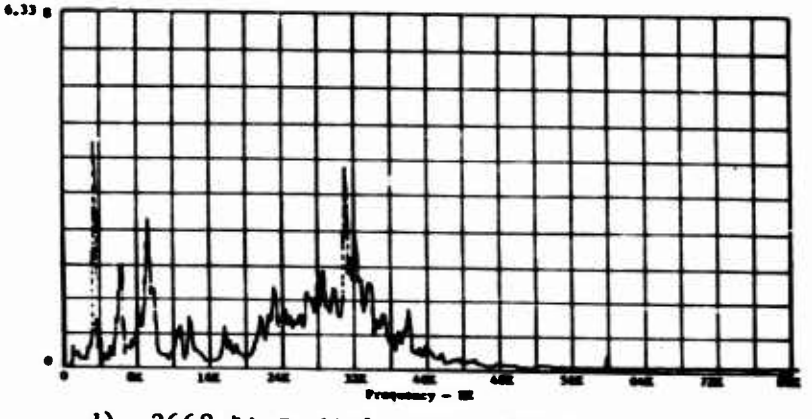

d) 2668-Lb Radial Load, 1856-Lb Thrust Load, Accelerometer No. 3

Figure 69. Bearing No. 4, Undamaged, 3050 RPM, Heavyweight Housing.

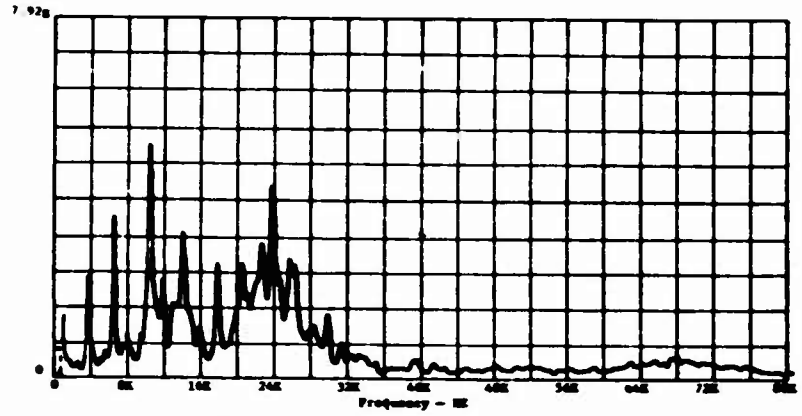

a) Damaged Outer Race, Accelerometer No. 1

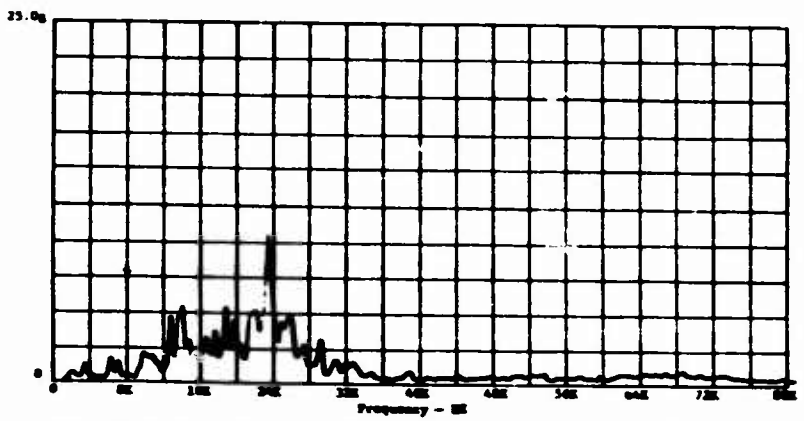

b) Damaged Inner Race, Accelerometer No. 1

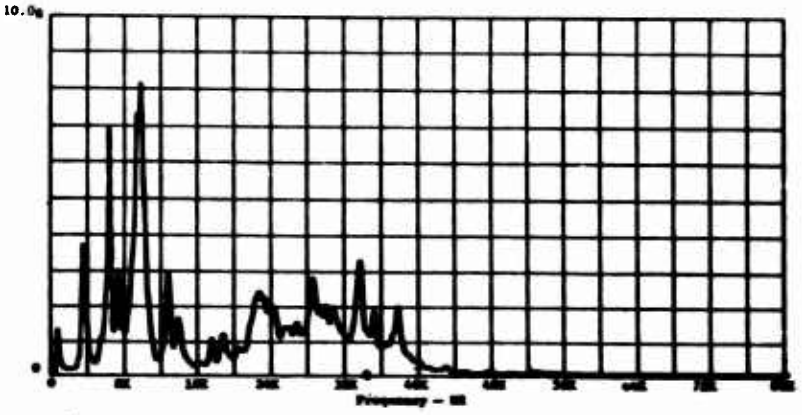

c) Damaged Outer Race, Accelerometer No. 3

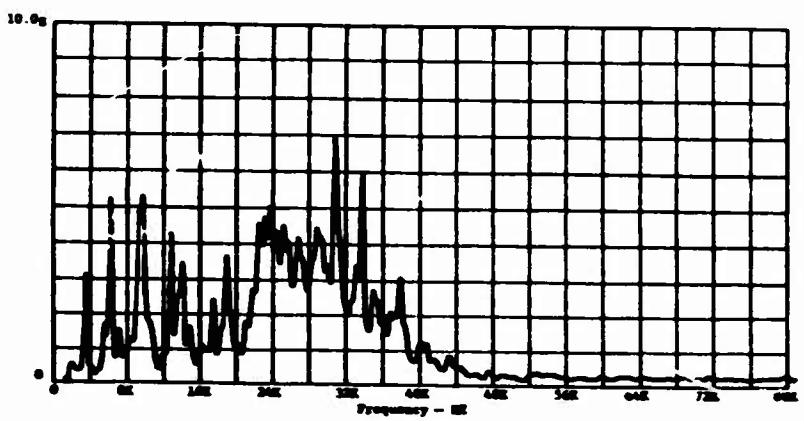

d) Damaged Inner Race, Accelerometer No. 3

Figure 70. Bearing No. 4, 3050 RPM, 2134-Lb Radial Load, 1303-Lb Thrust Load, Heavyweight Housing.

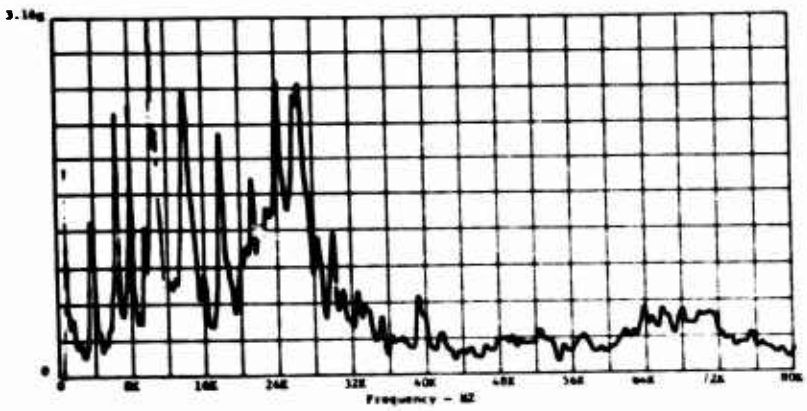

a) Damaged Outer Race, Accelerometer No. 1

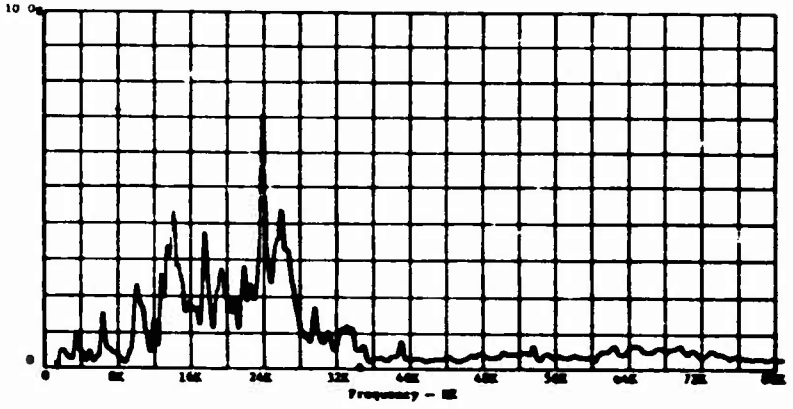

b) Damaged Inner Race, Accelerometer No. 1

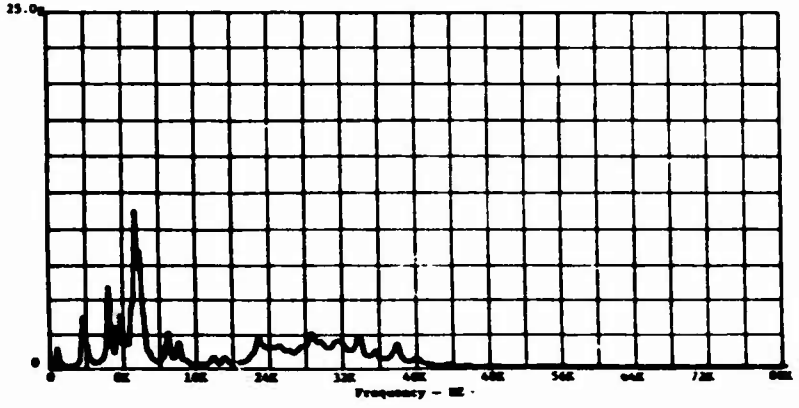

c) Damaged Outer Race, Acceleromter No. 3

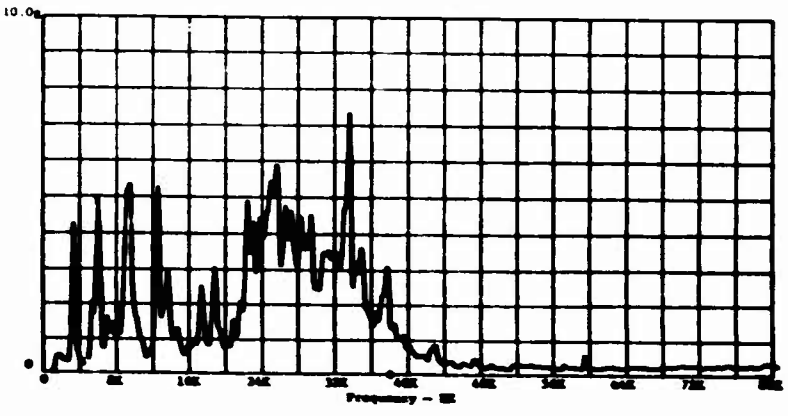

d) Damaged Inner Race, Accelerometer No. 3

Figure 71. Bearing No. 4, 3050 RPM, 2668-Lb Radial Load, 1856-Lb Thrust Load, Heavyweight Housing.

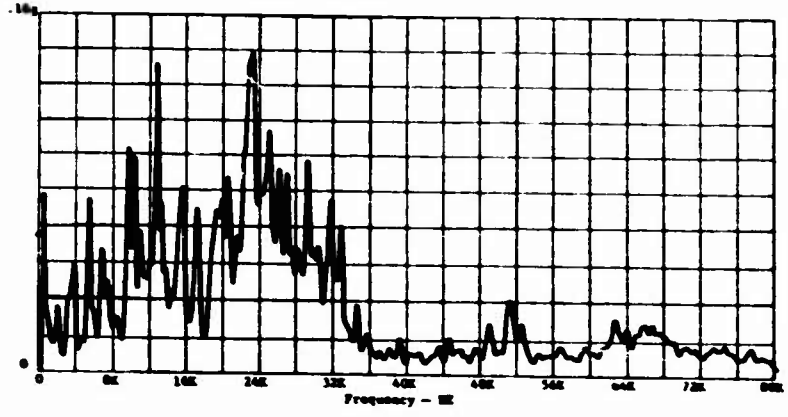

a) Lightweight Housing, Accelerometer No. 1

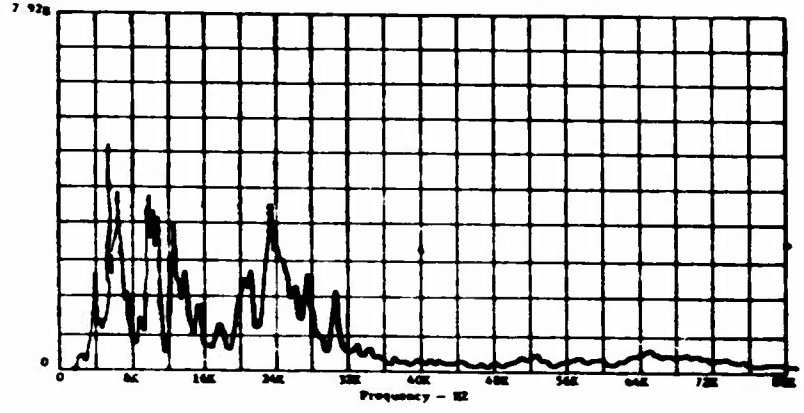

b) Lightweight Flexible Housing, Accelerometer No. 1

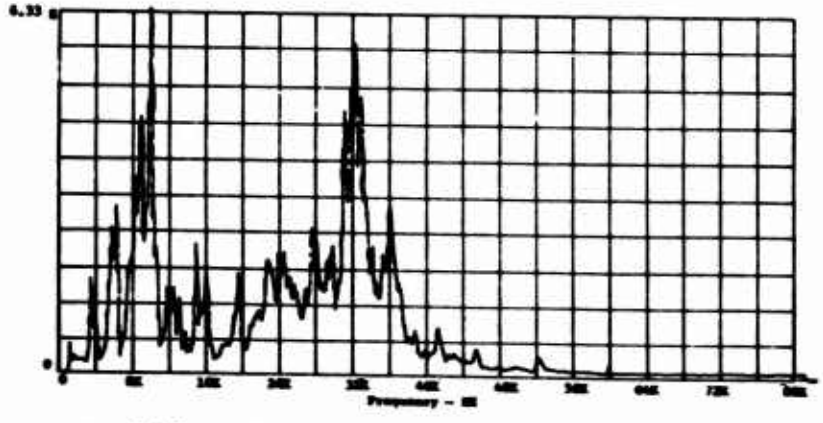

c) Lightweight Housing, Accelerometer No. 3

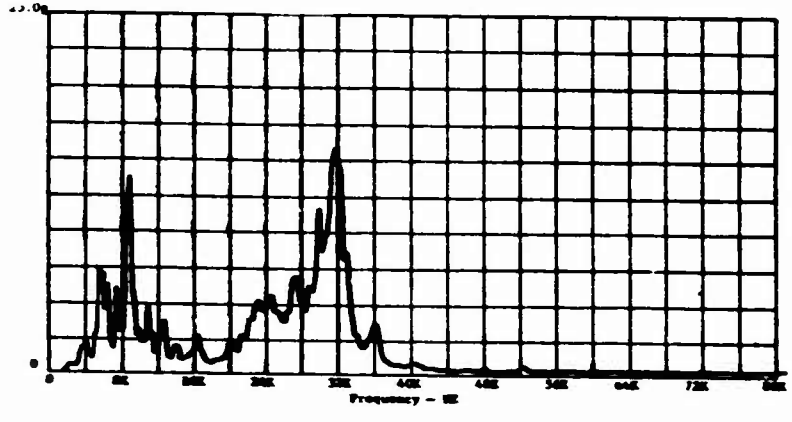

d) Lightweight Flexible Housing, Accelerometer No. 3

Figure 72. Bearing No. 4, 3050 RPM, 2668-Lb Radial Load, 1856-Lb Thrust Load, Damaged Outer Race.

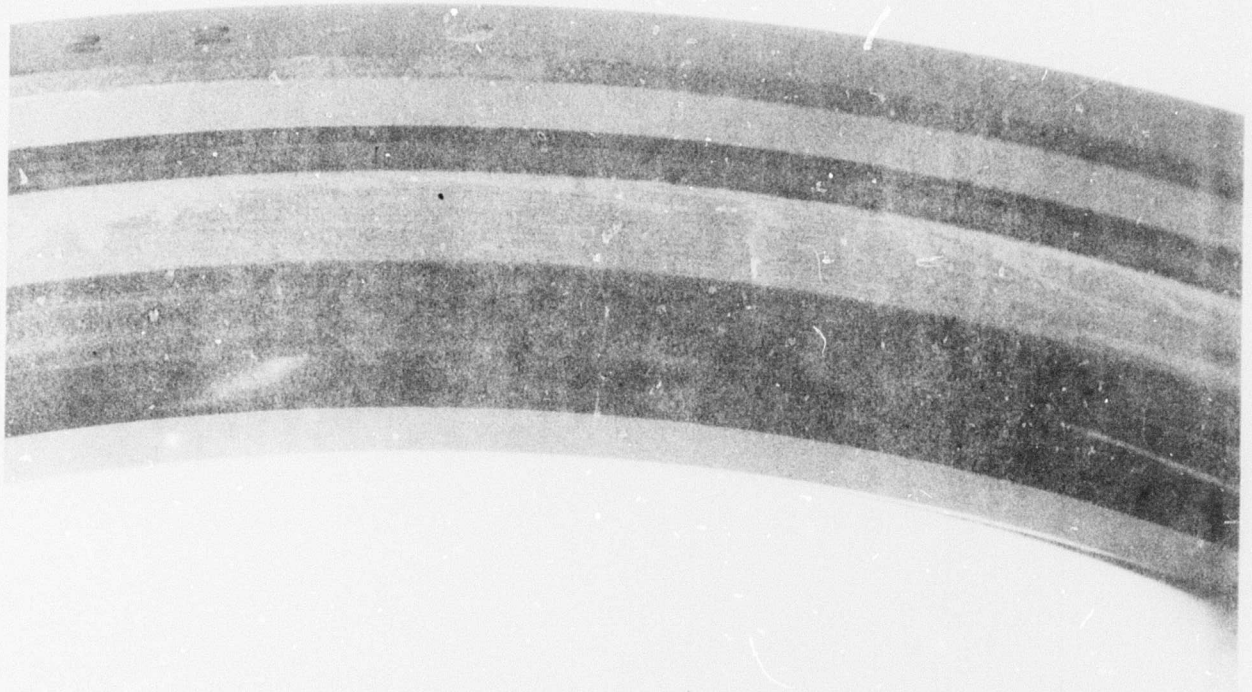

Figure 73. Outer Race Score for Bearing No. 5.

in Figure 74, were run with the heavyweight housing. In addition, the bearing with the artificially damaged outer race was run with the lightweight and lightweight flexible housings. The frequency spectrums obtained from the data for some of the bearing No. 5 tests are given in Figures 75 and 76.

TABLE XXVI. DATA SUMMARY FOR TESTS OF BEARING NO. 5

Record	Speed (rpm)	Radial Load (lb)	Thrust Load (lb)	Bearing Condition	Bearing Housing
1	324	2000	5000	Undamaged	Heavyweight
2	324	2000	5000	Damaged Outer Race	Lightweight
3	324	2000	5000	Damaged Outer Race	Heavyweight
4	324	2000	5000	Damaged Outer Race	Lightweight Flexible
5	324	2000	5000	Damaged Inner Race	Heavyweight

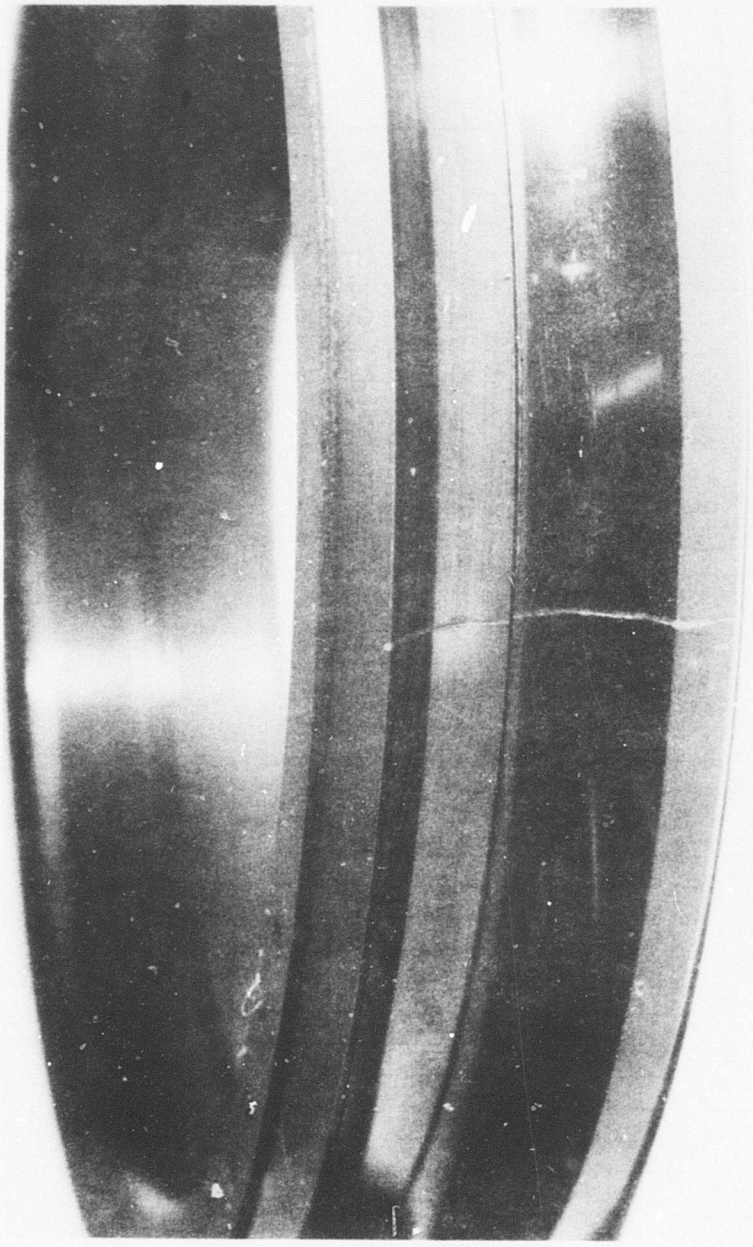

Figure 74. Inner Race Score for Bearing No. 5.

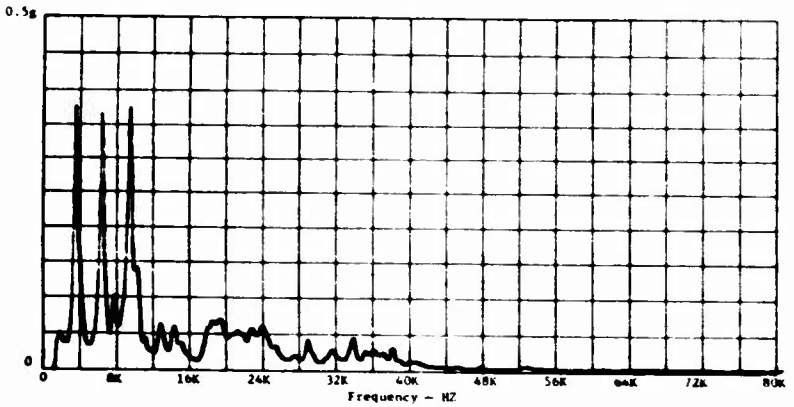

a) Undamaged Bearing, Heavyweight Housing

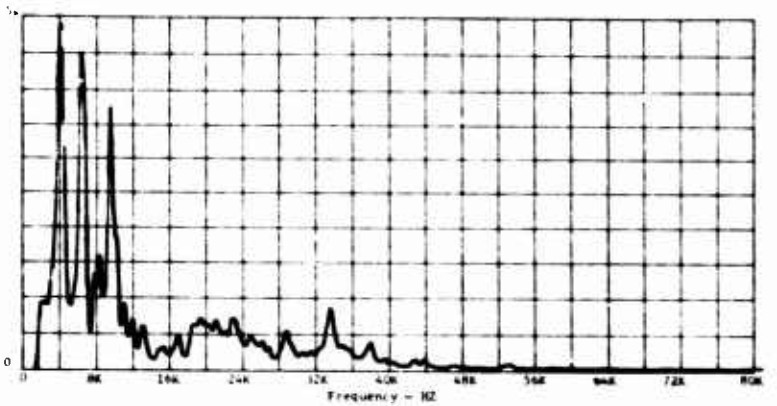

b) Damaged Outer Race Bearing, Lightweight Housin

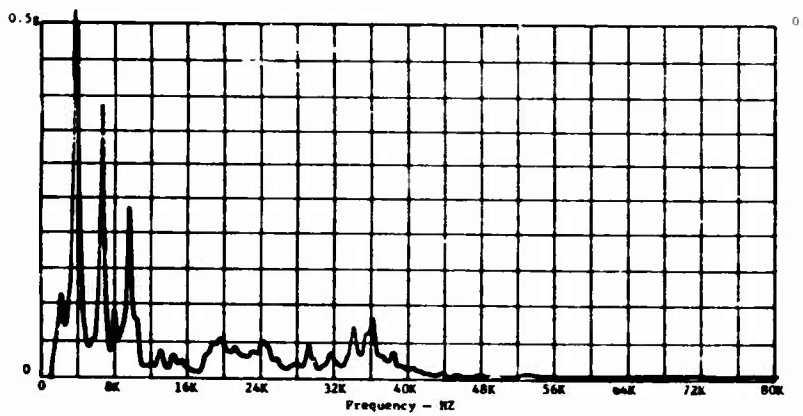

c) Damaged Outer Race Bearing, Heavyweight Housing

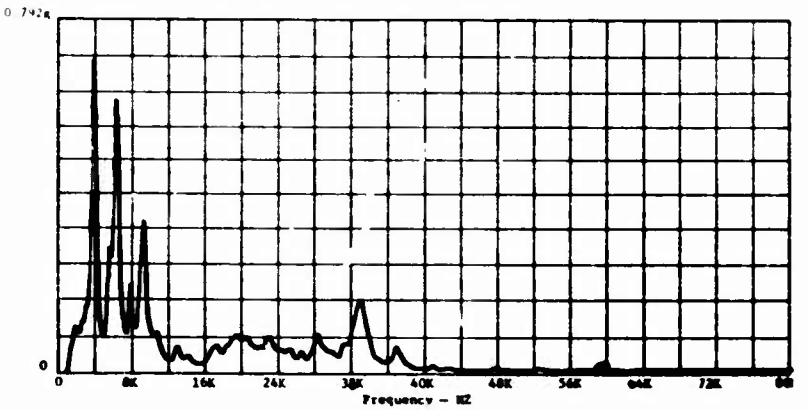

d) Damaged Outer Race Bearing, Lightweight Flexible Housing

Figure 75. Bearing No.5, 324 RPM, 2000-Lb Radial Load, 5000-Lb Thrust Load, Accelerometer No. 3.

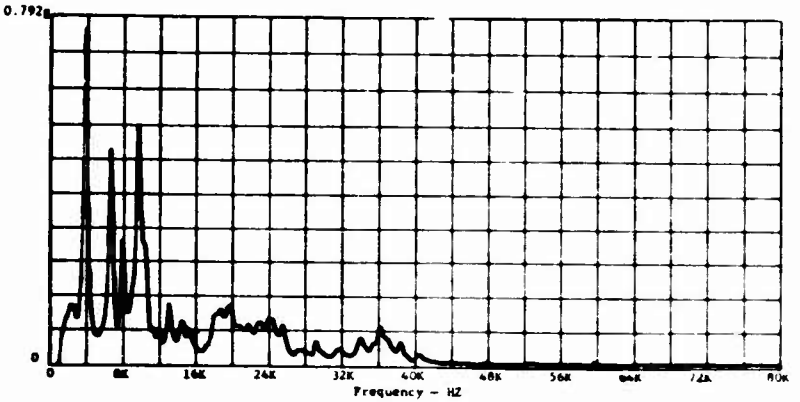

a) Damaged Inner Race Bearing, Accelerometer No. 3

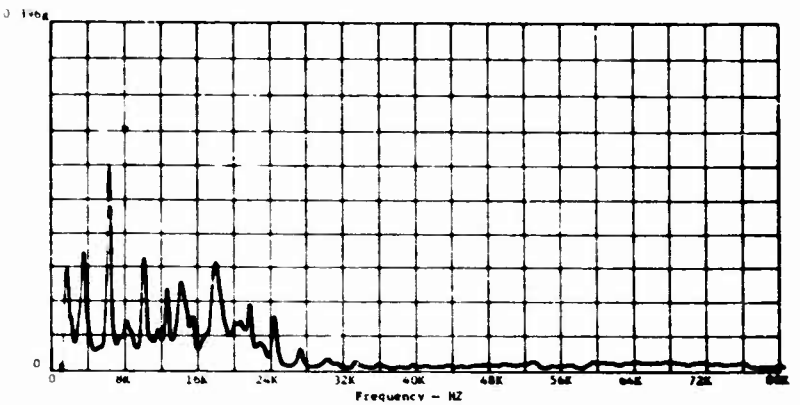

b) Undamaged Bearing, Accelerometer No. 1

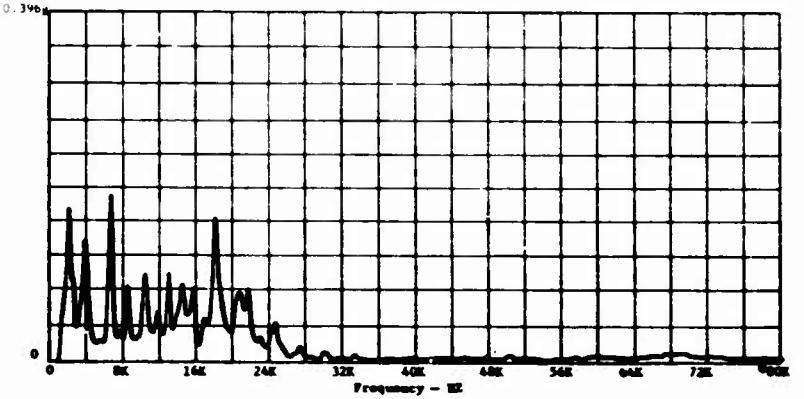

c) Damaged Inner Race Bearing, Accelerometer No. 1

Figure 76. Bearing No. 5, 324 RPM, 2000-Lb Radial Load, 5000-Lb Thrust Load, Heavyweight Housing.

EVALUATION AND ANALYSIS OF TEST RIG DATA

The data from the rotating dynamic response test rig was analyzed in order to determine what high-frequency resonances and accelerometer locations are likely to produce the best results for each bearing. The effect of speed, load and bearing housing design on those results was also determined from the analyzed test rig data.

The data analysis procedure for the test rig involved the detailed analysis of the data collected for each bearing tested. This analysis was done for one bearing at a time, in the same order as the tests were carried out.

Bearing No. 2

In order to better understand the dynamics involved in the creation of the test rig data, it was helpful to identify the origins of the outstanding peaks found in the frequency spectrum plots of that data. The bearing race resonance data was collected for that purpose. However, as the balls or rollers excited resonances in the bearing races, they may have also excited resonances in the bearing housings, which may have been responsible for some of those peaks. For that reason, the housing for bearing No. 2 was excited by an impulse load and the resulting vibration analyzed using a transient recorder and real-time frequency spectrum analyzer in a manner similar to that done for the bearing races. This was done for each of the three accelerometer locations used during the bearing tests. The resulting frequency spectrums are presented in Figure 77.

These plots were compared with those of the raw test rig data for bearing No. 2. It could be seen that the low-frequency peaks (below 20kHz) in the test rig data were probably due to bearing housing resonances since they correspond to some of the frequency peaks in the impact excited housing data. However, this is not true for the higher frequency peaks found in the test rig data. The most outstanding of these higher frequency peaks are located at approximately 31 kHz and 39 kHz. These peaks probably resulted from the purely circumferential bearing outer race resonances whose wave numbers are six and seven, respectively. These resonances occurred at frequencies somewhat lower than the calculated frequencies from Table IV because of inaccuracies in the analytical model. They occurred at frequencies higher than those experimentally determined, as shown in Table IV, because of the foundation stiffness provided by the bearing housing.

The bearing housing for bearing No. 3 was also similarly excited. The frequency spectrums for the three accelerometer locations are presented in Figure 78. The accelerometer signals analyzed in the bearing housing ringing tests were first filtered to remove signals above 50 kHz in order to prevent aliasing (a distortion of the frequency spectrum due to the inability of the spectrum analyzer to accurately handle analog to digital conversion of frequencies too close to its sampling rate).

The frequency spectrums for some of the envelope detected data of bearing No. 2 are presented in Figures 79 through 82. For comparison, frequency spectrums for some of the raw data covering the same frequency range

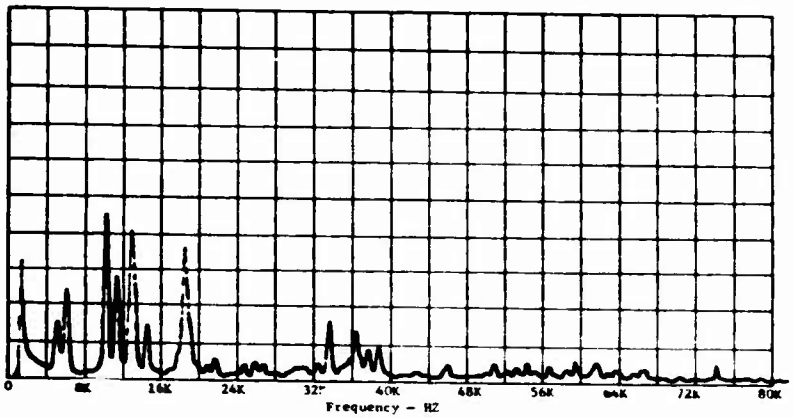

a) Accelerometer Location No. 1

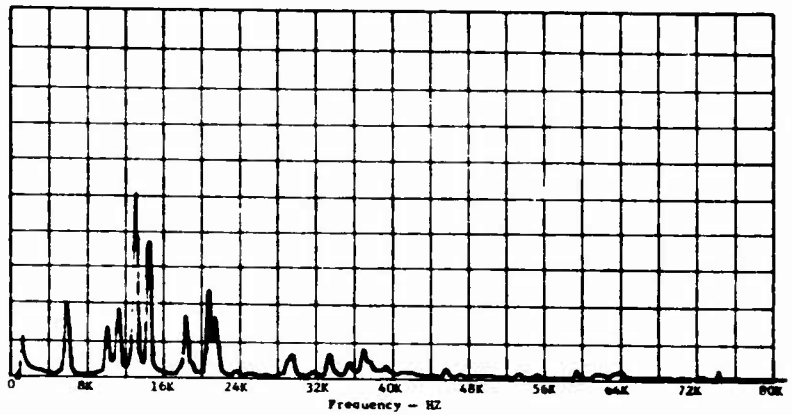

b) Accelerometer Location No. 2

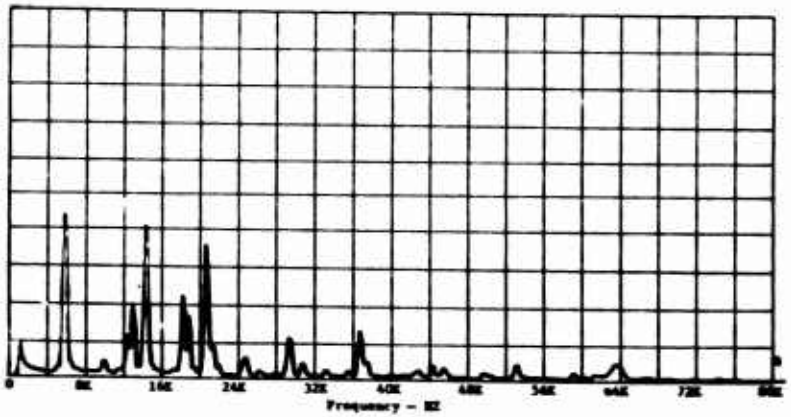

c) Accelerometer Location No. 3

Figure 77. Free Vibration of Bearing No. 2 Housing, Ball Drop Excitation.

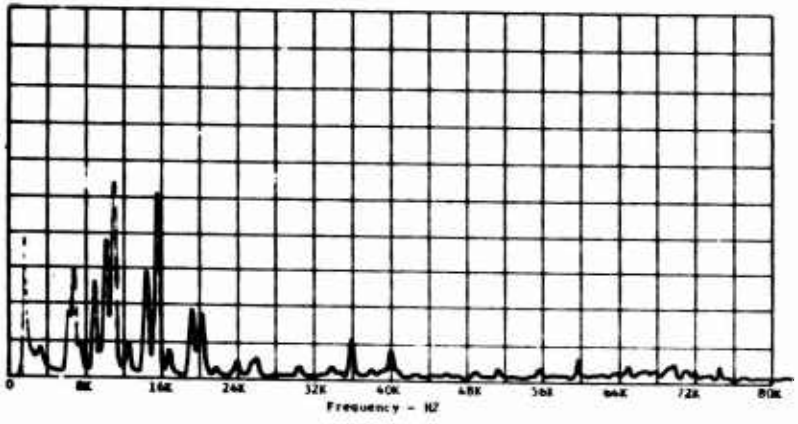

a) Accelerometer Location No. 1

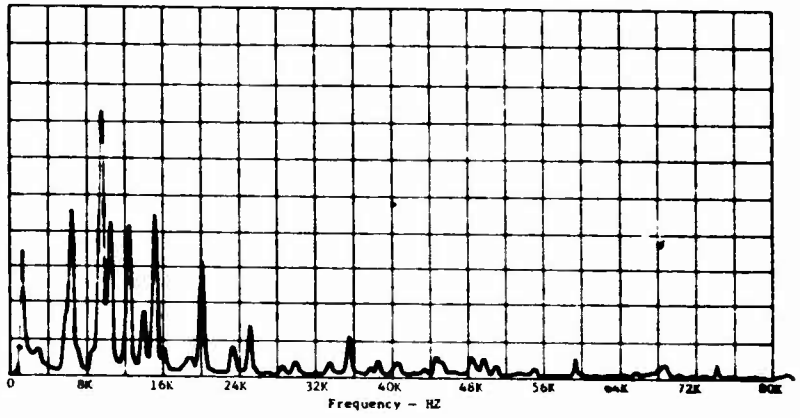

b) Accelerometer Location No. 2

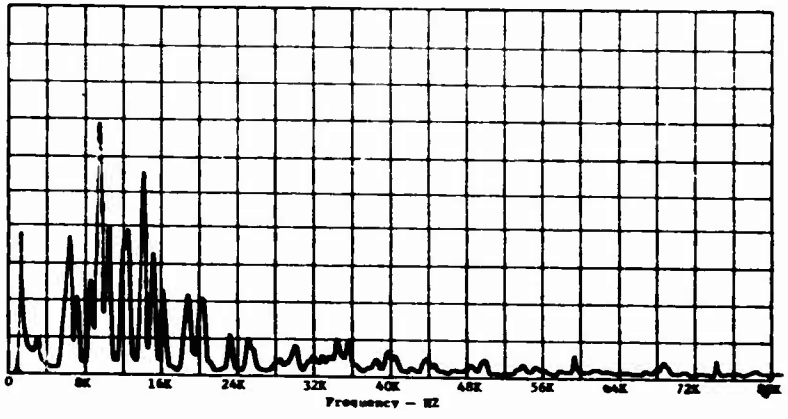

c) Accelerometer Location No. 3

Figure 78. Free Vibration of Bearing No. 3 Housing. Ball Drop Excitation.

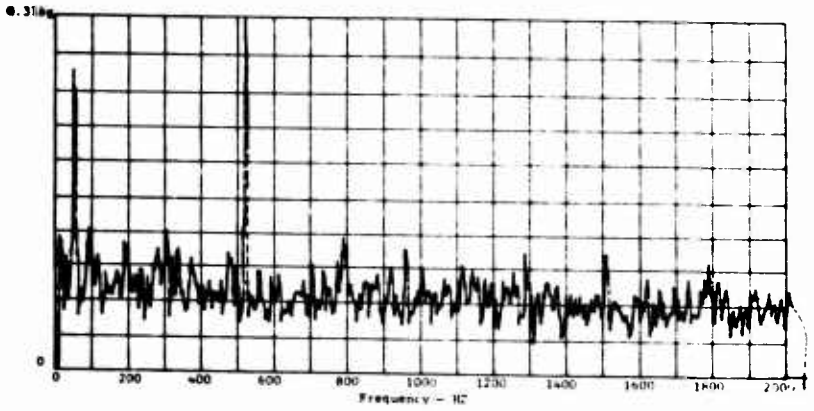

a) 6600 RPM, 726-Lb Load

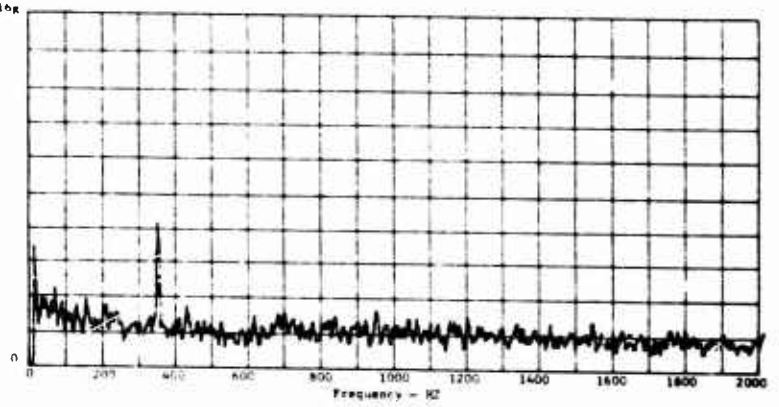

b) 4400 RPM, 726-Lb Load

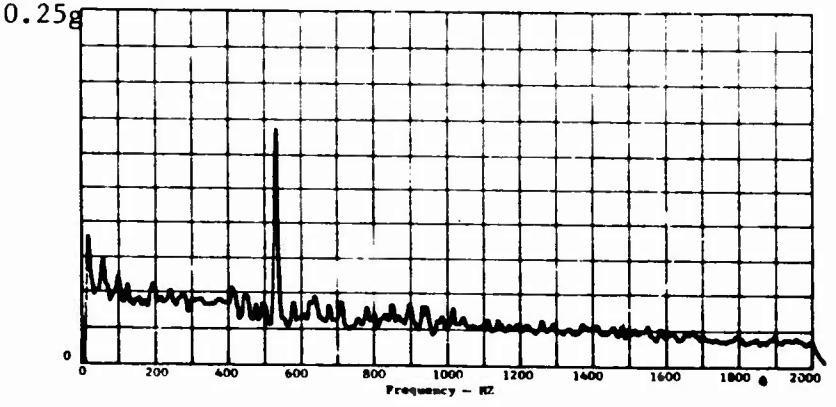

c) 6600 RPM 1817-Lb Load

Figure 79. Bearing No. 2, Undamaged, Accelerometer No. 3, Envelope Detected About 39 kHz.

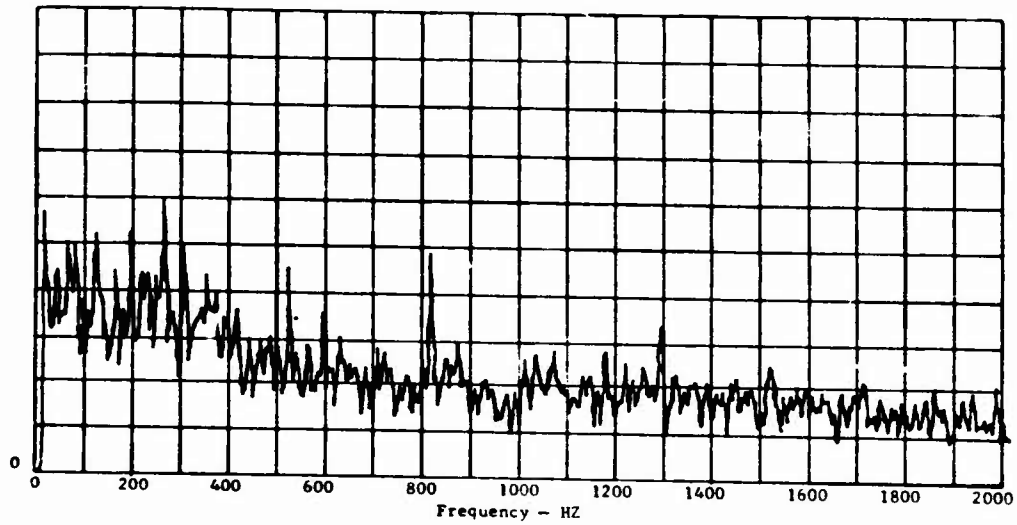

a) Envelope Detected About 14 kHz

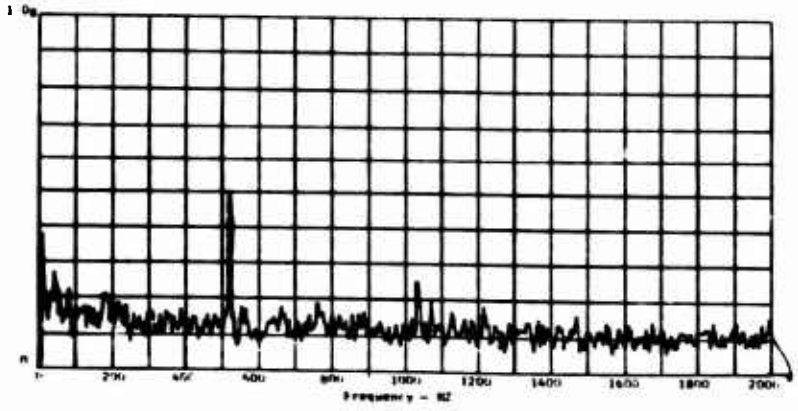

b) Envelope Detected About 31 kHz

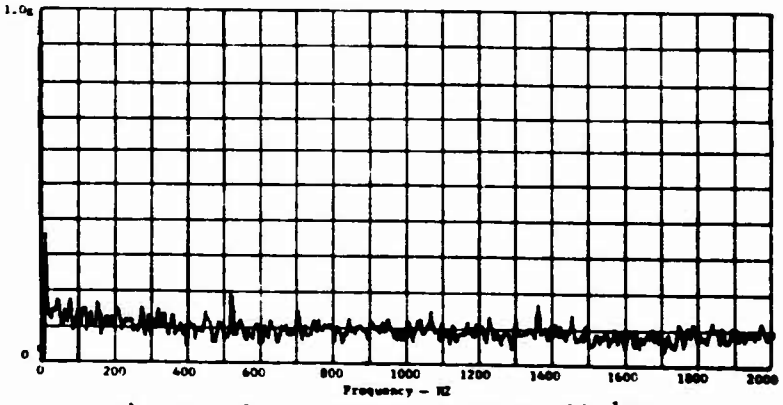

c) Envelope Detected About 39 kHz

Figure 80. Bearing No. 2, Undamaged, 6600 RPM, 3633-Lb Load, Accelerometer No. 3.

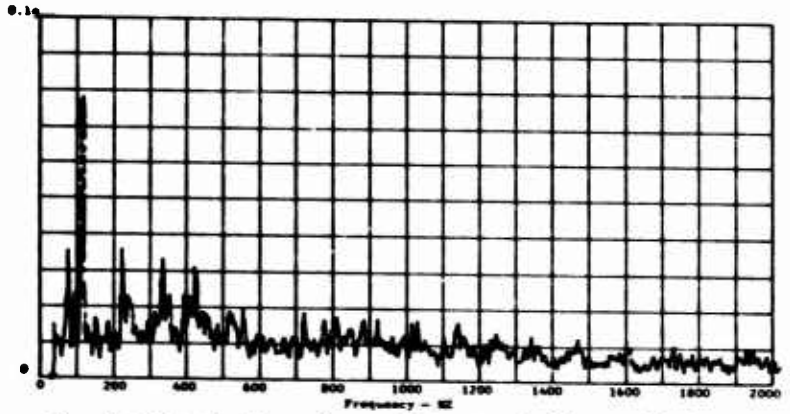

a) No Load, Envelope Detected About 39 kHz

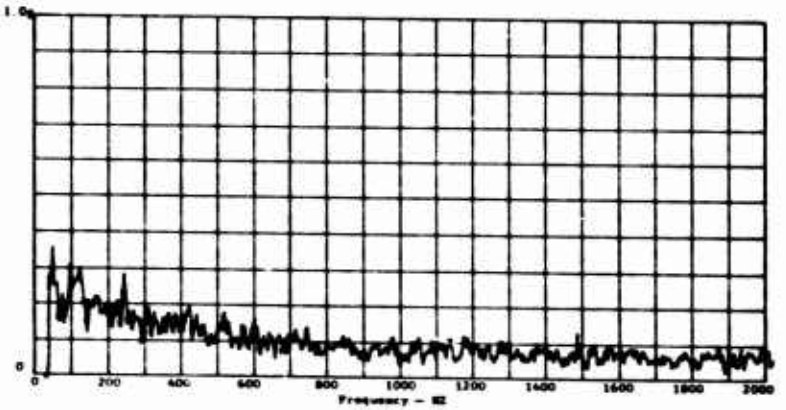

b) 3633-Lb Load, Envelope Detected About 14 kHz

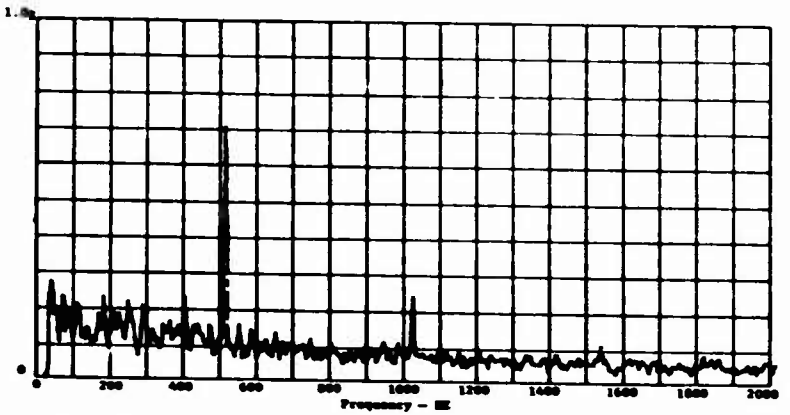

c) 3633-Lb Load, Envelope Detected About 31 kHz

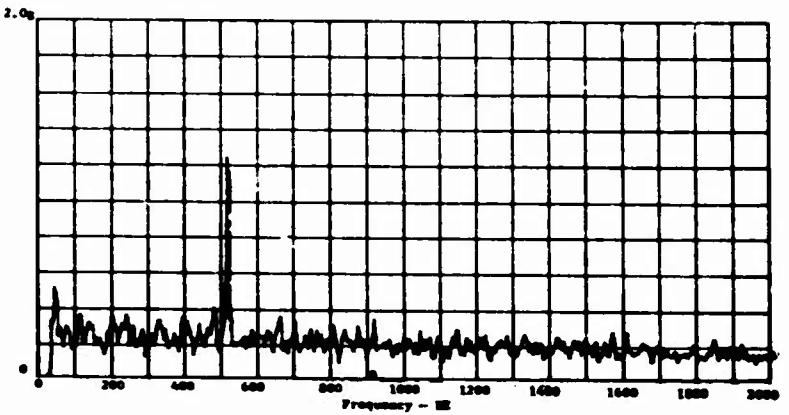

d) 3633-Lb Load, Envelope Detected About 39 kHz

Figure 81. Bearing No. 2, Damaged Outer Race, 6600 RPM, Accelerometer No. 3.

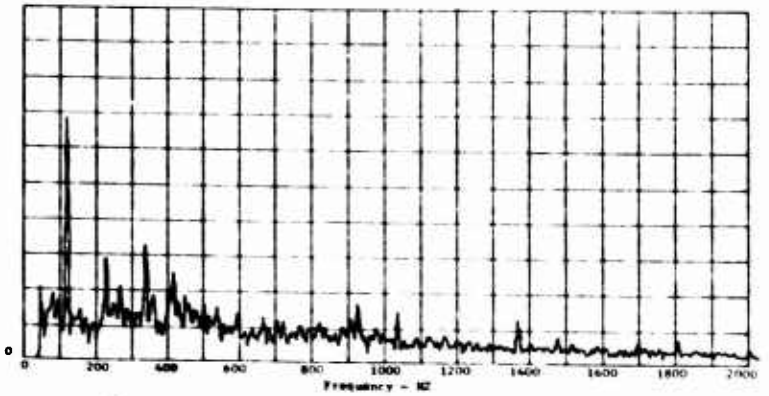

a) No Load, Accelerometer No. 3, Envelope Detected About 31 kHz

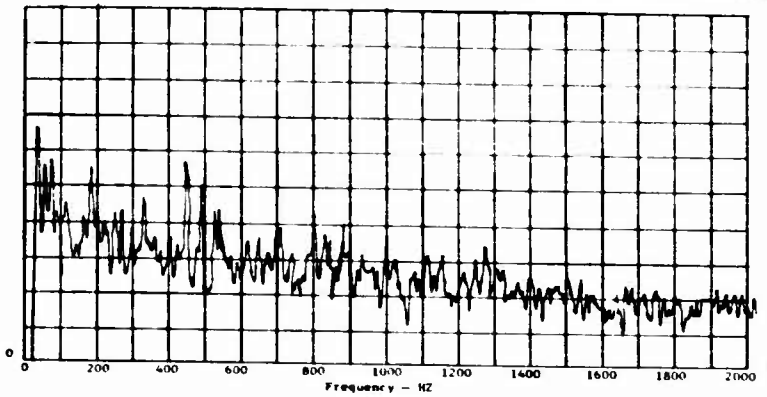

b) 3633-Lb Load, Accelerometer No. 1, Envelope Detected About 39 kHz

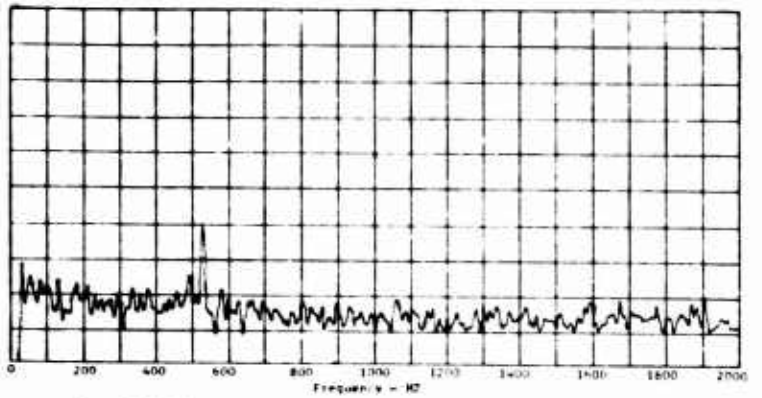

c) 3633-Lb Load, Accelerometer No. 2, Envelope Detected About 39 kHz

Figure 82. Bearing No. 2, Damaged Outer Race, 6600 RPM.

(0-2 kHz) are presented in Figure 83, which compare with Figures 80 and 81 (b, c and d), and 82 (b and c), respectively.

A number of conclusions can be drawn from this envelope detected data. Apparently, for bearing No. 2, the low-frequency peaks (i.e., 14 kHz) were not modulated by ball-pass to the extent that the higher frequency peaks (i.e., 31 kHz, 39 kHz) were, as shown in Figures 80 and 81. This is demonstrated by the fact that the envelope detection of the high-frequency peaks generally produced distinct ball-pass frequency peaks (518 Hz at 6600 rpm) for both undamaged and damaged bearings. However, no distinct ball-pass frequency peaks were produced by the envelope detection of the low-frequency peaks for even the damaged bearing. It appears that variations in speed, at least for the range covered in the test, had relatively little effect on the envelope detection results (Figures 79a and b). At the higher speed there was an increase in the amplitude of the ball-pass frequency peak. However, this was due to a general increase in excitation rather than to some variation in the consistency of the envelope detection results. The fact that the frequency at which the ball-pass peak occurred is directly proportional to speed further verifies that it is actually a ball-pass frequency that is being observed. Without any load on bearing No. 2, there was virtually no ball-pass frequency peak present in the envelope detected data, even for the damaged bearing (Figures 81a and 82a). However, once a reasonable amount of load was applied (726 lb in this test), a further increase in that load had relatively little effect on the envelope detection results (Figures 79a, 79c and 80c). This is probably due to the fact that a load was required to produce an intimate contact between the rollers and the outer race and thus produce a distinct ball-pass frequency excitation. However, once that contact was ensured, any additional load that was applied to the bearing had no effect on the envelope detection results.

The ball-pass frequencies for bearing No. 2 did not show up in the data from the accelerometer located in the axial direction (Figure 82b). This is not surprising since the motion of the rollers was only in the plane of the bearing and all load and reaction forces exerted on the rollers were exerted in that plane. Since the plane of the bearing was perpendicular to the axial direction, it is not likely that an accelerometer located in the axial direction would have picked up much ball-pass information. In comparing the data from the other two accelerometers, both located in the radial direction, it appeared that accelerometer No. 3 was located in a better position for detecting ball-pass information than was accelerometer No. 2 (Figures 81d and 82c). This was probably due to the fact that accelerometer No. 3 was located nearer the point of loading on the bearing housing. However, the bearings were installed in the housing arbitrarily, with the position of the defect in the damaged bearing not known in relation to the housing orientation. Thus, it is entirely possible that accelerometer No. 3 was also located nearer to the point of the defect, which could account for its more significant ball-pass signals.

A spall which would form in the outer race of a roller bearing during actual operation would probably occur very near the point of loading, since this is where the contact stresses would be the largest. In addition, any spalls which might occur at a distance from the point of loading would

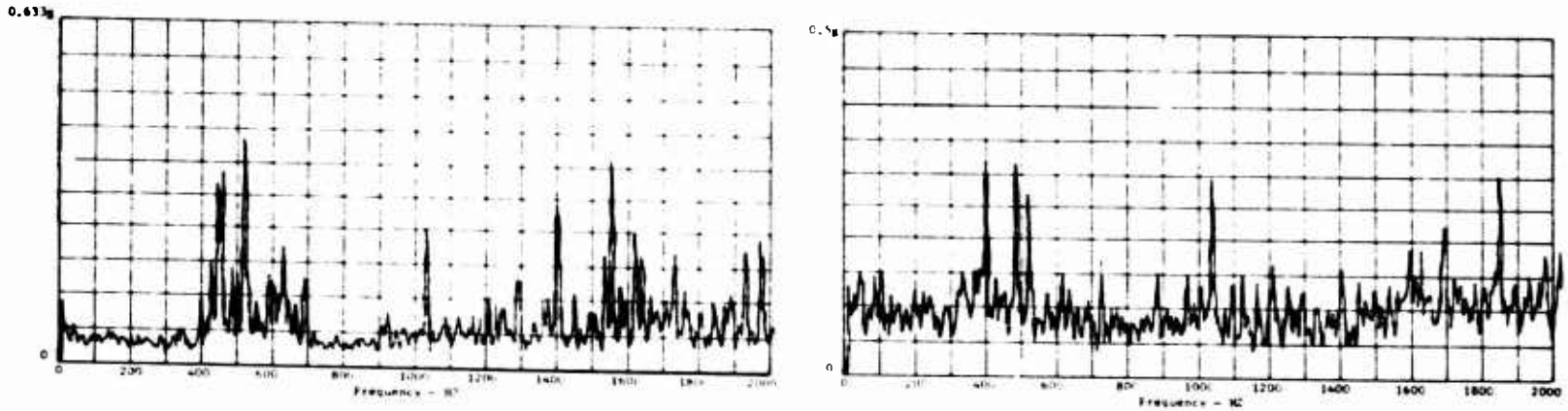

a) Undamaged Bearing

b) Damaged Outer Race Bearing

Figure 83. Bearing No. 2, 6600 RPM, 3633-Lb Load, Accelerometer No. 3, Raw Data.

not be as likely to cause a bearing failure as one in the vicinity of the point of loading. Therefore, since in an operating roller bearing the area of interest on the outer race and the point of loading are the same, the optimum accelerometer location would be in the radial direction as near to the point of loading as possible.

It would not be possible to use the ball-pass frequency peaks found in the raw data of bearing No. 2 to indicate the presence of a bearing defect. In most cases, the ball-pass frequency peaks in the raw data either did not exist or were not at all distinct (Figure 83). In addition, the amplitude of those peaks, when they occurred, did not appear to be at all dependent upon bearing condition. In general, the 39-kHz frequency peak in the bearing No. 2 data gave, through envelope detection, ball-pass frequency amplitudes which seemed to be most consistent and most indicative of bearing condition. The amplitude of the outer race ball-pass frequency peak (518 Hz), from the envelope detected 39-kHz peak, was six times as large for the bearing with the damaged outer race as for the undamaged bearing (Figures 80c and 81d). This was a very significant increase in amplitude.

Bearing No. 3

Bearing No. 3 is also a roller bearing. Most of the low-frequency peaks (below 20-kHz) were probably due to bearing housing resonances. However, some of the lower frequency peaks, notably the 4 kHz and 7.5-kHz peaks, were probably due to bearing outer race resonances. These two peaks apparently resulted from purely circumferential bearing outer race resonances whose wave numbers are four and five, respectively. These resonances were measured at frequencies slightly higher than those predicted because of the foundation stiffness provided by the bearing housing. The peaks found at higher frequencies were most likely also due to bearing outer race resonances.

Some of the frequency spectrum results of the envelope detection analysis of bearing No. 3 are presented in Figure 84. Not more than a trace of ball-pass information was present in even the damaged bearing. The bearings were installed in the housing in an arbitrary direction. Therefore, the lack of ball-pass information from the damaged bearing may have been due to the fact that the bearing was installed with the defect approximately opposite the load. If this were the case, there would not have been an intimate contact between the race defect and the rollers of the bearing. Consequently, any contact between a roller and the defect would not have created a large enough force to substantially excite any race resonances.

However, as previously mentioned in the discussion of the bearing No. 2 analysis, this is not a problem to be concerned about because it is not a situation that would be likely to occur under actual operating circumstances. For comparison, the raw data for one of the radially-mounted accelerometers is plotted on a 2-kHz scale in Figure 85. These spectrums do show slight ball-pass frequency peaks (755 Hz). These peaks have the same amplitude for both the undamaged and damaged bearings, and therefore were apparently not affected by the presence of the artificially induced defect.

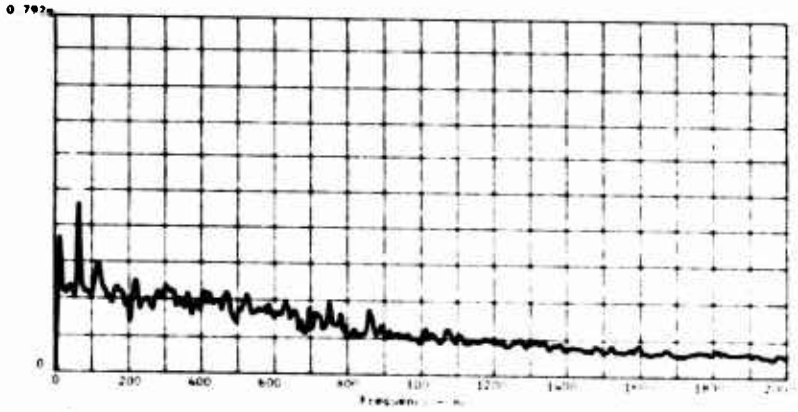

a) Undamaged Bearing, Accelerometer No. 2, Envelope Detected About 31 kHz

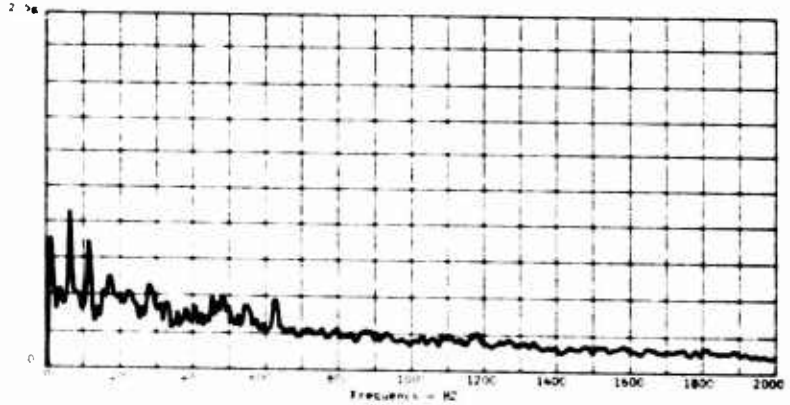

b) Undamaged Bearing, Accelerometer No. 3, Envelope Detected About 48 kHz

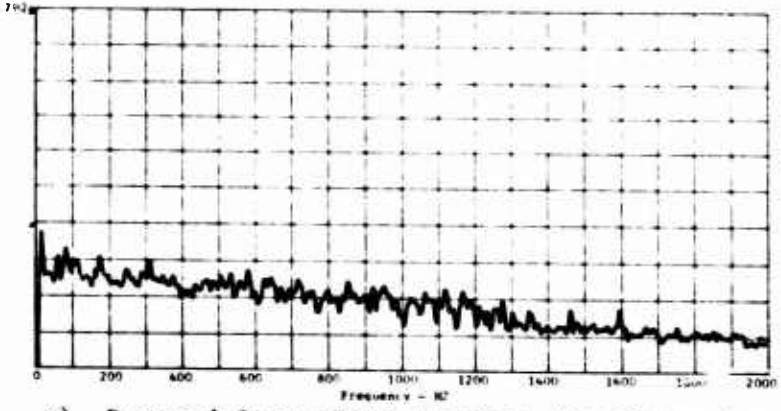

c) Damaged Outer Race Bearing, Accelerometer No. 2, Envelope Detected About 31 kHz

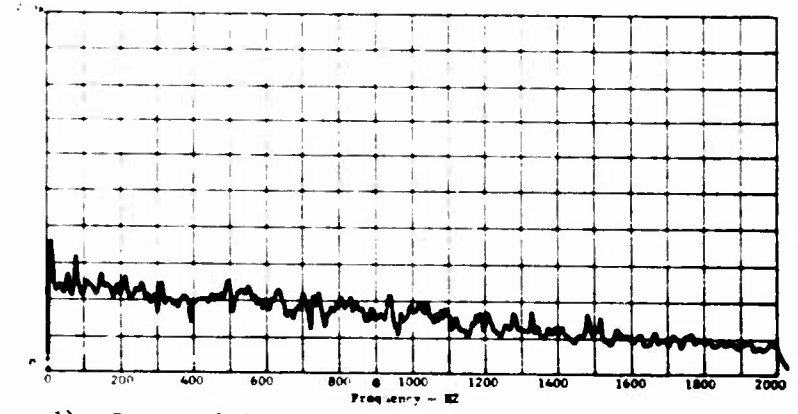

d) Damaged Outer Race Bearing, Accelerometer No. 3, Envelope Detected About 48 kHz

Figure 84. Bearing No. 3, 3050 RPM, 1588-Lb Load.

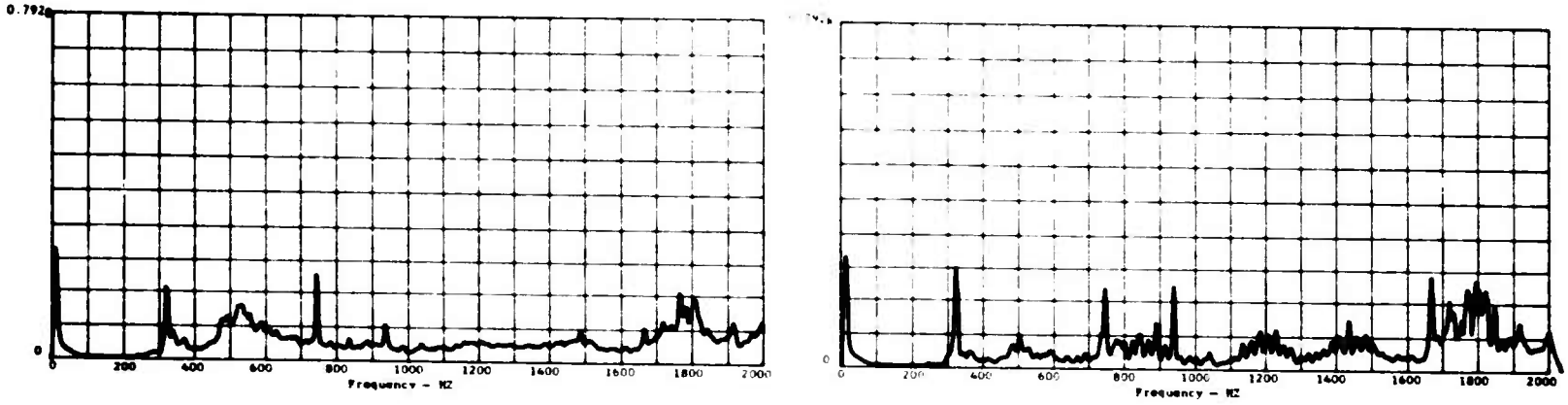

a) Undamaged Bearing

b) Damaged Outer Race Bearing

Figure 85. Bearing No. 3, 3050 RPM, 1588-LB Load, Accelerometer No. 3, Raw Data.

Bearing No. 1

Bearing No. 1 is an angular contact ball bearing. Since the contact between the outer race and the balls under thrust loading was at an angle between the radial and axial directions, it was not surprising to detect significant ball-pass information from both radially and axially mounted accelerometers. This was precisely the case for bearing No. 1.

For this bearing it was found that envelope detecting about the 24-kHz peak gave the best results for the radially mounted accelerometer data, while envelope detecting about the 31-kHz peak gave the best results for the axially mounted accelerometer data. This can be seen from Figures 86 through 88. These two frequency peaks are above the range of predicted race resonances for bearing No. 1. However, like the bearings previously tested, they are probably due to outer race resonances.

Each of the speed, load or housing variations run during the tests was envelope detection analyzed for both the best radial accelerometer case and the best axial accelerometer case. Both radial accelerometers produced roughly equivalent results for the envelope detection analysis of bearing No. 1 about the 24-kHz peak of the raw data. Accelerometer No. 3 (tape channel 6) was arbitrarily chosen to be used for comparison of the test data.

Some of the envelope detected results for this radial accelerometer for the tests run for bearing No. 1 are presented in frequency spectrum form in Figures 89 and 90. These results show some ball-pass information present for the damaged outer race bearing without any load, but it was not very significant (Figure 89a). When this same bearing was lightly loaded (less than 200 pounds radial and thrust), the amplitude of the outer race ball-pass frequency peak (690 Hz at 6600 rpm) increased substantially, though not as much as for the fully loaded case (Figures 89c and 88b). Either a radial or a thrust load by itself also increased the amplitude of this peak significantly (Figures 89b and d). These results also showed that under full load conditions, the ball-pass peak for the damaged outer race bearing is of considerably larger amplitude when run at 4400 rpm (460 Hz) than when run at 6600 rpm (Figures 88b and 90a). Apparently, for bearing No. 1, when the balls traveled across the artificially induced defect in the outer race at roughly two-thirds of full speed, they did a better job of forcing the 24-kHz race resonance. However, even at full speed, the ball-pass frequency peak for the damaged outer race bearing had a much larger amplitude than that for the undamaged bearing (Figures 88a and b). The results obtained for the tests with the various bearing housings were almost identical (Figures 88b, 90b and c). Therefore, the housings tested did not seem to have any effect on the transmission of ball-pass information in the radial direction with respect to the location of accelerometer No. 3. The inner race ball-pass frequency peak (960 Hz) did not show up at all in the results from the undamaged bearing (Figure 88a). However, this peak showed up very distinctly in the results from the damaged inner race bearing (Figure 88c).

Some of the envelope detected results for the axially mounted accelerometer

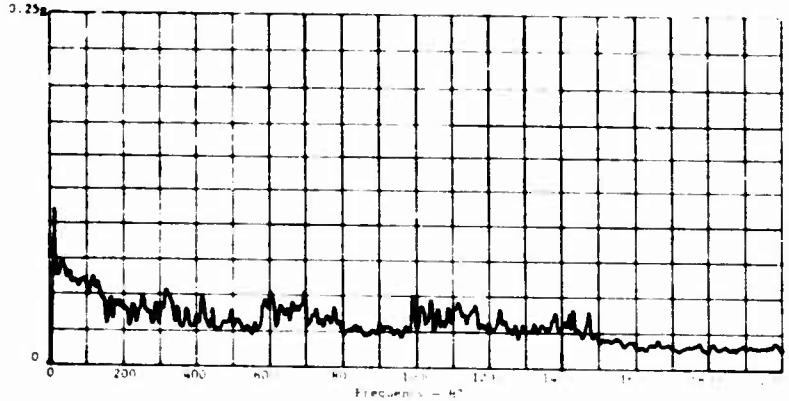

a) Undamaged Bearing

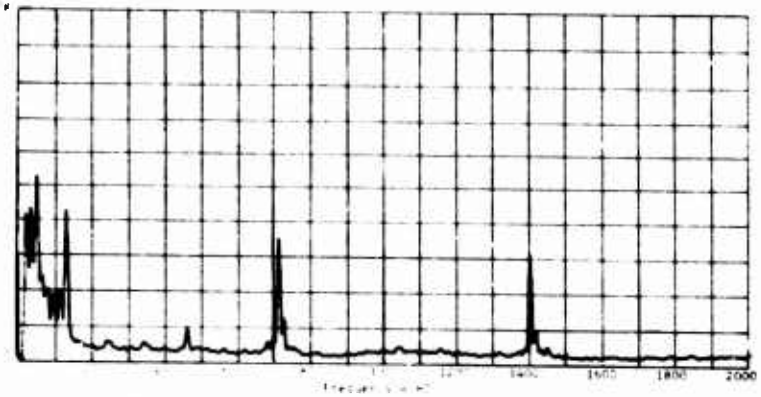

b) Damaged Outer Race Bearing

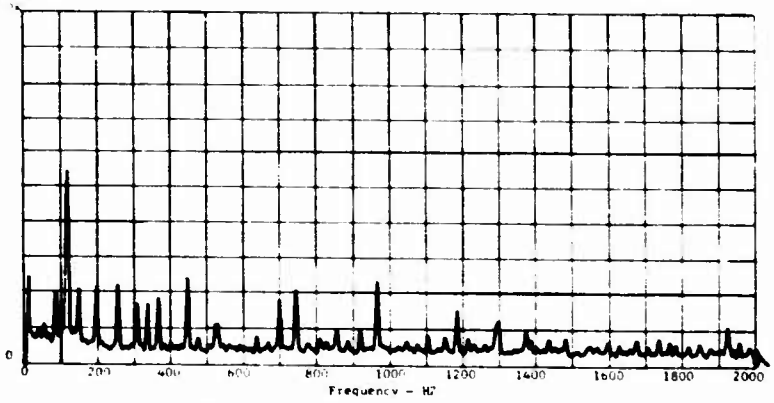

c) Damaged Inner Race Bearing

Figure 86. Bearing No. 1, 6600 RPM, 2860-Lb Radial Load, 4632-Lb Thrust Load, Heavyweight Housing, Accelerometer No. 1, Envelope Detected About 31 kHz.

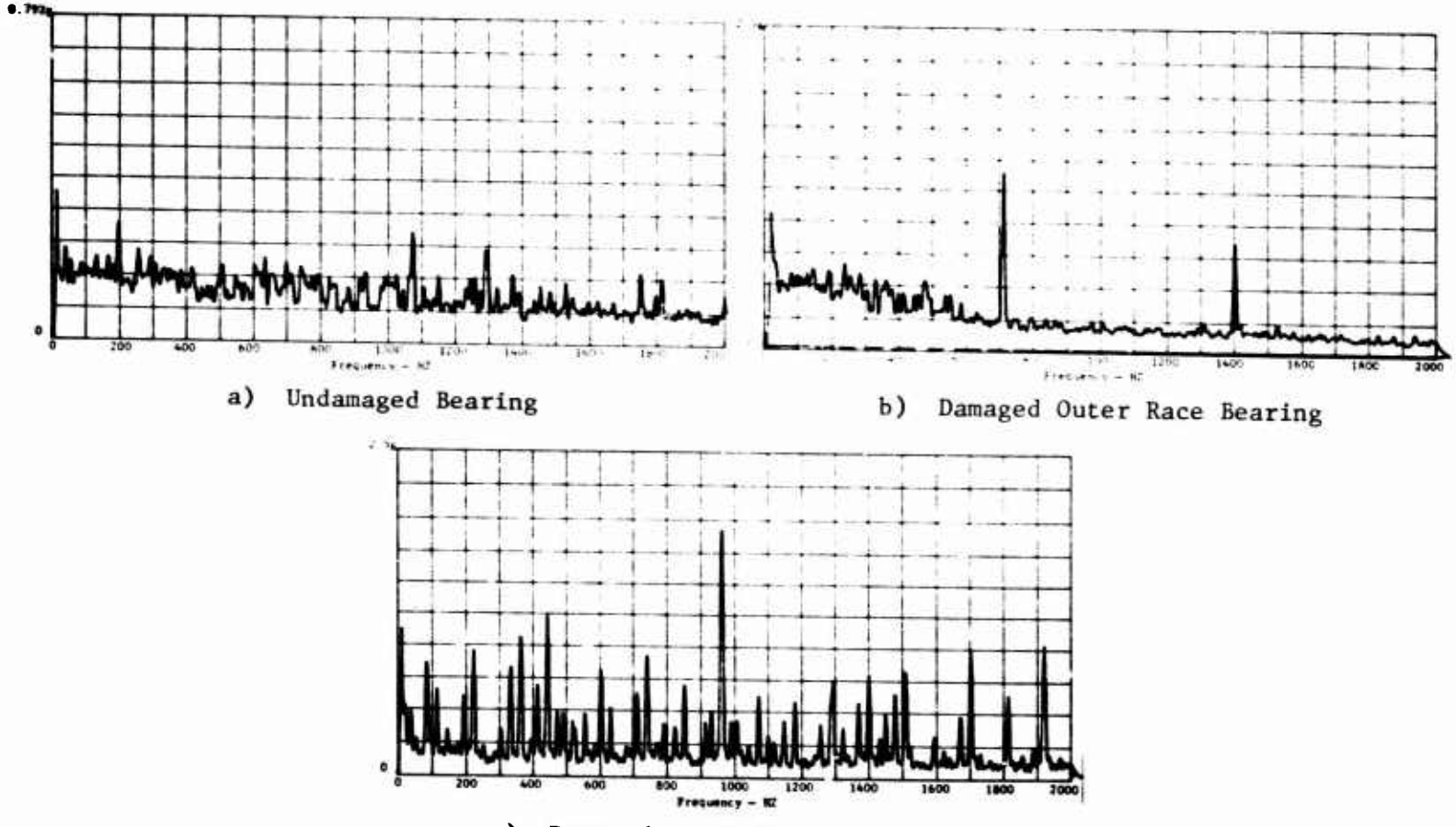

a) Undamaged Bearing

b) Damaged Outer Race Bearing

c) Damaged Inner Race Bearing

Figure 87. Bearing No. 1, 6600 RPM, 2860-Lb Radial Load, 4632-Lb Thrust Load, Heavyweight Housing, Accelerometer No. 2, Envelope Detected About 24 kHz.

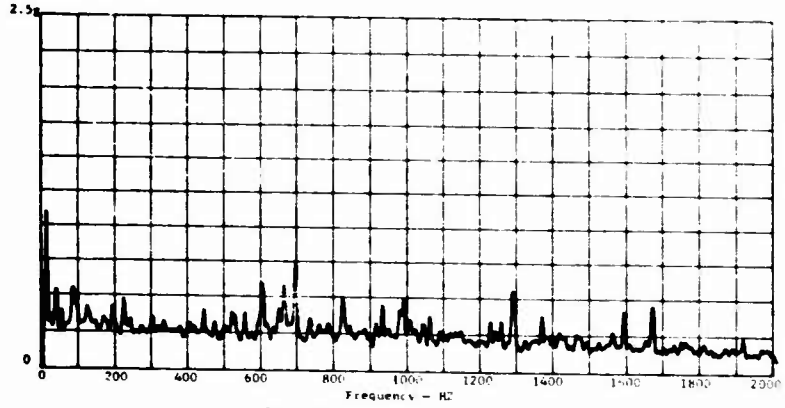

a) Undamaged Bearing

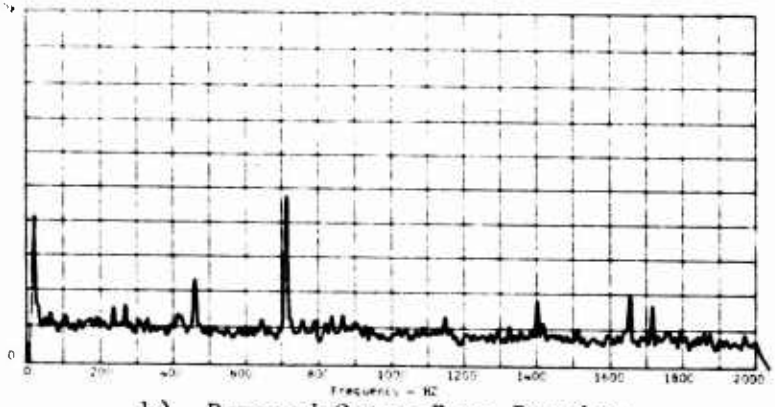

b) Damaged Outer Race Bearing

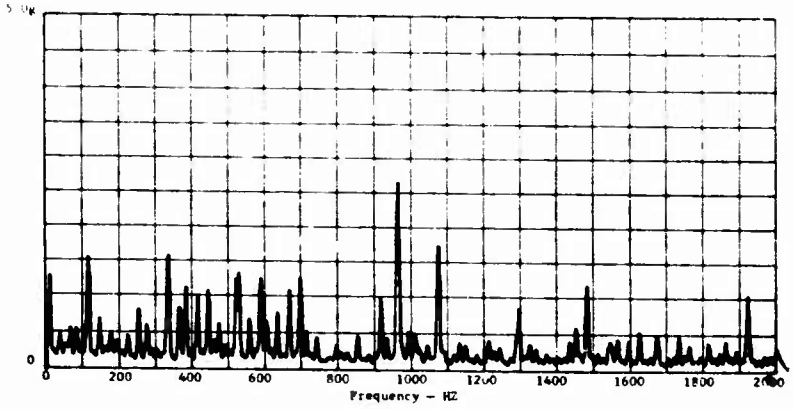

c) Damaged Inner Race Bearing

Figure 88. Bearing No. 1, 6600 RPM, 2860-Lb Radial Load, 4632-Lb Thrust Load, Heavyweight Housing, Accelerometer No. 3, Envelope Detected About 24 kHz.

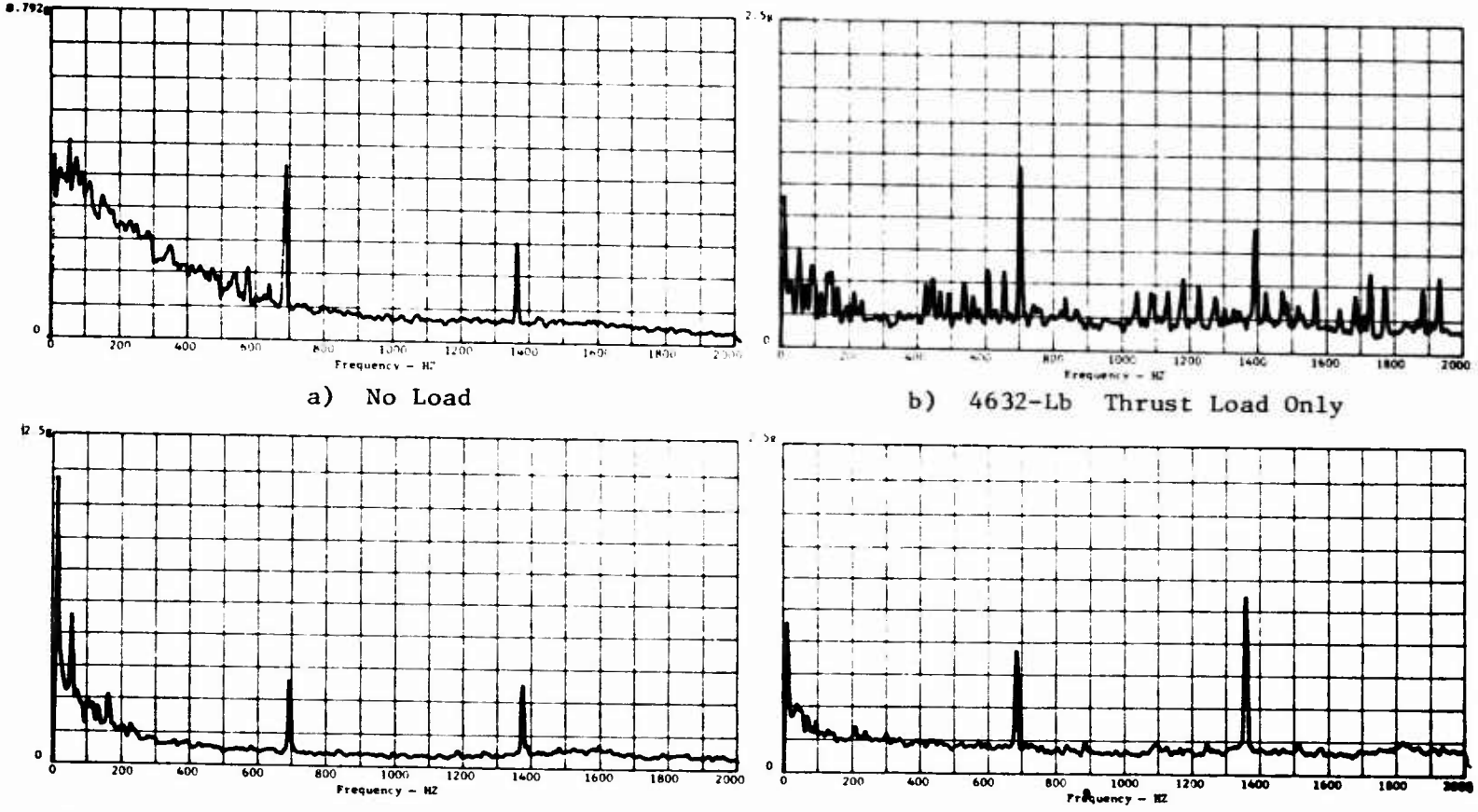

a) No Load

b) 4632-Lb Thrust Load Only

c) 198-Lb Radial Load, 192-Lb Thrust Load

d) 2860-Lb Radial Load Only

Figure 89. Bearing No. 1, Damaged Outer Race, 6600 RPM, Heavyweight Housing, Accelerometer No. 3, Envelope Detected About 24 kHz.

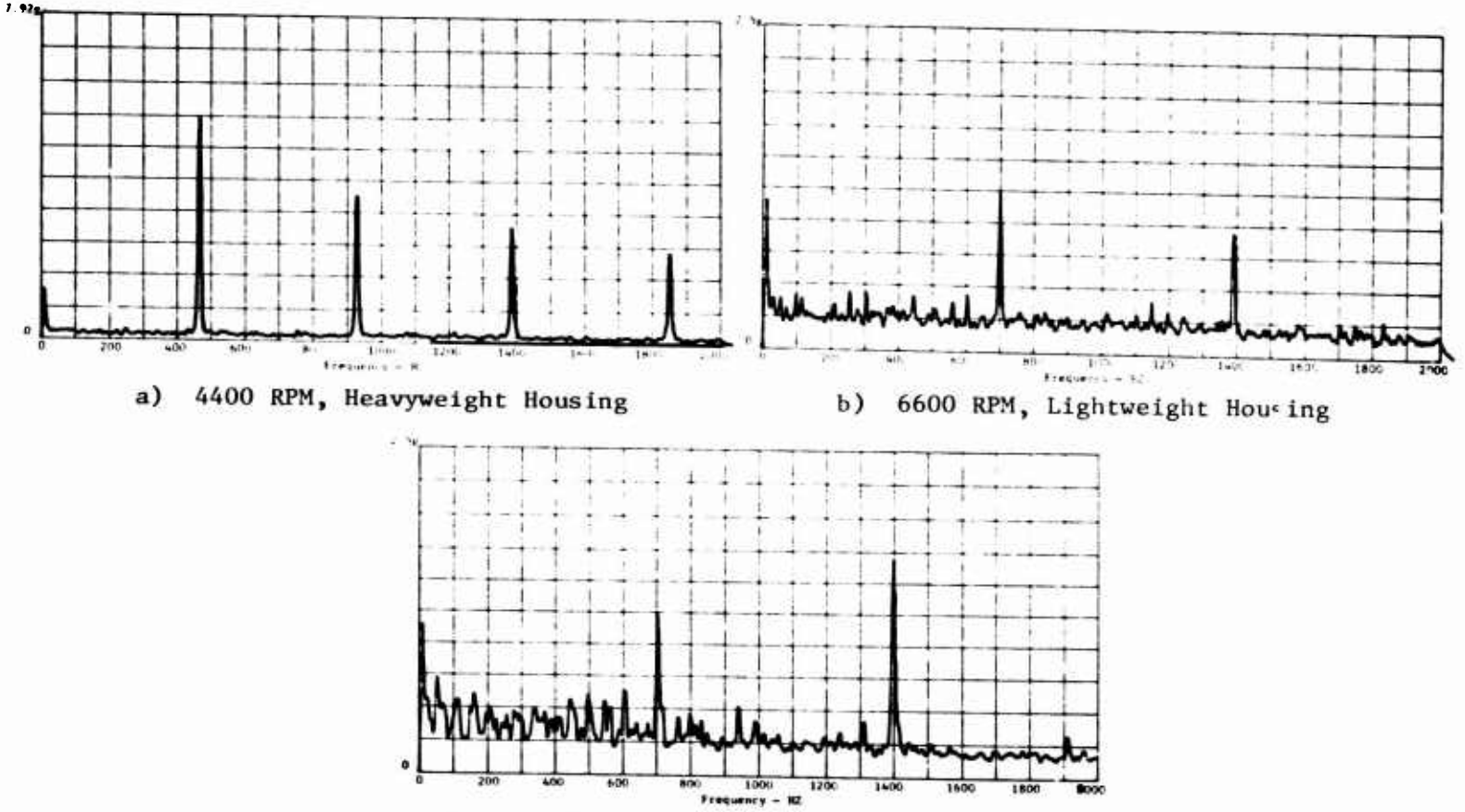

a) 4400 RPM, Heavyweight Housing

b) 6600 RPM, Lightweight Housing

c) 6600 RPM, Lightweight Flexible Housing

Figure 90. Bearing No. 1, Damaged Outer Race, 2860-Lb Radial Load, 4632-Lb Thrust Load, Accelerometer No. 3, Envelope Detected About 24 kHz.

for the same tests are presented in Figures 91 and 92. Similar to the results for the radial accelerometer, there was some ball-pass information present for the damaged outer race bearing without any load, and a light load (radial and thrust) increased that ball-pass peak significantly (Figures 91a and c). However, for the axial accelerometer, a radial load alone did not increase that peak, while a thrust load alone did (Figures 91d and b). This is reasonable, since with a radial load and no thrust load, the contact of the balls with the outer race was almost in a radial direction. Whereas, with a thrust load applied, this contact was at an angle roughly 30 degrees from radial. The results from the full load speed variations for the axial accelerometer show that there is a slight decrease in the amplitude of the ball-pass frequency peak when the speed of rotation is decreased (Figures 86b and 92a). This was probably as a result of a slight decrease in excitation force at the lower speeds. The amplitude of the ball-pass frequency peaks was slightly smaller for the tests run with the lightweight bearing housing and lightweight flexible housing than for the tests run with the heavyweight housing (Figures 86b, 92b and c). However, the results for the lightweight housing test were the same as for the lightweight flexible housing test. The only difference in the designs of these two housings was the holes drilled in the web of the lightweight flexible housing to make it flexible. Therefore, it appears that the lightweight housings did not transmit the ball-pass information as well in the axial direction as did the heavyweight housing. However, the holes in the lightweight flexible housing did not seem to make any difference. The ball-pass frequency peak for the inner race of bearing No. 1 did not show up at all in the results for the undamaged bearing from the axial accelerometer data (Figure 86a). This peak did show up in the results for the bearing with the damaged inner race (Figure 86c). However, it did not show up nearly as well for the data from the axial accelerometer as it did for the data from the radial accelerometer.

For comparison, some of the raw data for bearing No. 1 was plotted on a 2-kHz scale in Figure 93. The inner race ball-pass frequency peak (960 Hz) did not show up even for the bearing with the damaged inner race (Figure 93c). The outer race ball-pass frequency (690 Hz) did show up, but its amplitude was not indicative of bearing condition (Figures 93a and b). It appears that the 24-kHz peak from the radial accelerometer data was the best to analyze when concerned with the condition of the inner race of bearing No. 1 (Figure 88). Either the same peak or the 31-kHz peak from the axial accelerometer data was good to analyze when concerned with the condition of the outer race of bearing No. 1 (Figures 86 and 88). Using the radial accelerometer data and rotating the bearing at about 4400 rpm seemed to give the best results.

Bearing No. 4

Bearing No. 4 is also an angular contact ball bearing. The results of the envelope detection analysis for this bearing showed that ball-pass information could be found in both the radial and the axial accelerometer data. Some of these results are presented in frequency spectrum form in Figures 94 through 96. This bearing is found in a UH-1 helicopter transmission in a duplex set. Each member of the set undergoes a slightly different

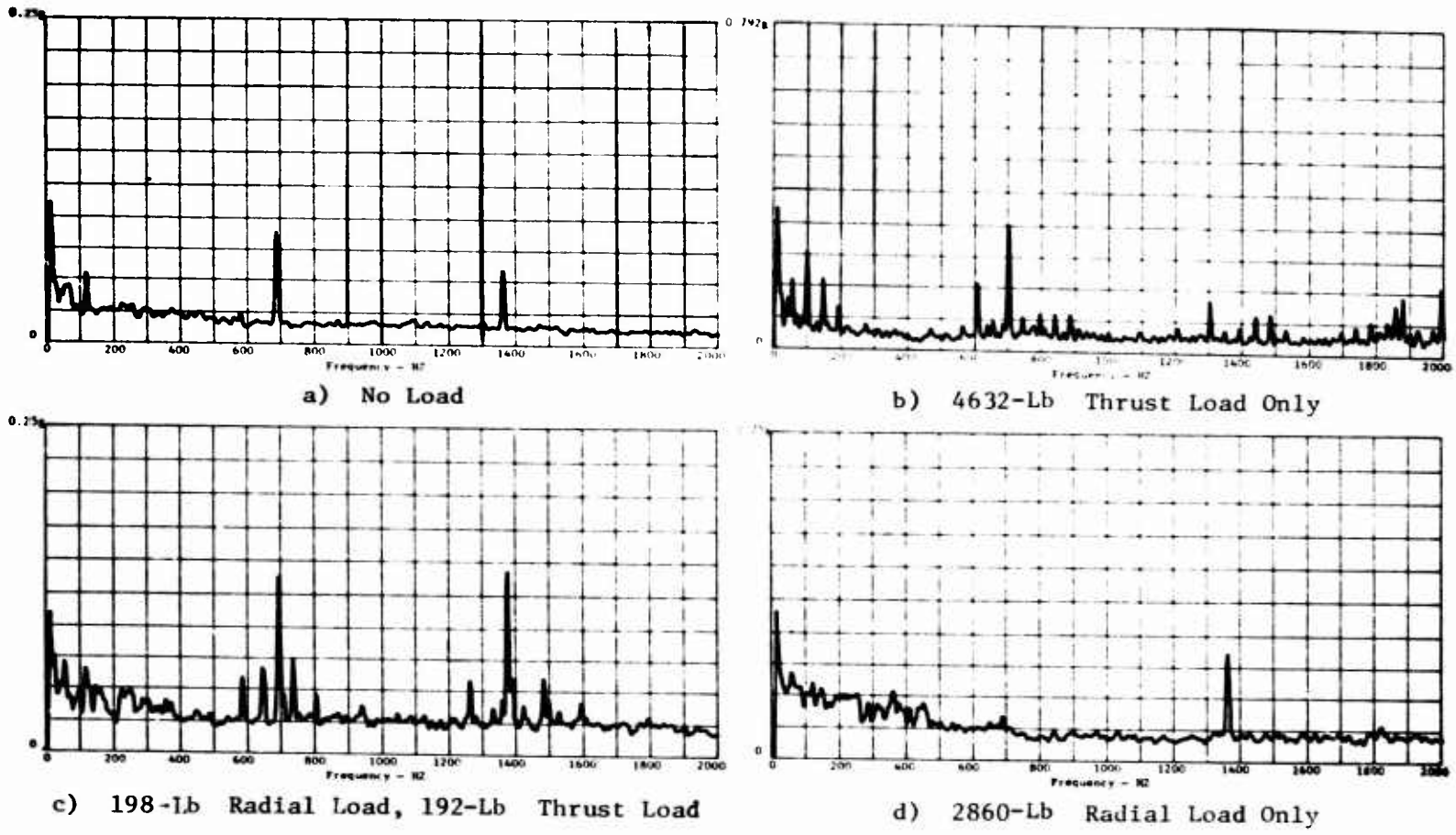

Figure 91. Bearing No. 1, Damaged Outer Race, 6600 RPM, Heavyweight Housing, Accelerometer No. 1, Envelope Detected About 31 kHz.

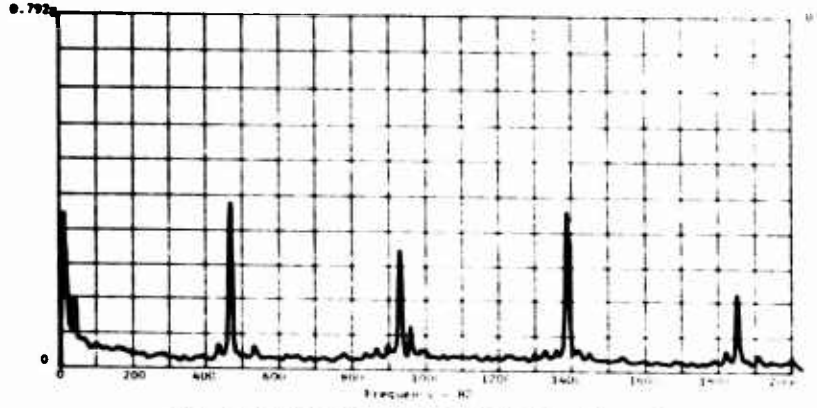

a) 4400 RPM, Heavyweight Housing

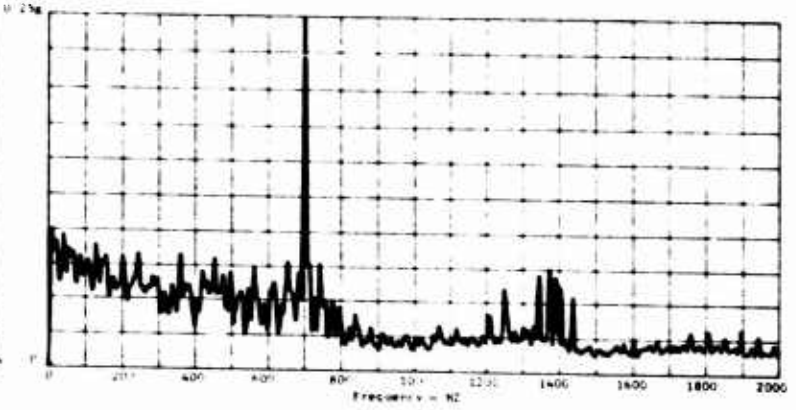

b) 6600 RPM, Lightweight Housing

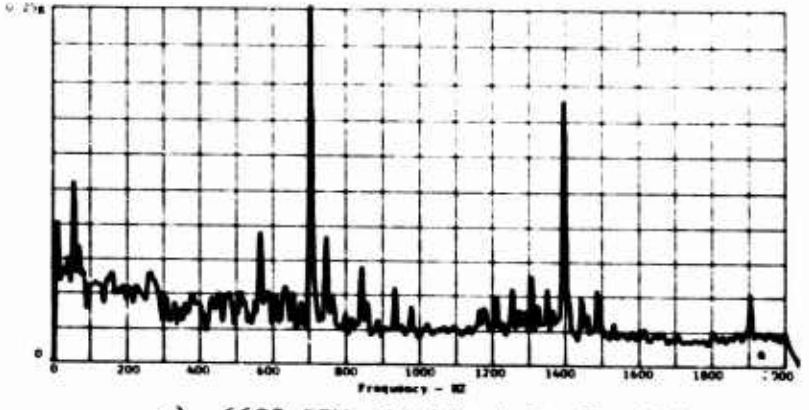

c) 6600 RPM, Lightweight Flexible Housing

Figure 92. Bearing No. 1, Damaged Outer Race, 2860-Lb Radial Load, 4632-Lb Thrust Load, Accelerometer No. 1, Envelope Detected About 31 kHz.

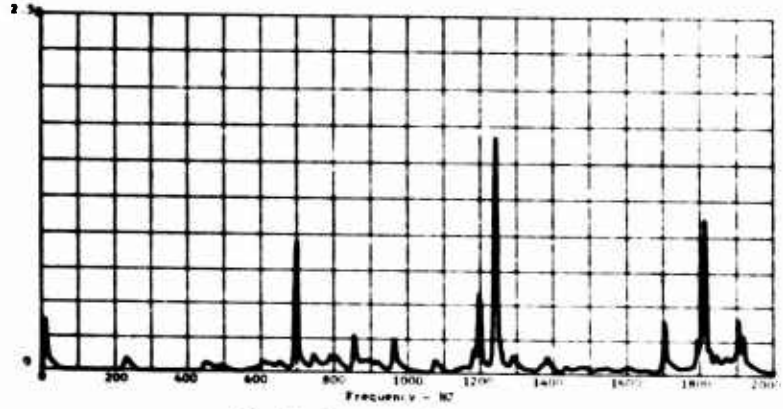

a) Undamaged Bearing

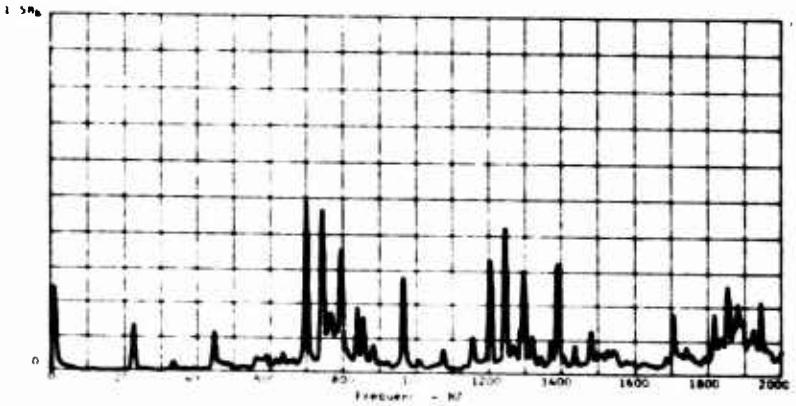

b) Damaged Outer Race Bearing

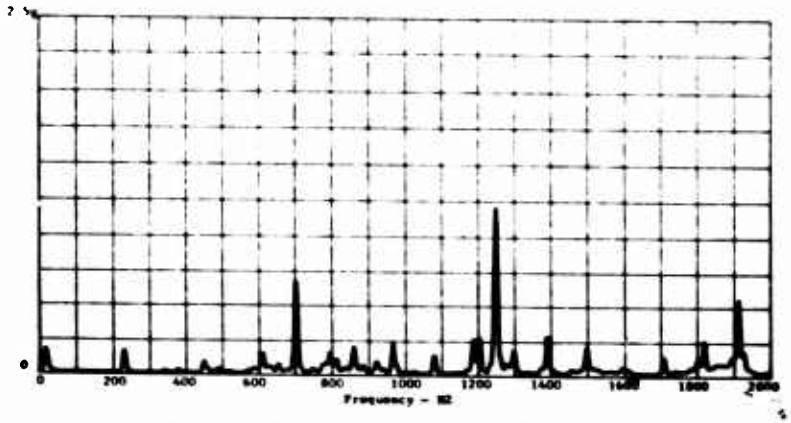

c) Damaged Inner Race Bearing

Figure 93. Bearing No. 1, 6600 RPM, 2860-Lb Radial Load, 4632-Lb Thrust Load, Heavyweight Housing, Accelerometer No. 1, Raw Data.

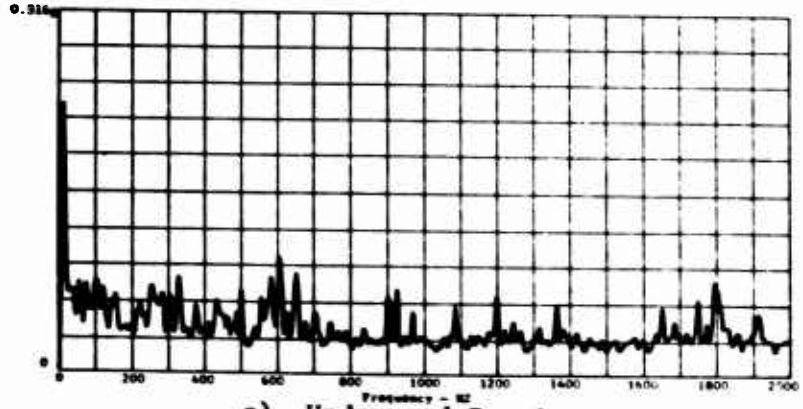

a) Undamaged Bearing

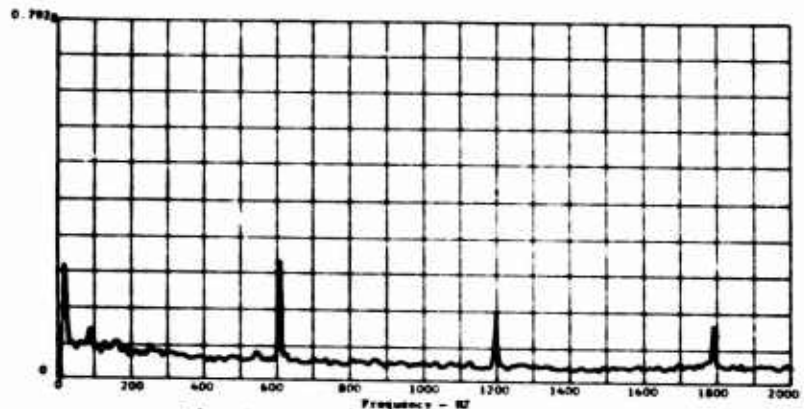

b) Damaged Outer Race Bearing

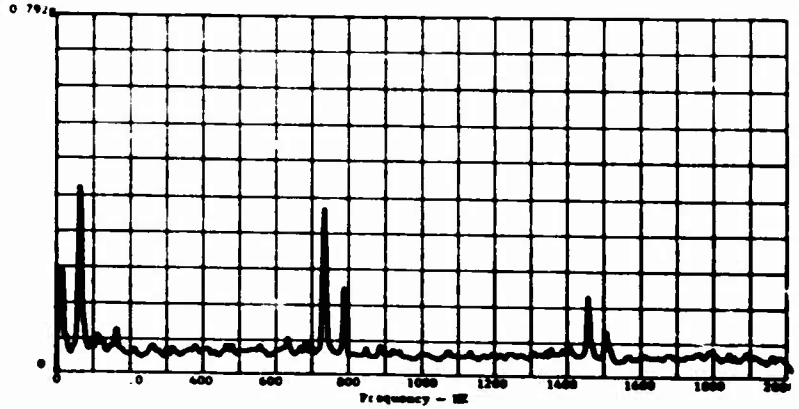

c) Damaged Inner Race Bearing

Figure 94. Bearing No. 4, 3050 RPM, 2134-Lb Radial Load, 1303-Lb Thrust Load, Heavyweight Housing, Accelerometer No. 2, Envelope Detected About 40 kHz.

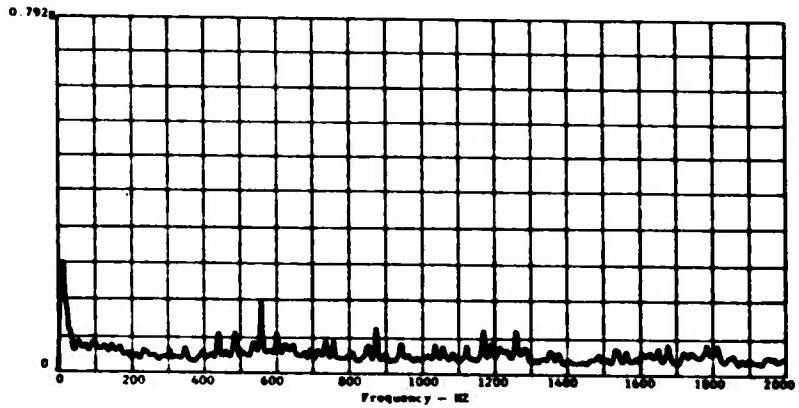

a) Undamaged Bearing, Heavyweight Housing

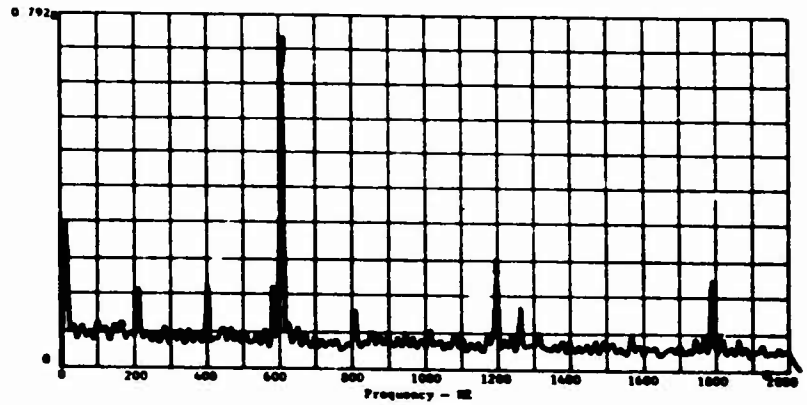

b) Damaged Outer Race Bearing, Lightweight Housing

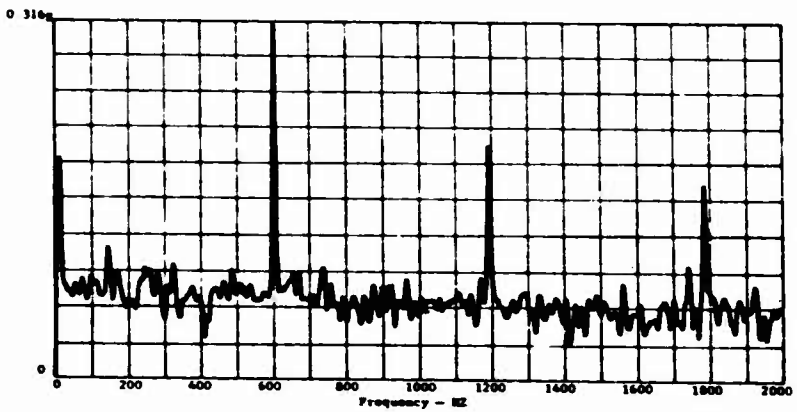

c) Damaged Outer Race Bearing, Heavyweight Housing

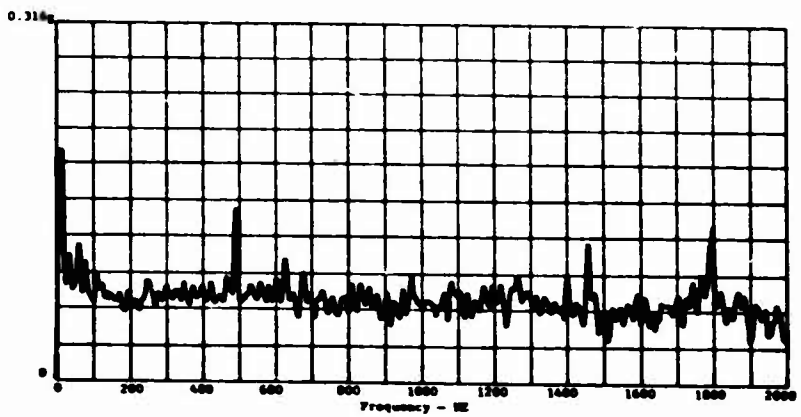

d) Damaged Outer Race Bearing, Lightweight Flexible Housing

Figure 95. Bearing No. 4, 3050 RPM, 2668-Lb Radial Load, 1856-Lb Thrust Load, Accelerometer No. 2, Envelope Detected About 40 kHz.

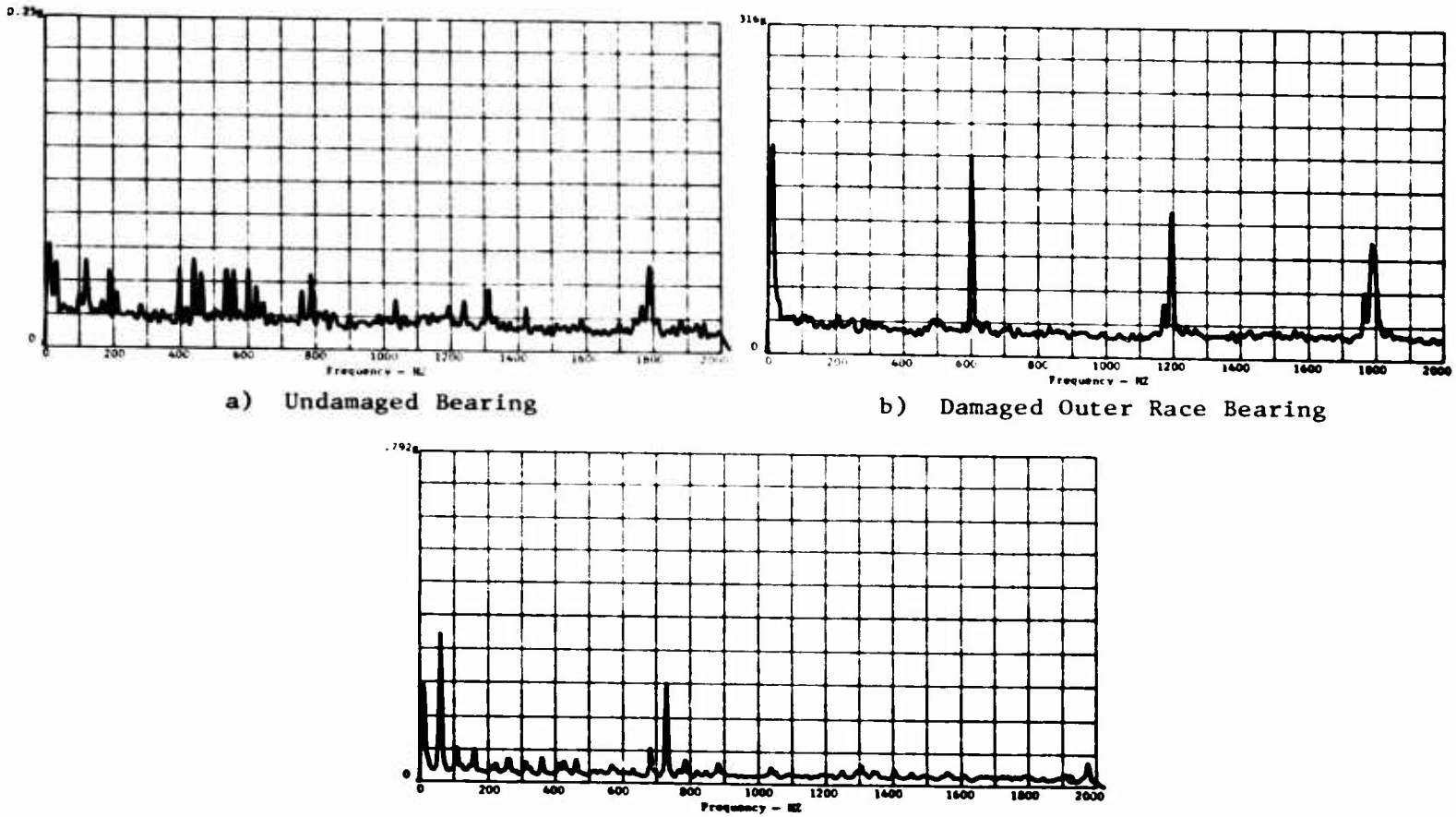

a) Undamaged Bearing

b) Damaged Outer Race Bearing

c) Damaged Inner Race Bearing

Figure 96. Bearing No. 4, 3050 RPM, 2668-Lb Radial Load, 1856-Lb Thrust Load, Heavyweight Housing, Accelerometer No. 1, Envelope Detected About 40 kHz.

combination of loads. Both sets of loads were used during the course of the tests. These different loads did not produce any significant difference in the test results (Figures 94b and 95c). The best frequency peak for envelope detection analysis was found to be 40-kHz for both the radial and the axial accelerometer data. This peak was probably due to a race resonance. However, it is above the range of the race resonances predicted. Outer race ball-pass information was easily found from both the radial and the axial data. However, the radial data was less affected by the type of bearing housing than the axial data was. The axial data appears to contain clearer inner race ball-pass information than the radial data, however (Figures 94c and 96c). For comparison, some of the raw data for bearing No. 4 is plotted on a 2-kHz scale in Figure 97. In this raw data, the outer race ball-pass frequency peak (606 Hz) had a lower amplitude for the damaged outer race bearing than for the undamaged bearing (Figures 97b and c). This raw data also did not show any significant inner race ball-pass frequency peak (732 Hz) for even the damaged inner race bearing (Figure 97d). Therefore, the raw data did not yield any information indicative of bearing condition.

Bearing No. 5

Bearing No. 5 is a split inner race ball bearing. During the tests, this bearing was rotated at only 324 rpm. Therefore, the contact between the balls and the race defects were of a much longer duration than for the other bearings that were tested. As a result, the higher race resonance frequencies were not modulated by ball-pass excitation to the extent that the lower frequencies were. The outer race ball-pass information was best found from envelope detection of the 5.8-kHz peak in the raw data (Figure 98). This peak appears to correspond to the outer race resonance of bearing No. 5 whose circumferential wave number is three and which has a single axial node, as predicted in Figure 24. The outer race ball-pass information was only present in the signals from the radially mounted accelerometers. Envelope detection of the 19-kHz peak produced the strongest inner race ball-pass signal (Figure 99). This peak appears to correspond to the outer race resonance of bearing No. 5 whose circumferential wave number is six and which has no axial nodes, as predicted in Figure 27. The inner race ball-pass information (61 Hz) was present in the signals from both the radially and axially mounted accelerometers. However, this ball-pass signal was slightly stronger in the axial data than in the radial data. The outer race ball-pass frequency peak (47 Hz) was reduced slightly and about equally in the data from the tests with the lightweight bearing housing and lightweight flexible housing. For comparison, some of the raw data for bearing No. 5 is plotted on a 200-Hz scale in Figure 100. None of this raw data has any truly distinct ball-pass frequency peaks, even for the cases with the damaged bearings.

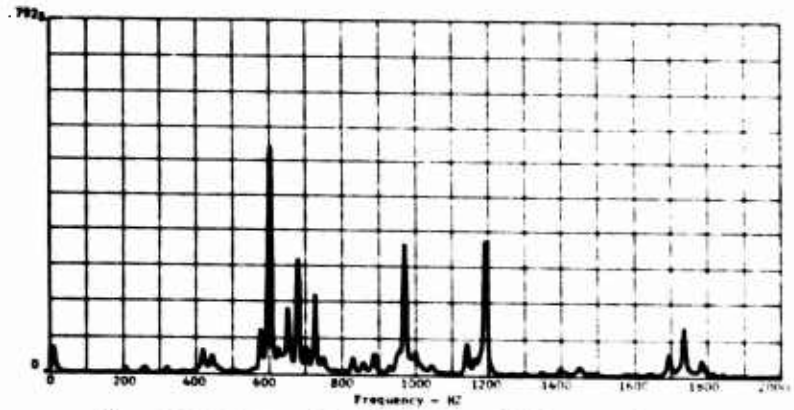

a) Accelerometer No. 1, Undamaged Bearing

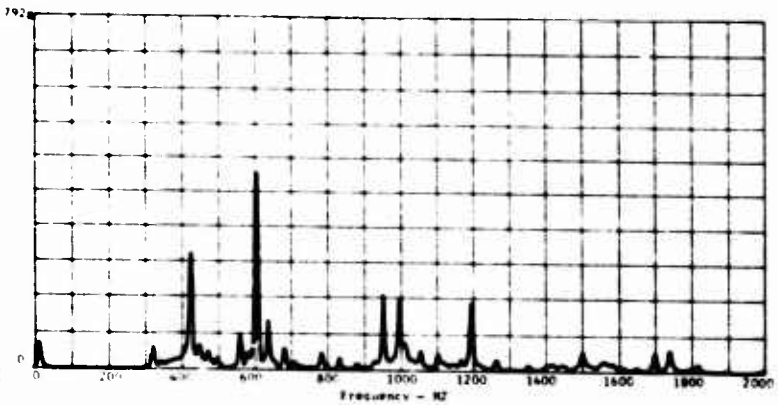

b) Accelerometer No. 2, Undamaged Bearing

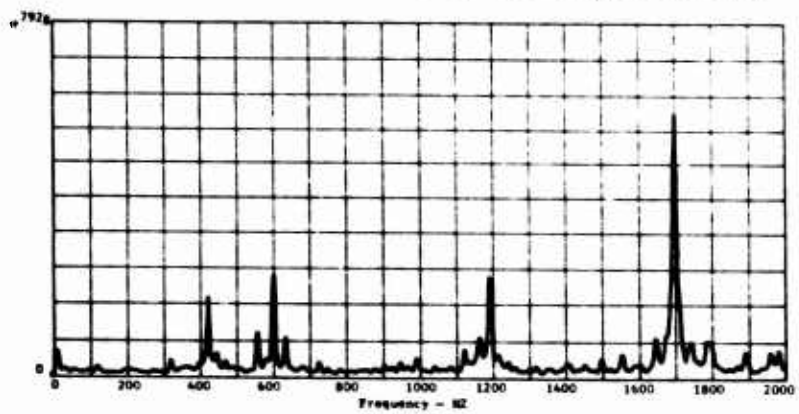

c) Accelerometer No. 2, Damaged Outer Race Bearing

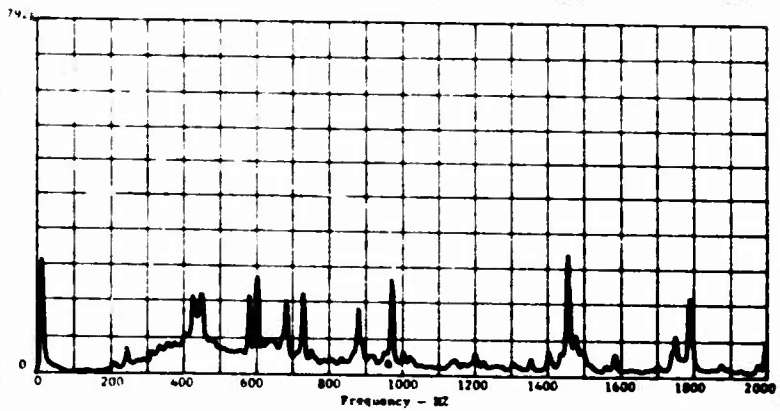

d) Accelerometer No. 1, Damaged Inner Race Bearing

Figure 97. Bearing No. 4, 3050 RPM, 2668-Lb Radial Load, 1856-Lb Thrust Load, Heavyweight Housing, Raw Data.

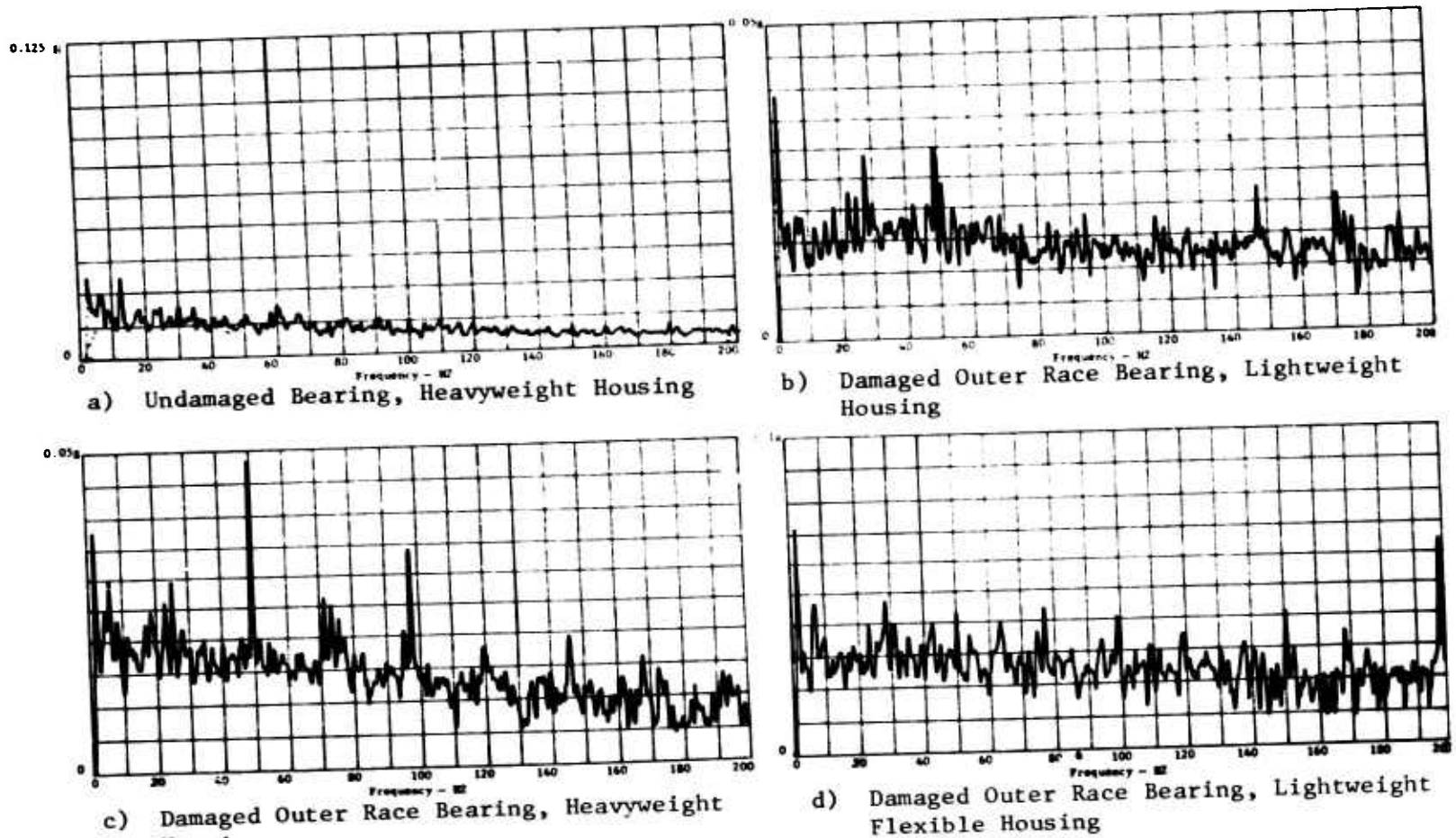

a) Undamaged Bearing, Heavyweight Housing

b) Damaged Outer Race Bearing, Lightweight Housing

c) Damaged Outer Race Bearing, Heavyweight Housing

d) Damaged Outer Race Bearing, Lightweight Flexible Housing

Figure 98. Bearing No. 5, 324 RPM, 2000-Lb Radial Load, 5000-Lb Thrust Load, Accelerometer No. 3, Envelope Detected About 5.8 kHz.

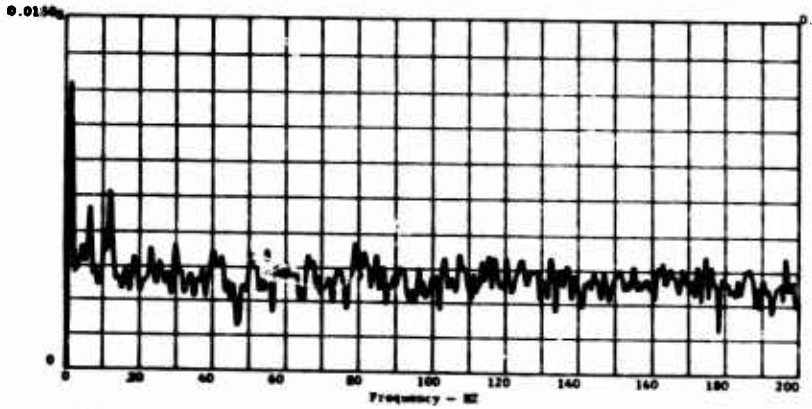

a) Undamaged Bearing, Accelerometer No. 1

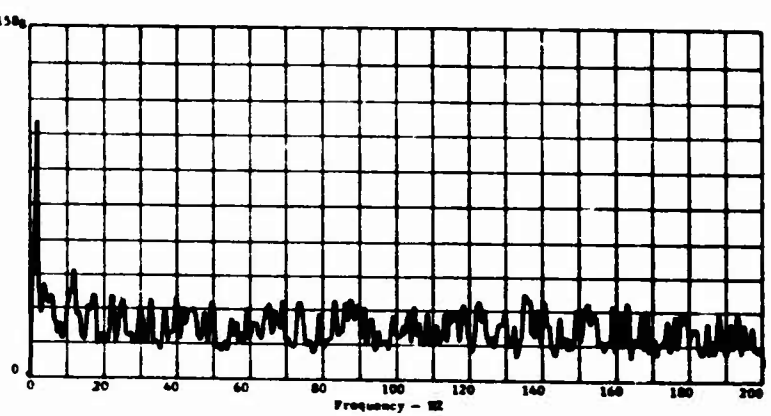

b) Undamaged Bearing, Accelerometer No. 3

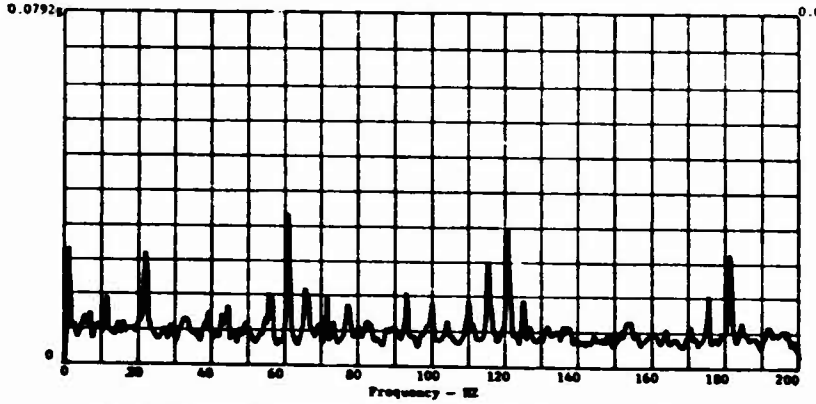

c) Damaged Inner Race Bearing, Accelerometer No. 1

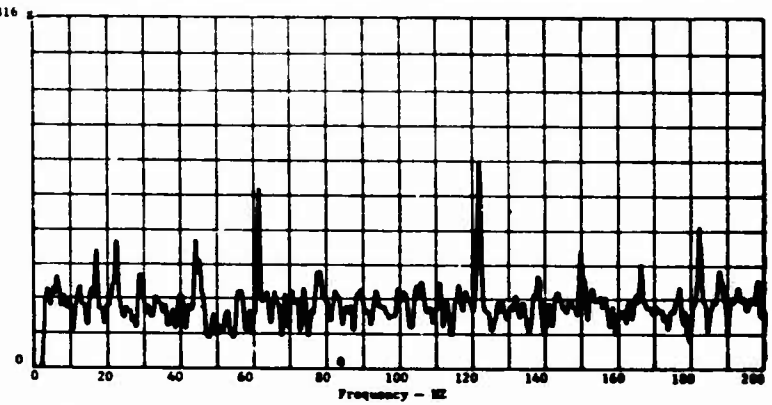

d) Damaged Inner Race Bearing, Accelerometer No. 3

Figure 99. Bearing No. 5, 324 RPM, 2000-Lb Radial Load, 5000-Lb Thrust Load, Heavyweight Housing, Envelope Detected About 19 kHz.

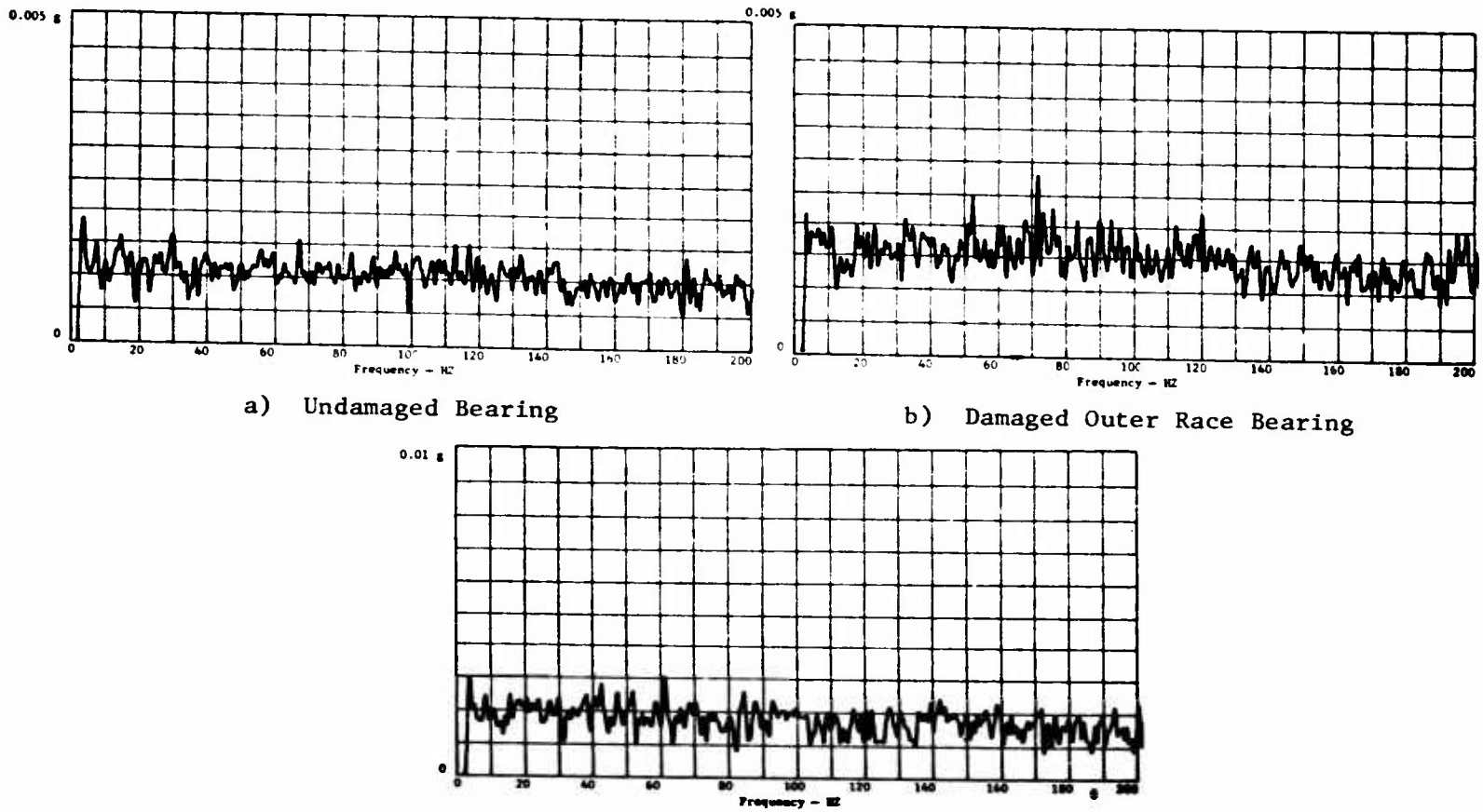

a) Undamaged Bearing

b) Damaged Outer Race Bearing

c) Damaged Inner Race Bearing

Figure 100. Bearing No. 5, 324 RPM, 2000-Lb Radial Load, 5000-Lb Thrust Load, Heavyweight Housing, Accelerometer No. 3, Raw Data.

MEASUREMENT OF BACKGROUND VIBRATION LEVELS IN UH-1 HELICOPTERS

In considering the practical problem of applying the high frequency resonance technique to an actual bearing system, a certain amount of experimental investigation such as that reported herein must be done in determining how the defect characteristic frequency components are to be extracted from the system vibrations. The total vibrations produced by the system, including background vibrations, carry the information to be extracted by the HFRT. The vibration levels vary according to the location at which they are being measured. It would thus be preferable to try to select the measurement location as close to the particular bearing being monitored as possible. This would make it generally less difficult to extract the defect information for that bearing from the overall vibration. However, transmission of bearing information can be dependent upon material interfaces and other less predictable factors, as well as location. Consequently, it is beneficial to measure background vibration levels at several locations around each bearing in order to determine the best sensor location for each bearing. This is especially true when dealing with a system as complex as a helicopter transmission.

DESCRIPTION OF INVESTIGATIVE PROCEDURE

Background vibration levels were recorded externally on the transmission of a UH-1H helicopter at the Logistics Branch of the USAAMRDL Eustis Directorate at Fort Eustis, Virginia.

Four accelerometers were used for each test run in order to determine the optimum location for measuring vibration levels for each bearing. The signals from the four accelerometers were recorded simultaneously on a multichannel tape recorder with a tape speed of 30 inches per second. Tests were run with the accelerometers located on the external surface of the transmission, yet as near as possible to each bearing, and for a variety of engine speeds for each location. A sketch of the transmission, as seen from the rear, is presented in Figure 101. The accelerometer locations are shown in Figures 102 through 105, as referenced in Figure 101. The numbers on the accelerometers refer to the channels on which the signals were recorded. All tests were run with zero collective pitch. Consequently, there was zero lift, leaving friction and windage losses and component weight as the only loads. Eleven separate tests were run.

In the MTI Analysis Center, the recorded data was evaluated by a real-time frequency spectrum analyzer in order to determine the frequency content of the accelerometer signals. In the course of this analysis, the data tape was played back at a tape speed of 7.5 inches per second. By playing the tape back at one-fourth the speed at which the data on it was recorded, all of the playback frequencies were one-fourth of their corresponding recorded frequencies. In this way, even though the maximum range of the real-time frequency spectrum analyzer was only 20-kHz, the actual accelerometer signals could be analyzed up to 80-kHz.

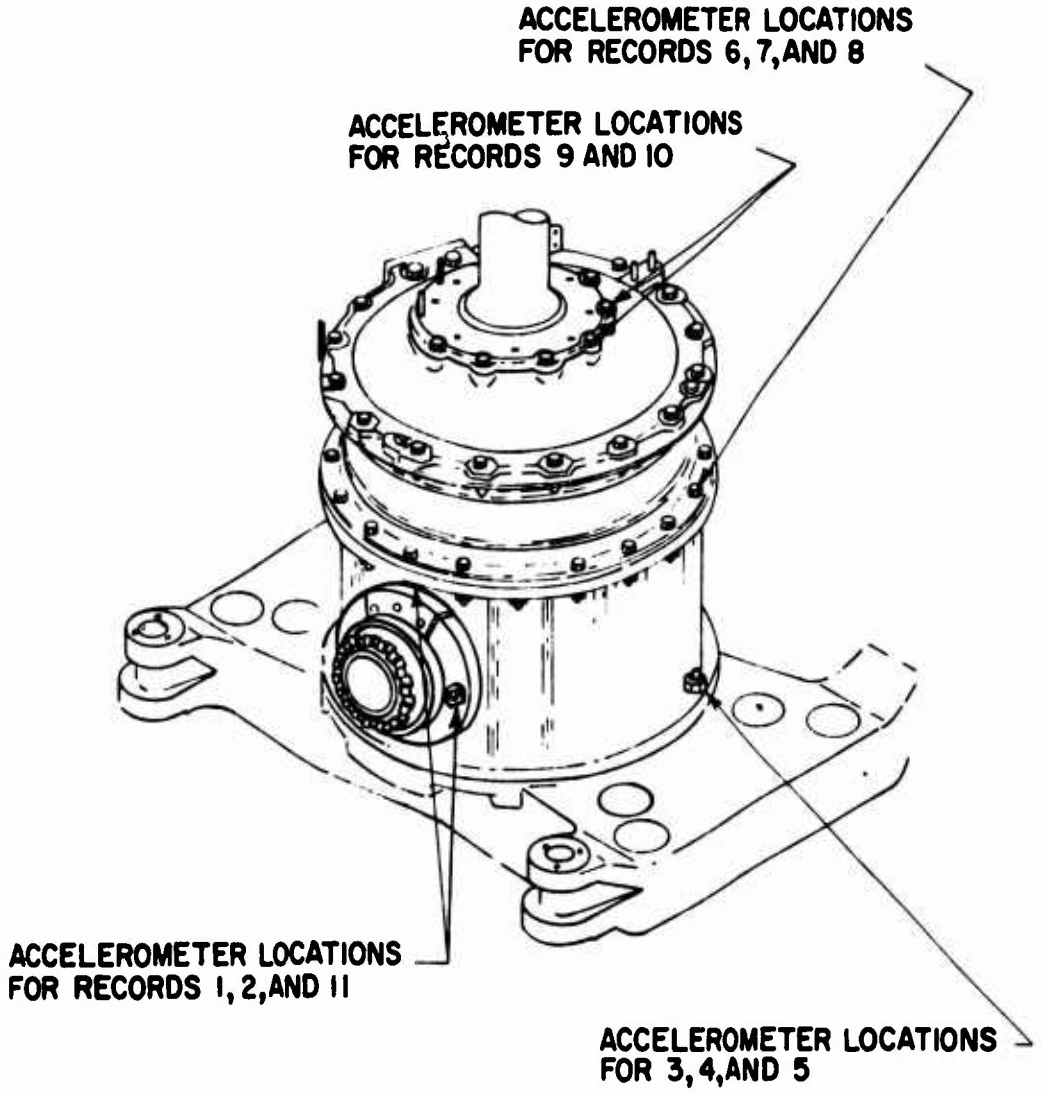

Figure 101. Sketch of UH-1 Helicopter Transmission and General Accelerometer Locations.

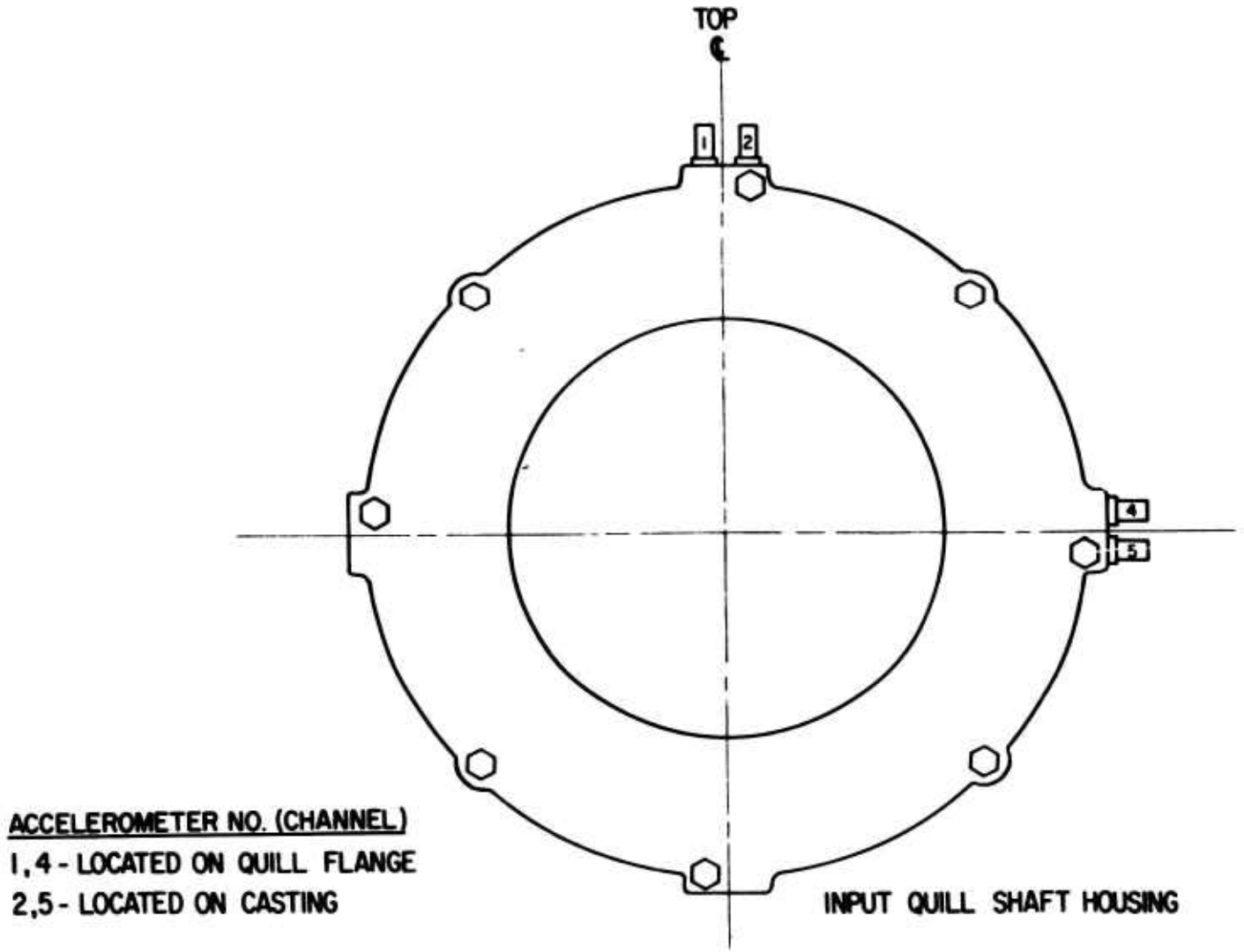

Figure 102. Accelerometer Location on UH-1 Helicopter Transmission for Records 1, 2, and 11.

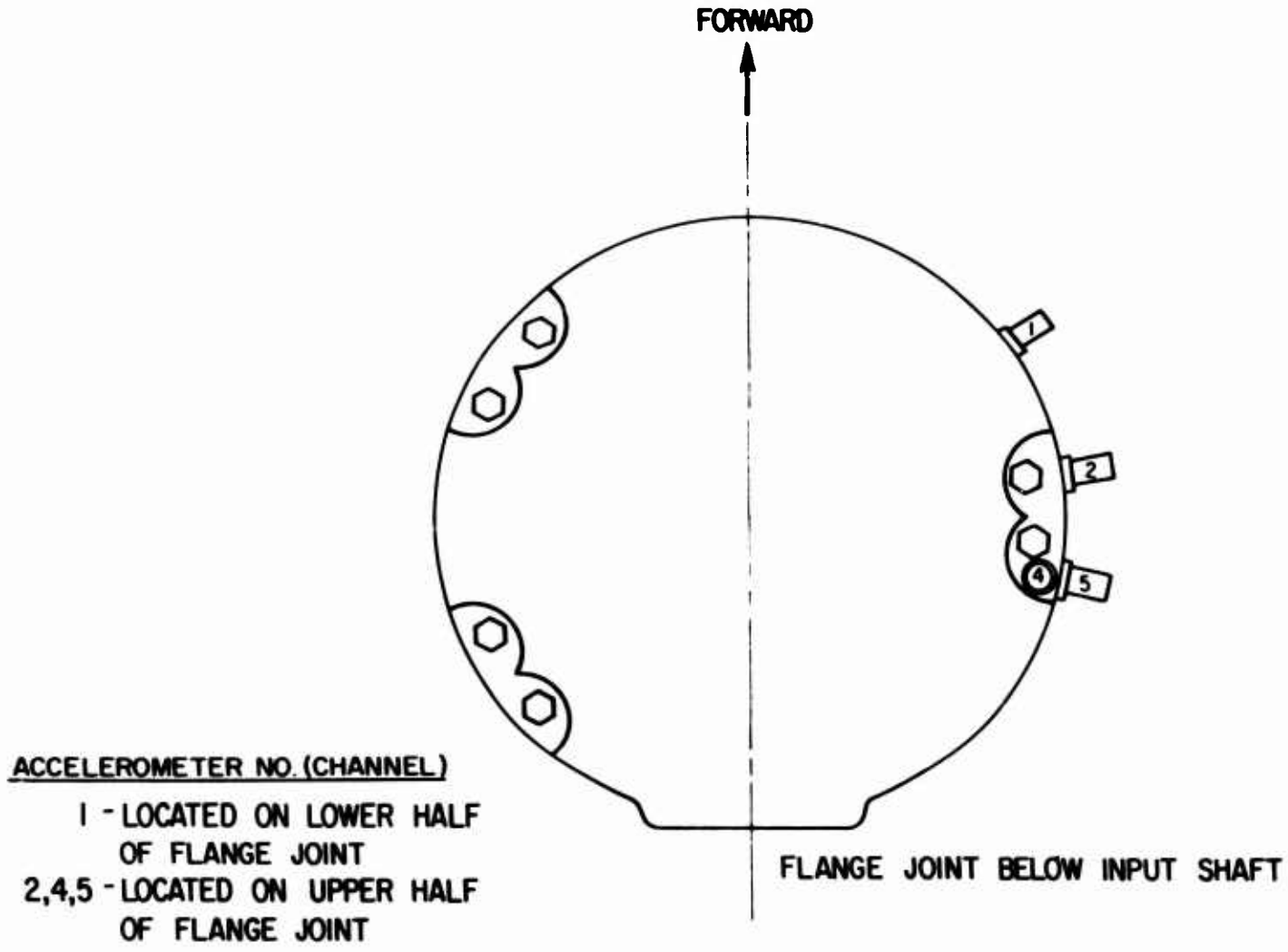

Figure 103. Accelerometer Locations on UH-1 Helicopter Transmission for Records 3, 4, and 5.

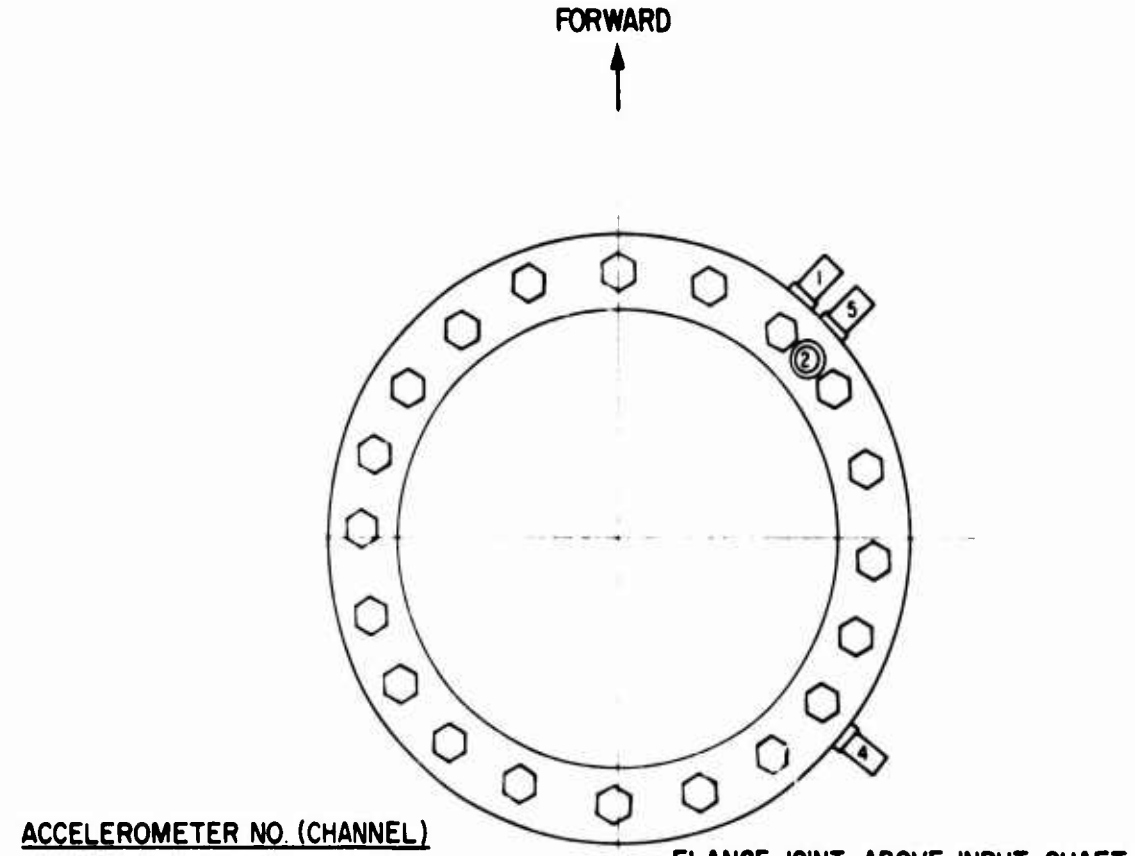

Figure 104. Accelerometer Locations on UH-1 Helicopter Transmission for Records 6, 7, and 8.

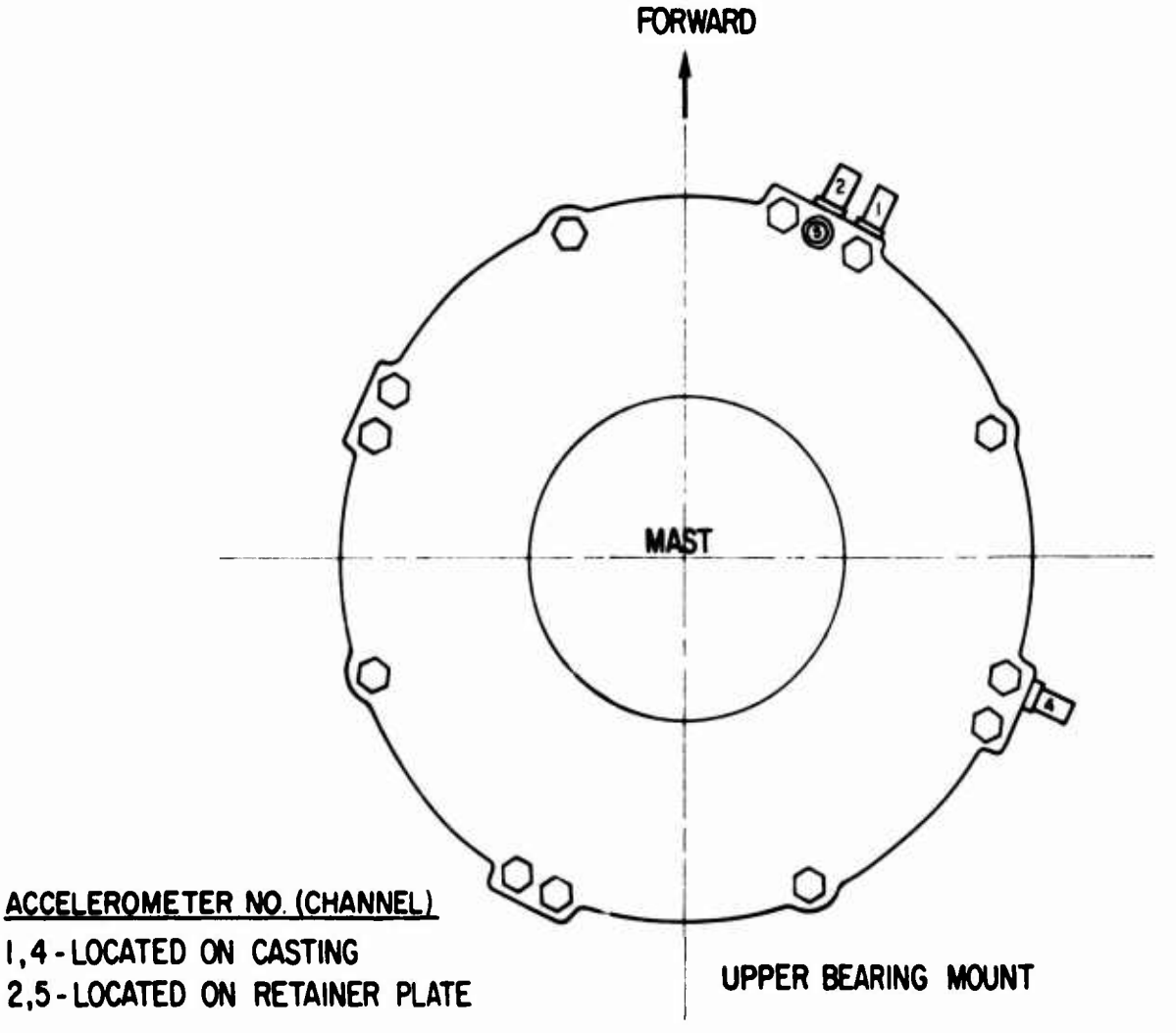

Figure 105. Accelerometer Locations on UH-1 Helicopter Transmission for Records 9 and 10.

The envelope detection portion of the data analysis was the same procedure as that used for the rotating dynamic response tests undertaken in Task II.

MEASURED VIBRATION LEVELS

The background vibration level data recorded on the helicopter consisted of eleven separate recordings, or records. Each record consisted of four channels of recorded data, where each channel contained the information from a separate accelerometer. The eleven records consisted of variations of accelerometer location as shown in Figures 102 through 105, and helicopter transmission input shaft speed. The input shaft speed varied from 4000 rpm to 6600 rpm. A data summary is presented in Table XXVII. The raw data from each of the cases was analyzed for frequency content with the aid of a real-time spectrum analyzer. Frequency spectrums for some of this data are presented in Figures 106 and 107.

TABLE XXVII. UH-1 HELICOPTER TRANSMISSION DATA SUMMARY

Record	Approximate Input Shaft Speed (rpm)	Bearing(s) of Interest
1	4000	1, 2
2	6600	1, 2
3	4000	3
4	4400	3
5	6600	3
6	4000	4
7	4400	4
8	6600	4
9	4400	5
10	6600	5
11	4400	1, 2

EVALUATION AND ANALYSIS OF HELICOPTER BACKGROUND VIBRATION TEST DATA

The data collected from the UH-1 helicopter transmission background vibration levels was analyzed for ball-pass frequency content using the High Frequency Resonance Technique. The procedure was the same as that used for analyzing the data collected from the rotating dynamic response test rig. The results from the test rig analyses were used as a guide during the analysis of the helicopter background vibration data. These results aided in the selection of accelerometer locations, running speeds and, especially, frequency peaks for envelope detection, for primary consideration during this analysis. During the course of this analysis, it was important to be able to distinguish between ball-pass frequencies and gear mesh frequencies

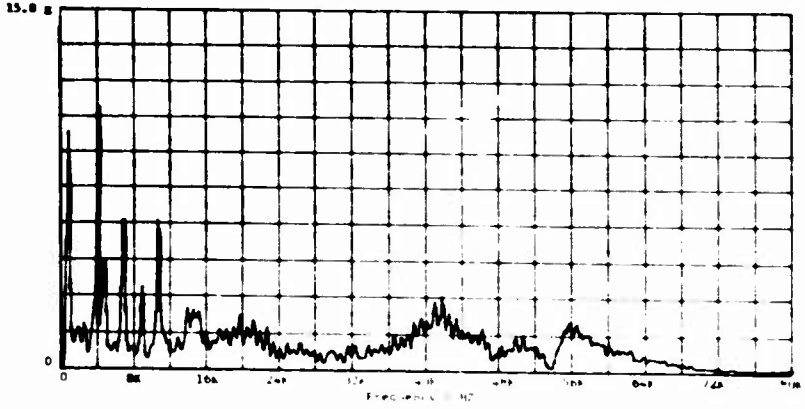

a) Accelerometer No. 4, Input Quill Shaft Housing

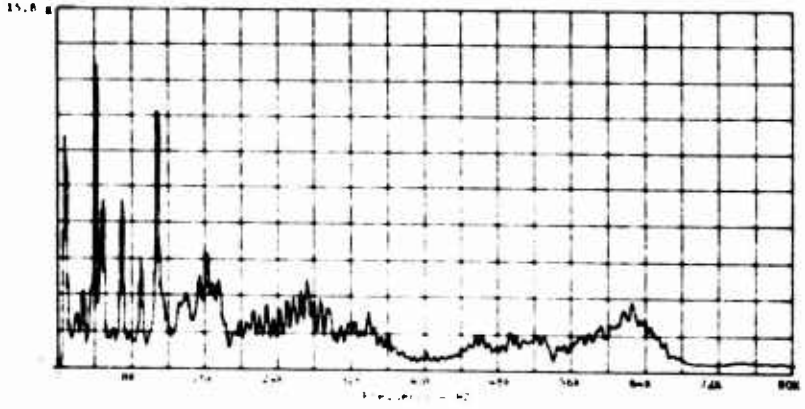

b) Accelerometer No. 5, Input Quill Shaft Housing

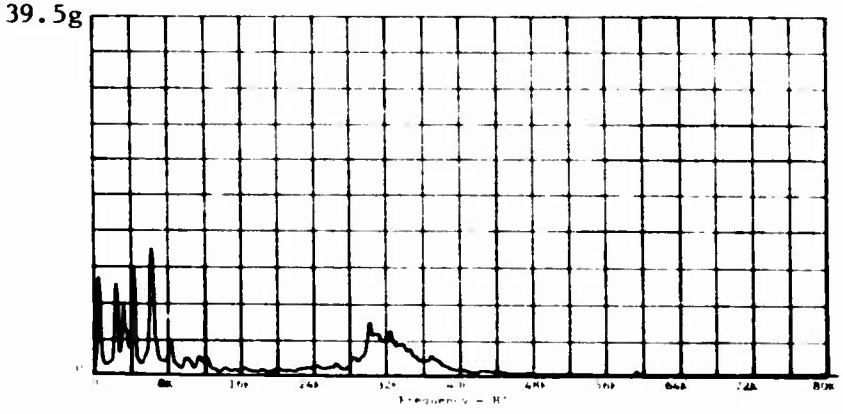

c) Accelerometer No. 2 on Flange Joint Below Input Shaft

Figure 106. Raw Helicopter Vibration Data, 6600 RPM.

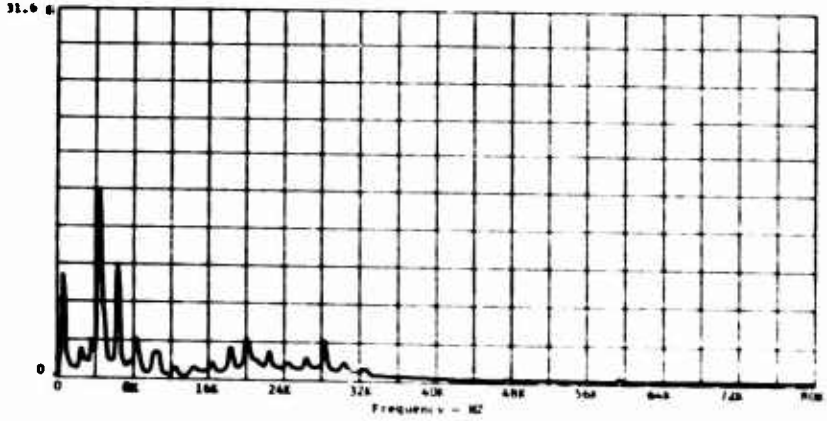

a) Accelerometer No. 2 on Flange Joint Above Input Shaft, 6600 RPM

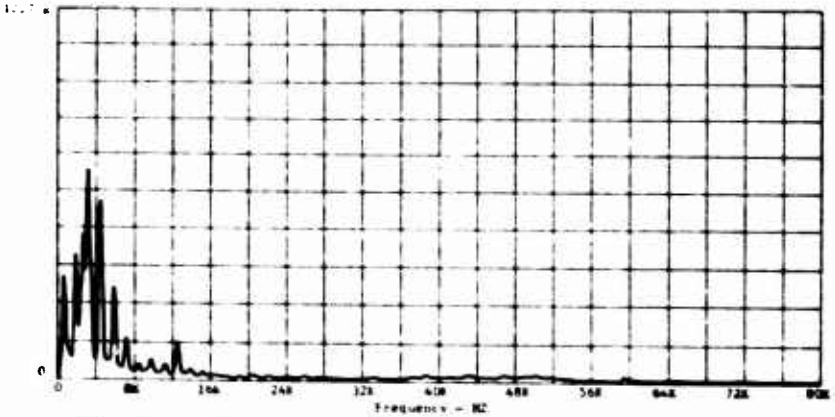

b) Accelerometer No. 1 on Upper Bearing Mount, 4400 RPM

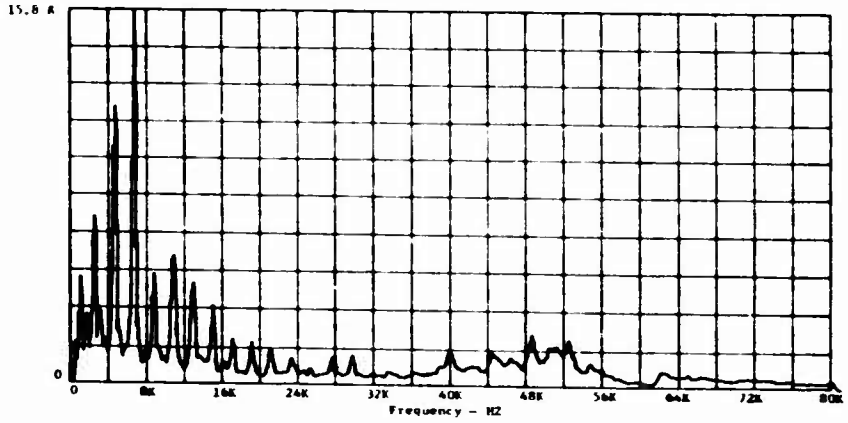

c) Accelerometer No. 1 on Upper Bearing Mount, 6600 RPM

Figure 107. Raw Helicopter Vibration Data.

for a UH-1 helicopter transmission. For this reason a list of gear mesh frequencies below 2-kHz is given in Table XXVIII.

TABLE XXVIII. LIST OF UH-1 HELICOPTER TRANSMISSION GEAR MESH FREQUENCIES BELOW 2-kHz

Gear Mesh	Harmonic	Frequency at Input Shaft Speed of 4400 rpm	Frequency at Input Shaft Speed of 6600 rpm
Upper Planetary	Fundamental	430	644
Upper Planetary	Second	859	1288
Upper Planetary	Third	1288	1932
Lower Planetary	Fundamental	1322	1982
Upper Planetary	Fourth	1718	2576

Bearing No. 1

The data for bearing No. 1 was envelope detected about its 24-kHz peak, as suggested by the results of the test rig data analysis. The most distinct outer race ball-pass signal was obtained from accelerometer No. 5 (channel 5) of record 2 with an input shaft speed of 6600 rpm. This is shown in Figure 108a. The same data is presented in raw form in Figure 108b. It is noted that the outer race ball-pass frequency peak (718 Hz) in Figure 108a and the upper planetary gear mesh fundamental (670 Hz) in Figure 108b are both about 4 percent higher than predicted. This is due to the inaccuracy of the helicopter tachometer used for determining the input shaft speed of the transmission during the background vibration tests. Judging from this data, the actual input shaft speed during the tests was roughly 4 percent higher than that registered on the helicopter tachometer. Further analysis of the helicopter background vibration data showed that this 4 percent speed error was carried through all of the tests. The outer race ball-pass frequency peak did not show up at all in the raw data, but the upper planetary gear mesh fundamental was very strong. However, the envelope detection results showed a very strong outer race ball-pass frequency peak and not more than a trace of the upper planetary gear mesh fundamental. The envelope detection analysis did not produce any inner race ball-pass frequency peaks for bearing No. 1. However, this is not surprising. The only bearings from the test rig tests which produced any inner race ball-pass frequency peaks were those with damaged inner races, and the bearings in the helicopter transmission were, presumably, all undamaged bearings.

Bearing No. 2

During the helicopter background vibration tests, the same accelerometer locations were used for collecting data for bearing No. 2 as were used for bearing No. 1. However, bearing No. 2 is located considerably deeper in the transmission and further from the accelerometers than bearing No. 1. Consequently, it was expected to be much more difficult to obtain ball-pass information from bearing No. 2 than from bearing No. 1. As suggested

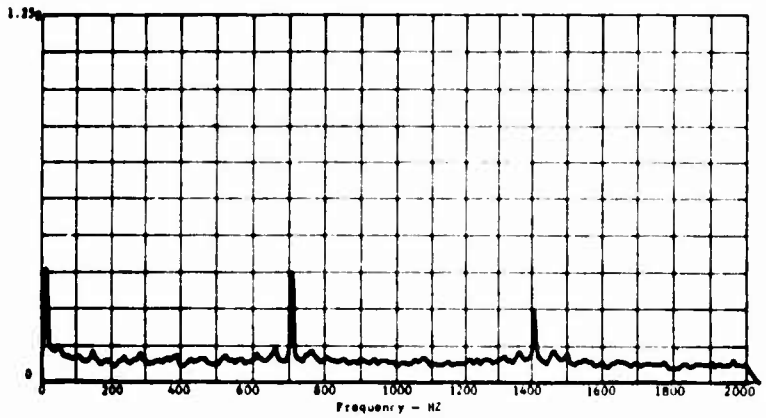

a) Envelope Detected About 25-kHz.

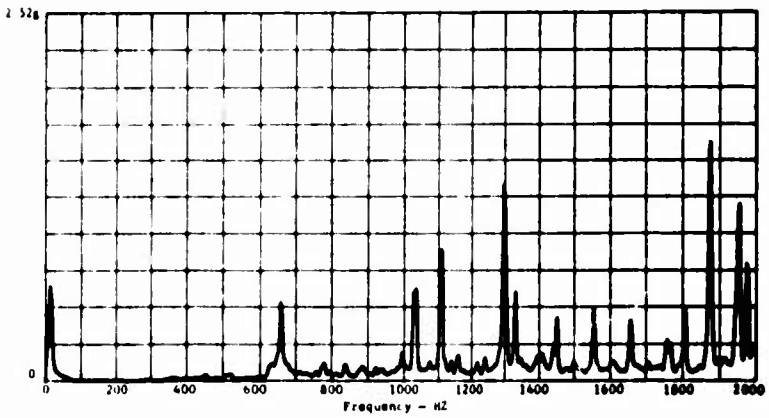

b) Raw Data

Figure 108. Helicopter Vibration Data, Bearing No. 1, 6600 RPM, Accelerometer No. 5, Located on Input Quill Shaft Housing.

by the test rig results for bearing No. 2, the helicopter data was envelope detected about 39-kHz and 31-kHz. Some of the results are presented in frequency spectrum form in Figure 109. There was no ball-pass frequency peak (539 Hz) for bearing No. 2 found in these results. However, there is a very substantial outer race ball-pass frequency peak for bearing No. 1 present in both spectrums. This shows that if the ball-pass contact of bearing No. 2 was exciting any race resonances around those frequencies, they did not produce nearly as strong signals as resonances in the same frequency regions being excited by outer race ball contact in bearing No. 1. It is entirely possible that a damaged bearing No. 2 would excite a strong enough race resonance signal to be detected at those accelerometer locations. However, all that can be determined from these test results is that the presumably undamaged bearing No. 2, which was in the transmission at the time of the tests, did not produce that strong a signal.

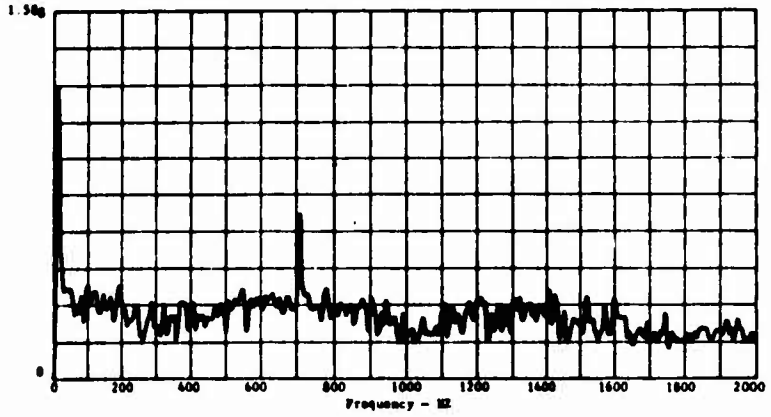

a) Envelope Detected About 39-kHz

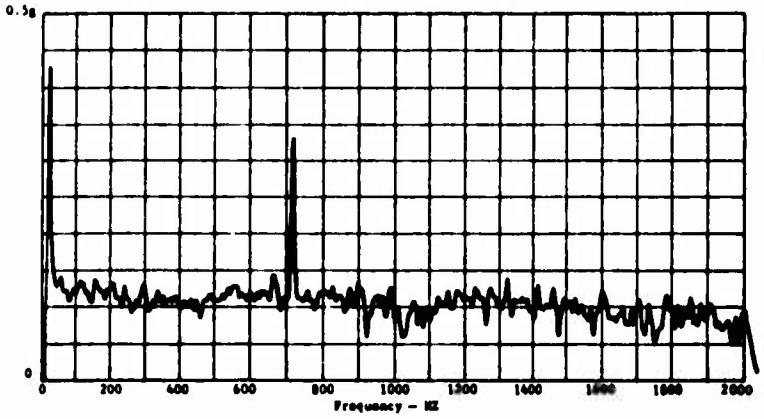

b) Envelope Detected About 31-kHz

Figure 109. Helicopter Vibration Data, Bearing No. 2, 6600 RPM, Accelerometer No. 4 Located on Input Quill Shaft Housing.

Bearing No. 3

Envelope detection of the data for Bearing No. 3 about 48-kHz produced a small, but distinct, outer race ball-pass frequency peak (785 Hz), as shown in Figure 110a. However, there was also a strong, upper planetary gear mesh fundamental frequency peak (670 Hz) present, which was also present in the raw data shown in Figure 110b. Although this gear mesh was present in the envelope detected results and had a somewhat larger amplitude than the ball-pass frequency peak, it would not present an insurmountable obstacle to accurate defect analysis of bearing No. 3. This is because a narrow band pass filter could be used effectively to separate the two frequency peaks.

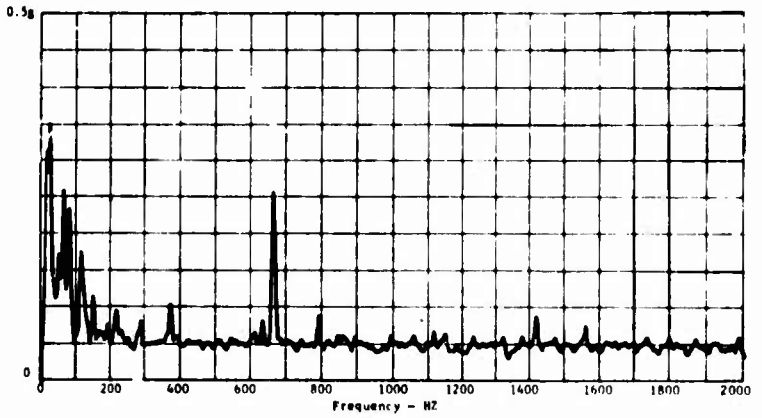

a) Accelerometer No. 2, Envelope Detected About 48-kHz

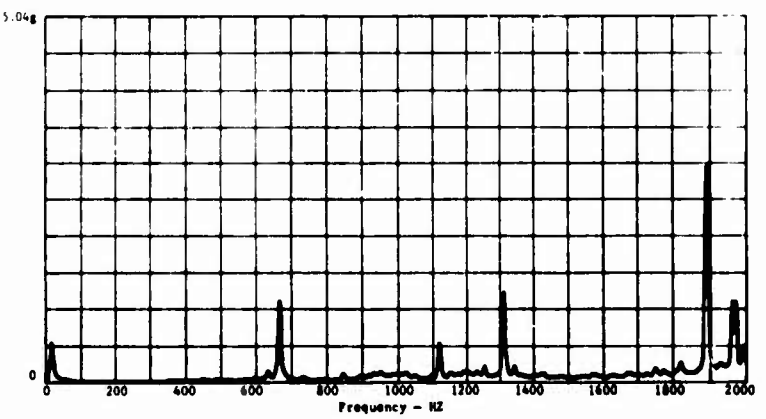

b) Accelerometer No. 1, Raw Data

Figure 110. Helicopter Vibration Data, Bearing No. 3, 6600 RPM, Accelerometer Located on Flange Joint Below Input Shaft.

Bearing No. 4

The helicopter data for bearing No. 4 was envelope detected about 40-kHz, as suggested by the test rig results for that bearing. A small outer race ball-pass frequency peak (630 Hz) could be seen in the results of the analysis of the data collected by accelerometer No. 2 (channel 2) of record 8. It is interesting to note that this accelerometer was mounted in the axial direction. These results are shown in frequency spectrum form in Figure 111a. In this case, the upper planetary gear mesh fundamental, shown clearly in the frequency spectrum of the raw data in Figure 111b, did not show up at all in the envelope-detected results. No inner race ball-pass frequency peak (761 Hz) was found for bearing No. 4 during the envelope detection analysis of the helicopter data.

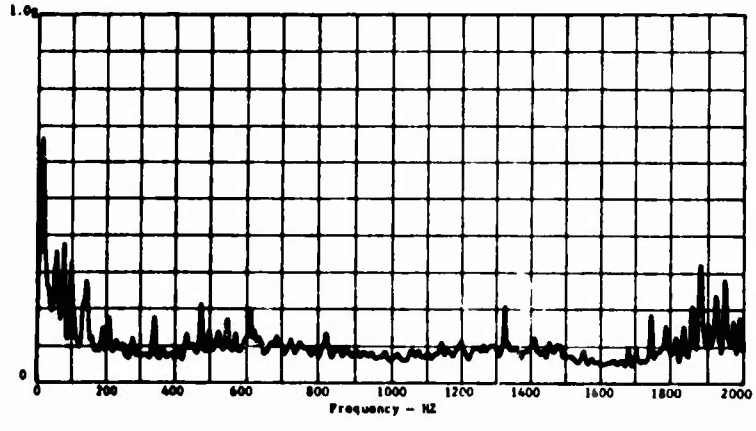

a) Accelerometer No. 2, Envelope Detected About 40-kHz

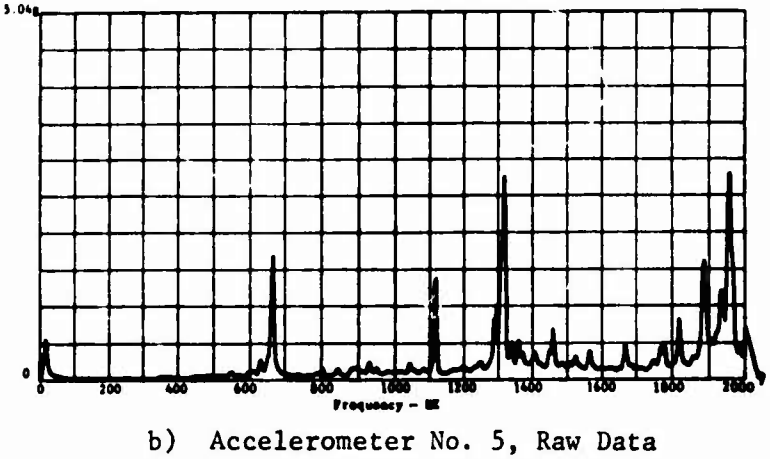

b) Accelerometer No. 5, Raw Data

Figure 111. Helicopter Vibration Data, Bearing No. 4, 6600 RPM, Accelerometers Located on Flange Joint Above Input Shaft.

Bearing No. 5

Both outer and inner race ball-pass frequency peaks were found in the analysis of the helicopter data for bearing No. 5. In addition, a ball defect ball-pass frequency peak was found. The ball defect ball-pass frequency peak (44 Hz) showed up when the helicopter data was envelope detected about 5.8-kHz. The frequency spectrum for these results is presented in Figure 112a. As predicted by the test rig results, the inner race ball-pass frequency peak (45 Hz) showed up strongest when the helicopter data was envelope detected about 19-kHz. Also, the outer race ball-pass frequency peak (35 Hz) appeared in the same results. The frequency spectrum for these results is presented in Figure 112b. The analysis for both of these cases was conducted on data collected by the same accelerometer which was mounted in the radial direction. However, the ball defect ball-pass frequency signal was found for an input shaft speed of 6600 rpm, while the inner and outer race signals were found for a speed of 4400 rpm. There was no raw data under 200 Hz, or at least none that could be detected and analyzed by the instrumentation used for these tests.

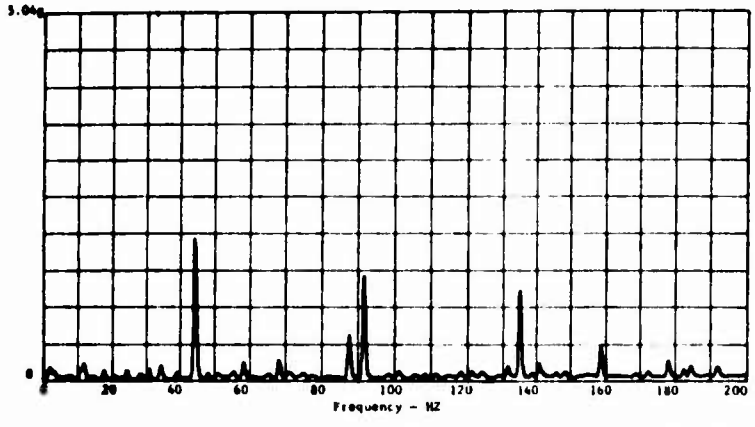

a) 6600 RPM, Envelope Detected About 5.8-kHz

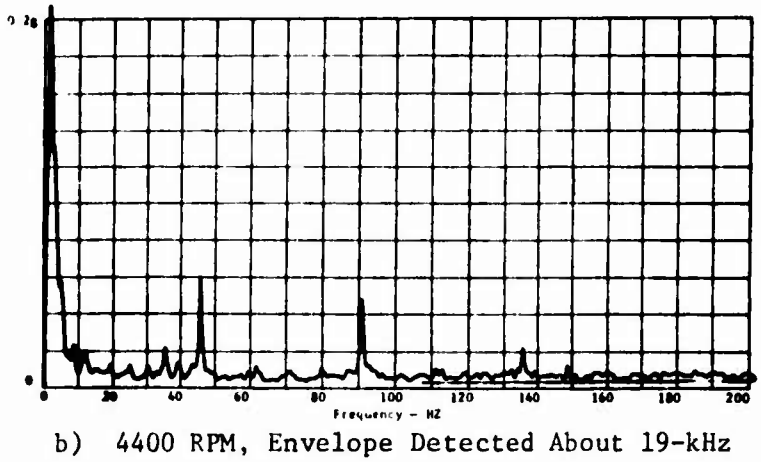

b) 4400 RPM, Envelope Detected About 19-kHz

Figure 112. Helicopter Vibration Data, Bearing No. 5, Accelerometer No. 1 Located on Upper Bearing Mount.

Summary

The outer race ball-pass frequencies for bearings Nos. 1, 3, 4, and 5, and the inner race and ball defect ball-pass frequencies for bearing No. 5, showed up distinctly in the results of the envelope detection analysis of the UH-1 helicopter transmission background vibration data. With the exception of the analysis performed for bearing No. 3, none of the gear mesh frequencies appeared in any of the envelope detected results. In the case of bearing No. 3, although a gear mesh frequency was present in the envelope detected results, it was distant enough from the outer race ball-pass frequency peak to be easily separated from it by a narrow band-pass filter.

CONCLUSIONS

GENERAL

Results of the High-Frequency Resonance Technique (HFRT) evaluation clearly show the feasibility of using this technique for detecting faults in rolling-element bearings.

Lab tests in the dynamic response test rig showed the ability of the technique to detect faults in both inner and outer races of the five UH-1 helicopter main-rotor-drive transmission bearings investigated. The envelope detection procedure was found to be very successful in detecting artificial faults in these bearings. The HFRT principle was further investigated to provide confidence in the application to both roller and ball bearings in general. The high-frequency peaks used for envelope detection were selected by empirical methods rather than by predictions. Although the results of the race resonance investigation were used to identify some of those high-frequency peaks, these results could not be solely used to choose those peaks, because the reasons why certain resonances are excited and others are not, are not presently well understood.

A comparison of the HFRT with raw data detection techniques showed that the HFRT could readily be used where defect signal components in the raw data were masked by noise. This truly demonstrated the value of the HFRT. These results were obtained as part of a study of UH-1 helicopter transmission background vibration levels conducted under this contract. They demonstrated clearly the practicality of using the High-Frequency Resonance Technique for evaluating the condition of bearings in an actual, installed UH-1 helicopter transmission. It appears that determination of bearing conditions can probably be accomplished through the use of accelerometers located on the exterior surface of the transmission. The results of these tests showed that in most cases, significant ball-pass or roller-pass signal components could be detected from the presumably good bearings that were in the installed transmission. While the laboratory tests indicated that ball-pass or roller-pass signals would very likely be detectable in the aircraft environment, the results of the helicopter transmission background vibration tests showed these signals to be considerably more vivid than anticipated. This could be caused by combinations of static and dynamic loading actually encountered in the transmission, or could be due to worn bearings. In any case, the signals from distressed bearings should be considerably more pronounced. Detecting such signals is expected to be reasonably easy and straightforward.

The HFRT appears to be suited to the detection of both outer and inner race faults. The test rig results showed that a bearing with an artificially damaged outer race has an outer race ball-pass or roller-pass signal component of significantly higher magnitude in the envelope detected data than does an undamaged bearing. The differences for inner race defects were even more dramatic. The results for the damaged inner race bearings showed very significant inner-race-related signal components, while the results for the undamaged bearings showed virtually none.

BEARING DESIGN AND OPERATING PARAMETERS

Several specific conclusions can be drawn with respect to the effect of certain design and operating parameters on the presence and magnitude of the defect vibration signal components. In general, variations of speed did not appear to cause large changes in defect signal component magnitudes. Thus, once a resonance has been selected as an information carrier for the particular UH-1 transmission bearing, that resonance should be usable over the entire operating speed range.

It appears that much more ball-pass or roller-pass signal component information was collected by the accelerometers when the bearing being tested was loaded than when it was not loaded. However, as long as there was enough load on the bearing to maintain intimate contact between the balls or rollers and the races, the exact level of that load, in general, did not appear to have a significant effect on the envelope detection results. The minimum loads encountered in a UH-1 helicopter transmission are certainly large enough to maintain this intimate contact. Therefore, the variation in loads encountered in the transmission should not have a significant effect on the envelope detection results.

For roller bearings, the accelerometer should be mounted with its axis in the bearing radial direction and located as near to the roller-race loading point as possible. For the ball bearings tested, the accelerometer locations and orientations were not as critical, and the locations which produced the best data varied from bearing to bearing. In some cases, the lightweight and flexible lightweight bearing housings used in the tests did not transmit the ball-pass excited race resonance signals quite as well as the heavyweight housings. However, the differences were never very great.

UH-1 HELICOPTER TRANSMISSION BEARINGS

With respect to application of the results of this contract to the UH-1 helicopter main-rotor-drive transmission, certain preliminary conclusions can be drawn as to the best accelerometer locations and envelope detection frequencies for the defect analysis of each of the five bearings tested; as demonstrated in the results of both the test rig and helicopter background vibration level tests:

a) For both the inner and outer races of bearing No. 1, the best test rig results were obtained with the accelerometer axis oriented in the bearing radial direction and the envelope detection analysis done at 24-kHz. The best accelerometer location found in the helicopter data analysis was accelerometer No. 5, as shown in Figure 102. The test rig results showed that an outer race defect for bearing No. 1 could also be found by envelope detecting the 31-kHz resonance data obtained from an axially-mounted accelerometer. However, there were no accelerometers mounted axially with respect to bearing No. 1 during the helicopter background vibration tests.

b) For bearing No. 2, the best test rig results were obtained with the accelerometer axis oriented in the bearing radial direction and as near as possible to the load point, and with the envelope detection analysis done at 39 kHz.

c) For bearing No. 3, the best test rig results were obtained with the accelerometer axis in the bearing radial direction and as near as possible to the load point, and with the envelope detection analysis done at 48 kHz. From the helicopter data analysis, the best accelerometer location for roller-pass signal component detection for bearing No. 3 was accelerometer No. 2 in Figure 103.

d) For bearing No. 4, the best test rig results were obtained from both axially and radially-mounted accelerometers for outer race defect detection, while axially mounted accelerometers gave the best data for inner race defect analysis. The best frequency for envelope detection analysis was found to be 40 kHz for both inner and outer race defect detection. The best results from the helicopter data analysis for bearing No. 4 were obtained from the data collected by the axially mounted accelerometer, designated as accelerometer No. 2 in Figure 104.

e) The best frequencies for envelope detection defect analysis for bearing No. 5 were 5.8 kHz for outer race defects and 19 kHz for inner race defects. In both cases, the best accelerometer location, as determined from the helicopter data analysis, was that designated as accelerometer No. 1 in Figure 105.

RECOMMENDATIONS FOR FURTHER INVESTIGATION

The results obtained in this program demonstrate the capability and advantages of using the HFRT for the detection of bearing faults. However, the limits within which this technique is effective have not been determined, and a detailed relationship between bearing defect severity and envelope detected ball-pass frequency vibration component amplitude has not been defined. These areas must be investigated before the HFRT can be confidently and accurately used for bearing fault detection in the UH-1 helicopter transmission.

Two avenues of investigation should be followed: The first is a continuation of the rotating dynamic response test rig investigation. Using the test rig, detailed information can be obtained about the UH-1 helicopter transmission bearings as related to the topics of investigation discussed above. In addition, the test rig concept can be developed into a practical instrument for the defect analysis of both new and used bearings in a controlled laboratory environment.

The second avenue of investigation involves the performance of similar tests on an actual UH-1 helicopter transmission, operated in a laboratory environment. The transmission should be altered so as to simplify installation and removal of test bearings. The results obtained from these tests may be used to establish bearing fault criteria which could be applied directly to the defect analysis of the bearings in an actual operating UH-1 helicopter transmission.

The tests to be conducted in the course of both of these avenues of investigation can include, in addition to the evaluation of bearings with various discrete defects, the evaluation of evenly worn bearings or bearings with various surface finishes on the contacted surfaces to simulate even wear. In this way it can be determined whether the HFRT could be used to effectively define the degree of normal bearing wear present as well as to detect the presence of a discrete bearing fault.